Channel Estimation in Half and Full Duplex Relays

by

Xiaofeng Li

A Dissertation Presented in Partial Fulfillment
of the Requirements for the Degree
Doctor of Philosophy

Approved June 2018 by the
Graduate Supervisory Committee:

Cihan Tepedelenlioğlu, Chair
Antonia Papandreou-Suppappola
Daniel W. Bliss
Oliver Kosut

ARIZONA STATE UNIVERSITY

August 2018

ABSTRACT

Both two-way relays (TWR) and full-duplex (FD) radios are spectrally efficient, and their integration shows great potential to further improve the spectral efficiency, which offers a solution to the fifth generation wireless systems. High quality channel state information (CSI) are the key components for the implementation and the performance of the FD TWR system, making channel estimation in FD TWRs crucial.

The impact of channel estimation on spectral efficiency in half-duplex multiple-input-multiple-output (MIMO) TWR systems is investigated. The trade-off between training and data energy is proposed. In the case that two sources are symmetric in power and number of antennas, a closed-form for the optimal ratio of data energy to total energy is derived. It can be shown that the achievable rate is a monotonically increasing function of the data length. The asymmetric case is discussed as well.

Efficient and accurate training schemes for FD TWRs are essential for profiting from the inherent spectrally efficient structures of both FD and TWRs. A novel one-block training scheme with a maximum likelihood (ML) estimator is proposed to estimate the channels between the nodes and the residual self-interference (RSI) channel simultaneously. Baseline training schemes are also considered to compare with the one-block scheme. The Cramer-Rao bounds (CRBs) of the training schemes are derived and analyzed by using the asymptotic properties of Toeplitz matrices. The benefit of estimating the RSI channel is shown analytically in terms of Fisher information.

To obtain fundamental and analytic results of how the RSI affects the spectral efficiency, one-way FD relay systems are studied. Optimal training design and ML channel estimation are proposed to estimate the RSI channel. The CRBs are derived and analyzed in closed-form so that the optimal training sequence can be found

via minimizing the CRB. Extensions of the training scheme to frequency-selective channels and multiple relays are also presented.

Simultaneously sensing and transmission in an FD cognitive radio system with MIMO is considered. The trade-off between the transmission rate and the detection accuracy is characterized by the sum-rate of the primary and the secondary users. Different beamforming and combining schemes are proposed and compared.

To My Family.

ACKNOWLEDGMENTS

Five years have already passed since the beginning of my PhD By the time I was close to finishing, my PhD duration became surprisingly short. All of my achievements will not be possible without the help of many people.

First and foremost I would like to extend my deepest appreciation to my advisor, Cihan Tepedelenlioğlu. He has given me so much inspiration for my academic career and provided me countless support for almost any matters. His insightful ideas and experience inspired my interest in channel estimation and guided my research. I am extremely grateful to him for his numerous proofreads that greatly improved my papers. Without him, it will be uncertain if I can make it all the way through my PhD.

I would also like to thank other members in my thesis committee, Dr. Daniel W. Bliss, Dr. Antonia Papandreou-Suppappola, and Dr. Oliver Kosut for their precious time in serving on my thesis committee member, and for providing feedback to my thesis. I would like to thank the ECEE department at Arizona State University for offering me such a stimulating, inspiring and caring environment to pursue my PhD degree.

I also wish to thank my colleagues (in chronological order) whom I have learned so much from: Adithya Rajan, Jonghoon Lee, Ahmed Ewaisha, Xue Zhang, Ruochen Zeng, and Sai Zhang. I am grateful to them for their friendship and many useful discussions.

Last but not least, I would like to express special thanks to my family. I thank my parents for their love, help and encouragement. My wife has always supported me during my PhD life with her true love and extreme patience. They have been and will always be my strongest support!

TABLE OF CONTENTS

CHAPTER Page

CHAPTER Page

LIST OF ABBREVIATIONS

5G	Fifth Generation
ADC	Analog-to-Digital Converter
AF	Amplify-and-Forward
AWGN	Additive White Gaussian Noise
BER	Bit Error Rate
BFGS	Broyden-Fletcher-Goldfarb-Shanno
CRB	Cramer-Rao Bound
CSI	Channel State Information
DAC	Digital-to-Analog Converter
DF	Decode-and-Forward
FD	Full-Duplex
FIM	Fisher Information Matrix
i.i.d.	independently identically distributed
IIR	Infinite Impulse Response
ISI	Inter-Symbol Interference
LoS	Line-of-Sight
LS	Least Square
LTE	Long Term Evolution
MIMO	Multi-input Multi-output
ML	Maximum Likelihood
MF	Matched Filter

MSE	Mean Square Error
MMSE	Minimum Mean Square Error
MRC	Maximum-Ratio Combining
OFDM	Orthogonal Frequency Division Multiplexing
PDF	Probability Density Function
PU	Primary User
SC	Selection Combining
SI	Self-Interference
SIC	Self-Interference Cancellation
SINR	Signal to Interference plus Noise Ratio
SNR	Signal to Noise Ratio
SU	Secondary User
RSI	Residual Self-Interference
TWR	Two-Way Relay

LIST OF FIGURES

Figure Page

Chapter 1

INTRODUCTION

Both two-way relays (TWRs) and in-band full-duplex (FD) are not new concepts in wireless communications but they have been re-discovered recently since they and their integration are potential solutions to provide efficient utilization of spectrum to support the fifth generation (5G) wireless systems [1–4]. Bidirectional or two-way direct communication between two nodes was first studied by Shannon in [5]. However, at that time it was more practical to decompose the two-way communication into two conventional uni-direction communication. Hence, the two-way communication did not draw much attention until the last decade when the TWR architecture significantly improves the spectral efficiency with a low-complexity implementation [6, 7]. Systems with paired users are typical applications of TWRs [8–10]. Especially in the internet of things (IoT) era where huge number of devices simultaneously access a router [11, 12], as shown in Figure 1.1, spectrally efficient architecture becomes more and more crucial [13].

Practical relays usually work in half-duplex mode that includes one receiving phase and one forwarding phase of the same length [14–16], which cuts down the throughput of such relay systems to one half. Therefore, it is natural to apply FD on the relays to compensate the throughput loss. The terminology full-duplex means transmitting and receiving at the same time either over the same frequency band (in-band) or different bands (out-band). Clearly, in-band FD has the potential to double the spectrum efficiency. The history of in-band FD dates back to 1940s. Though FD was extensively used in continuous wave radars [17], it was considered to be impractical in wireless communications since the strong self-interference (SI) from the

transmitter overwhelms the desired signal at the receiver. Recently development of self-interference cancellation (SIC) [18,19] acts as an enabler of in-band FD and makes it a candidate solution for 5G.

The integration of FD radios and TWRs shows great potential to further improve the spectrum efficiency [20], especially in the scenario shown in Figure 1.1 where TWRs provide pair-wise two-way communication for devices while FD makes the router efficient. However, the high spectrum efficiency in theory is fundamentally limited by the quality of channel state information (CSI) used in SIC. In FD relays, the residual self-interference (RSI) caused by the imperfect CSI in the SIC process [21,22] reduces the spectrum efficiency of the system. The efficiency and overhead of the channel estimation methods are also major concerns when optimizing the spectrum efficiency of the whole system. For instance, a half-duplex mode channel estimation approach is not preferred in an FD system for the following reasons. First, the half-duplex training approach increases the overhead compared to a specially designed approach for FD. Second, extra complexity is needed to switch duplex modes between training phase and data phase for the system. Therefore, it is challenging for channel estimation methods to be of both high quality and high efficiency. This motivates my work in this thesis to develop suitable channel estimation methods for the particular FD TWR system.

1.1 Two-Way Relay Systems

Shannon firstly raised the problem that in two-way communication, how to communicate in both directions through the channel as effectively as possible, if not decomposing the two-way into one-way communication. Later, the TWR was investigated when the physical layer network coding came out which significantly improves the network throughput of ad hoc and cellular systems [23, 24]. Inspired by the

Figure 1.1: A scenario where FD TWRs are spectrally efficient - in the IoT era where huge number of devices simultaneously access a router, spectrally efficient architecture becomes more and more crucial. TWRs provide pair-wise two-way communication for devices while FD makes the router efficient.

network coding, the TWR architecture in which two nodes exchange their messages via a relay inherited the throughput improvement and became an active research area [6, 25–27]. Relay architectures including one-way and two-way relays are investigated for the present standards such as LTE-Advanced and WiMAX in which relays are deployed efficiently in cellular systems [28, 29]. TWRs can be relevant to ad hoc networks, networks with a centralized controller through which all messages must pass, and cell phones talking via a satellite, which would be widely used.

In a TWR system, as shown in Figure 1.2, two source nodes exchange information with the help of a relay node in between. There is either direct link or not between the source nodes. The TWR system can be classified by the scheme of how the relay forwards information and the protocol of two source nodes exchanging information. The relaying schemes and protocols will be discussed in detail in the next chapter. The TWR system can operate in either full-duplex or half-duplex. In half-duplex communication, a node may either transmit or receive at a given time. This is in contrast to in-band FD where nodes transmit and receive over the same frequency simultaneously. The channels between nodes are referred to as individual channels while the effective channels from one source to the other, which are products of two individual channels, are referred to as cascaded channels.

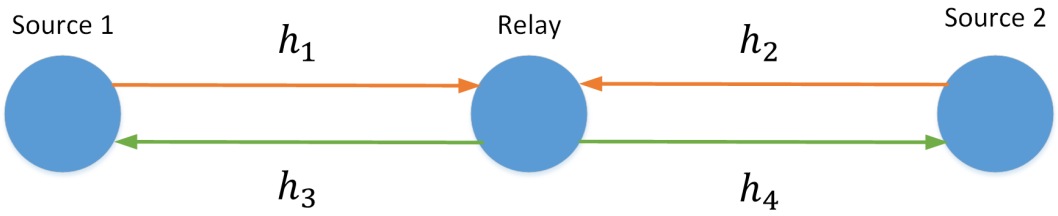

Figure 1.2: A two-way relay system - two sources exchange their messages with the help of a relay node in between. There is no direct link between the two sources. The channels h_1, h_2, h_3, and h_4 are individual channels and h_1h_4 and h_2h_3 are cascaded channels.

1.2 Full-Duplex Radios

In-band FD wireless radios are able to transmit and receive simultaneously over the same frequency band and are used in FD relays [20,30,31], continuous wave radars [17], and FD bidirectional communications [32–34]. In the past, in-band FD radios were generally thought infeasible due to strong SI from the transmitter to the receiver. Here is an example to illustrate how strong the SI is. According to [19], in femtocell networks, femto base stations transmit at 21 dBm with a receiver noise floor of 100 dBm. If a physical isolation of 15 dB between the base station's transmit and receive antennas is assumed, then the SI from the base bastion will be $21-15-(-100) = 106$ dB above the noise floor. Compared to a half-duplex counterpart, the FD base station has to suppress the SI by a fantastic value of 106 dB to achieve the same received signal to noise ratio (SNR) for the desired signal. That explains why half-duplex systems, which transmit and receive either at different time slots, or over different frequency bands, are commonly used.

However, recently, FD radios have drawn great attention from both industry and academia for the following reasons. First, the traditional approaches to increase spectral efficiency such as MIMO, coding and advanced modulation have been exhausted. Second, most contemporary wireless communication terminals/devices such as base stations, relays and mobiles have the function of both transmitters and receivers,

and largely benefit from FD. Besides, SIC techniques have been developed with great promise [3,18,19], which leverages the implementation of FD devices. As a typical application of in-band FD radios, an FD relay, which receives the current symbols from a source while transmits the previously received symbols to a destination over the same frequency, is of great interest for the 5G wireless communication systems [4, 20] due to its potential to double the spectrum efficiency. As in-band FD is the promising technology, we will use FD to generally refer to in-band FD throughout this thesis unless otherwise stated.

The implementation of FD relays can be devices equipped with either separate-antenna [30,35,36] or shared-antenna [37]. Two antenna sets are used for transmission and reception respectively in the former implementation while only one antenna set is adopted to transmit and receive simultaneously with a duplexer/circulator connected to it in the latter case. More detailed comparison of the two implementations can be found in [19, 20]. We will adopt the separate-antenna implementation in this thesis since the advantages of such implementations are two-fold. First, it is relatively easy to implement the separate-antenna sets with current antennas and circuits and to install those sets on large size terminals, e.g., base stations, infrastructure-based relays. Second, physical isolation for SIC can take advantage of the physical distance between the antenna sets which provides natural isolation. The space between the antenna sets also allows obstacles to block the line-of-sight component of the SI.

1.3 Contributions

Here we summarize the main contributions of this thesis.

- For the half-duplex TWRs, we investigate the trade-off between training and data in a MIMO scenario. In the symmetric power case of two sources, a closed-form expression of the optimal ratio of data energy to training energy is derived

to maximize the achievable rate of the data phase. The optimal ratio is found by solving a fourth order equation and reduces to a quadratic equation when the number of antennas at the source is large. We also show that the achievable rate is a monotonically increasing function of the data time. The results can be extended to the asymmetric case in which the minimum of the two source SNRs is maximized.

- In the FD TWR system, we propose a spectrally efficient one-block training scheme which suits the FD transmission. A maximum likelihood (ML) estimator with zero-forcing initialization are derived and efficiently solved by the Broyden-Fletcher-Goldfarb-Shanno (BFGS) algorithm. Baseline schemes including the multi-block training scheme and the cross-correlation method for ISI channels are also proposed for comparison. The Cramer-Rao bounds (CRBs) for the training schemes are derived and compared. We analyze how the channel parameters and transmit powers affect the Fisher information by using the theorem of asymptotic Toeplitz matrices. We also show analytically that the Fisher information exploiting the channel structure arising form the RSI is greater than the counterpart which does not take the structure into account. To show the importance of estimating the RSI channel and canceling the RSI, matched filter detector and Viterbi equalizer are implemented and compared.

- In the FD one-way relay, we propose a block-based training scheme with an ML estimator to estimate the RSI channel and the end-to-end channel at the destination. Closed-form expressions of CRBs for the channel and RSI parameters are derived. We approximate the CRB for large training length by using asymptotic Toeplitz matrices, and minimize it with respect to the training sequence. We show that the optimal training sequence is sinsoid and charac-

terize its frequency. Extensions to the case when the channels between nodes are frequency-selective and the case of multi-relay systems are considered. We show that our training scheme applies also for frequency-selective case when the length of training sequence is large. For the multi-relay case we also derive an asymptotic CRB which captures the effect of the number of relays.

- Simultaneously sensing and transmission problem in an FD cognitive radio system with MIMO is considered. The probabilities of detection in the presence of RSI are derived. The sum-rate of the PU and the SU is proposed as a metric to characterize the trade-off between the transmission rate and the detection accuracy. Different beamforming and combining schemes are compared and how the schemes affect the sum-rate is discussed.

1.4 Thesis Outline

The rest of this thesis is organized as follows. Chapter 2 provides the reader the background of the channel estimation problem in FD TWRs. Chapter 3 begins with a system model for the half-duplex MIMO TWR. The trade-off between training and data for TWR is investigated. In Chapter 4, we focus on the channel estimation problem of an FD TWR system, aiming to estimate and eliminate the RSI at the sources. The Fisher information of the channels are also analyzed to show the benefit of estimating the RSI. Chapter 5 discusses the optimal training design of a FD one-way relay system with closed-form expression of CRBs. Simultaneously sensing and transmission in FD is considered in Chapter 6. Chapter 7 draws the conclusion of this thesis.

Chapter 2

BACKGROUND

In this chapter, background knowledge on three main topics is provided, namely relaying schemes and protocols, the unique channel estimation problem in two-way relays (TWRs), and residual self-interference (RSI). The relaying schemes and protocols are important since they affect the accuracy and efficiency of the training schemes. Roughly speaking, traditional channel estimation methods can work with low efficiency protocols while new training schemes need to be designed to suit high efficiency protocols, especially for FD relays. Before getting into the FD training schemes, we will explain the unique channel estimation problem which is the ambiguity of estimating the individual channels in TWRs. Without sophisticated training schemes, the two sources can only estimate the cascaded channels, which result in ambiguity when the cascaded channels are used to recover the individual channels. Lastly, we illustrate the point that RSI is unavoidable in FD relays even all the self-interference cancellation (SIC) approaches are applied, and discuss the RSI channel model by considering the residual error from SIC and transceiver distortions from hardware impediment. An accurate and effective RSI channel model is essential in designing effective channel estimation methods for FD TWRs.

2.1 Relaying Schemes and Protocols

2.1.1 Relaying Schemes

Relay schemes are the strategies of how the relay processes its received signal. Amplify-and-forward (AF) [38–43] and decode-and-forward (DF) [38, 44–48] are two

main schemes that can be adopted to both half-duplex and FD TWRs. In the AF scheme, the relay constructs its transmit signal by simply replicating and amplifying the received signal and does not decode the received signal. Hence, it has a much shorter forwarding delay. The AF relay has lower complexity than the DF relay and can be implemented by analog circuits only if necessary [6]. Another advantage of the AF relay is that it is transparent to the transmit signal of the source, which means the received signal at the destination is an explicit function of the transmit signal at the source [49]. This flexibility which is not limited to particular modulation types of the transmit signal allows end-to-end optimization in AF relays. However, one of the intrinsic drawbacks of the AF relay is that it also amplifies its receiver noise and propagates it to the destinations, which will degrade the bit error rate (BER) performance. In an FD AF relay, the RSI after SIC is also amplified and would result in distortion and clipping of the signal which must be prevent from by carefully controlling the power scaling factor at the relay [50,51]. Moreover, the RSI link forms a feedback at the relay, which makes the overall channel a single pole infinite impulse response (IIR) channel and causes inter-symbol interference (ISI) [52–55].

On the contrary, in the DF scheme the relay decodes both messages from the two sources, then encodes them and transmits the new codeword. Thus, the relay requires the full codebooks of both source 1 and source 2 and a large mount of calculation to decode. The processing delay and the implementation complexity are high but the noise-propagation is stopped. For FD relays, the SI again has a large impact on the decoding such that more rigorous SIC process is needed otherwise the received signal is not decodable. In addition to the AF and the DF schemes, there are other relaying schemes but not as commonly used as AF and DF. For instance, compress-and-forward [56] is a scheme performs in between AF and DF. It compress the received to satisfy certain constraints and then forwards the signal. Though the relay does

not require codebooks, it really requires some channel state information (CSI) such as the distribution of the source-to-relay channel. In detect-and-forward scheme [57] the relay detects the received signal to reduce the relay noise and in partial decode-and-forward [58] the relay decodes the sum or XOR sum of the two messages from source 1 and source 2 respectively.

2.1.2 Relaying Protocols

The relaying protocol plays an important role in increasing the spectrum efficiency. The protocols for half-duplex TWRs are four time slots, three time slots and two time slots protocols, as shown in Figure 2.1. Traditionally, the four time slots protocol of a half-duplex relay system is $1 \rightarrow R$, $R \rightarrow 2$, $2 \rightarrow R$,$R \rightarrow 1$, where the time slots are listed chronologically. Therefore, the two-way communication is decomposed into two conventional one-way communication. There is no overlap of the two signals of the two source nodes in this protocol so that interference can be avoided. However, the protocol is spectrally inefficient and does not take full advantage of the broadcast nature of wireless channels. One intuitive way to take advantage of the broadcast channel is to combine the second and the fourth time slot into a single broadcast transmission by using network coding [23]. This protocol works as the following. If the relay can decode the messages m_1 and m_2 from the two sources respectively, it is sufficient for the relay to broadcast $m_{\mathrm{R}} = m_1 \oplus m_2$ to both sources. This three time slots protocol is also called the time division broadcast protocol. The time slots needed can be further reduced to two by using network coding which is the key to improve the efficiency. In [6], the authors introduce analog network coding in AF-based TWRs which allows the two source nodes transmit their signals simultaneously to the relay, then the relay amplifies and broadcasts the superimposed signal. Either of the source receives the superimposed signal and remove its own part from it. Consequently, the

source can get the message from the other source. The advantage of analog network coding is the simplicity of the scheme which can be implemented totally in analog and does not largely depend on CSI. In most of the cases the relay only needs to keep the power constraint. In [24], Zhang et al. show that network coding applied at the physical layer enables the source nodes to transmit simultaneously to the relay in DF scheme. The two time slots scheme is also called the multiple access broadcast protocol since in the first time slot the TWR channel is a multiple access channel while in the second time slot it is a broadcast channel. Though the exact capacity region of TWRs with the two time slots scheme is still unknown [7,38], the reduction in time slot already achieves significant throughput increase compared with the four and the three time slots protocols.

The two time slot protocol can be extended to FD relays, where the relay receives the current symbols while it forwards the previously received symbols. A forwarding process delay of at least one symbol duration cannot be ignored when formulating the forwarded signal due to causality. In FD relays, the SIC process also results in a delay which inhibits the FD relays from achieving the theoretical spectral efficiency. However, the spectral efficiency gain from reducing two time slots to one is considerable and the rate loss due to the delay is negligible when the duration of the time slot is long. The synchronization of the two sources is a common problem in TWR systems with the two time slot protocol. Some studies [6, 59, 60] provide practical methods to synchronize the two sources and analyze the effect of asynchronization on the system performance as well. Though these methods are designed for half-duplex, they can be extended to FD and used in conjunction without methods. Since the synchronization is an unavoidable cost of both half-duplex or FD TWR system, it is not taken into account when considering the efficiency of spectrum. Hence, we will assume perfect synchronization throughout this thesis.

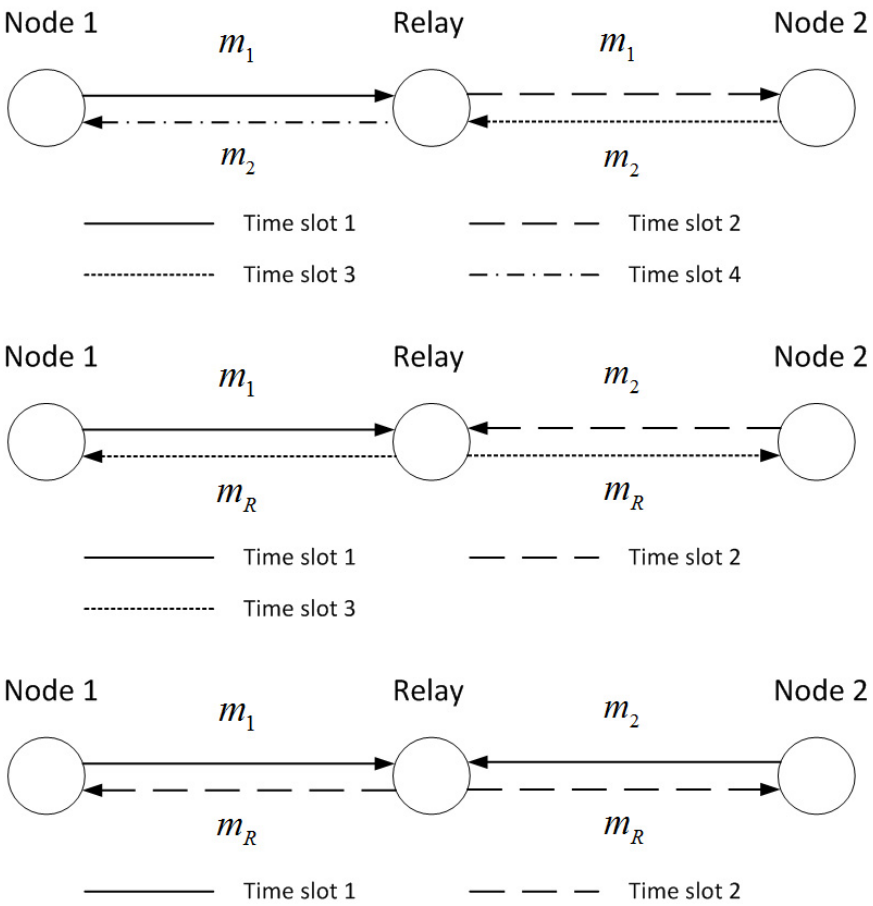

Figure 2.1: Relaying protocols for half-duplex TWRs - the four time slots protocol decomposes the two-way communication into two conventional one-way communication. In the three time slots protocol, the relay receives messages separately, then broadcasts a coded message to both sources. In the two time slots protocol, the relay receives a superimposed signal and then broadcasts it.

2.2 Channel Estimation Problem in Two-Way Relays

2.2.1 Cascaded and Individual Channel Estimation

The channel estimation problem in TWRs with the two time slot protocol has its own characteristics. As the relay forwards the signal from one source to another, the effective channels between the two sources are cascaded channels which are the product of the channels between the sources and the relay (i.e. the individual chan-

nels). The individual channels cannot be directly estimated or recovered without sophisticated training schemes, which will be explained in the following example.

Consider a half-duplex TWR system with two source nodes Source 1 and Source 2 and one relay node, as shown in Figure 1.2. The AF relaying scheme and the two time slots protocol are adopted. In the first time slot, the two sources transmit messages to the relay simultaneously while in the second time slot the relay amplifies and broadcasts its received signal to both the source nodes. For simplicity, we assume that both of the nodes are equipped with a single antenna. The channels between nodes are h_1, h_2, h_3, and h_4, and they are assumed to be flat fading modeled by independent complex Gaussian random variable with zero mean and variance σ_{h}^2. In the training phase, both sources transmit training sequences $\boldsymbol{x}_{1\mathrm{t}}$ and $\boldsymbol{x}_{2\mathrm{t}}$ to the relay at the first time slot. The received signal at the relay is

$$\boldsymbol{y}_{\mathrm{rt}} = \sqrt{P_1} h_1 \boldsymbol{x}_{1\mathrm{t}} + \sqrt{P_2} h_2 \boldsymbol{x}_{2\mathrm{t}} + \boldsymbol{n}_{\mathrm{rt}}, \tag{2.1}$$

where P_1 and P_2 are transmit powers of Source 1 and 2 respectively, and $\boldsymbol{n}_{\mathrm{rt}}$ is a noise vector composed of independent samples from a complex Gaussian distribution with zero mean and variance σ_{v}^2. The relay scales the superimposed signal $\boldsymbol{y}_{\mathrm{rt}}$ by a power scaling factor α such that

$$\alpha = \sqrt{\frac{P_r}{P_1\sigma_{\mathrm{h}}^2 + P_2\sigma_{\mathrm{h}}^2 + \sigma_{\mathrm{v}}^2}}, \tag{2.2}$$

where P_{r} is the maximum relay transmit power. Then the relay broadcasts the superimposed training signal at the second time slot. The received training signal at Source 1 can be expressed as

$$\boldsymbol{y}_{1\mathrm{t}} = \alpha\sqrt{P_1} h_3 h_1 \boldsymbol{x}_{1\mathrm{t}} + \alpha\sqrt{P_2} h_3 h_2 \boldsymbol{x}_{2\mathrm{t}} + \alpha h_3 \boldsymbol{n}_{\mathrm{rt}} + \boldsymbol{n}_{1\mathrm{t}}, \tag{2.3}$$

where noise vector $\boldsymbol{n}_{1\mathrm{t}}$ is defined in the same way as $\boldsymbol{n}_{\mathrm{rt}}$. We define the cascaded channels as $p := \alpha h_3 h_1$, $q := \alpha h_3 h_2$. Therefore, we can rewrite (2.3) as

$$\boldsymbol{y}_{1\mathrm{t}} = [\boldsymbol{x}_{1\mathrm{t}}\ \boldsymbol{x}_{2\mathrm{t}}][p\ q]^T + \alpha h_3 \boldsymbol{n}_{\mathrm{rt}} + \boldsymbol{n}_{1\mathrm{t}}. \tag{2.4}$$

A least square (LS) estimator of the cascaded channels for Source 1 is given by

$$[\hat{p}\ \hat{q}]^T = \left(\boldsymbol{X}_{\mathrm{t}}^H \boldsymbol{X}_{\mathrm{t}}\right)^{-1} \boldsymbol{X}_{\mathrm{t}}^H \boldsymbol{y}_{1\mathrm{t}}, \tag{2.5}$$

where $\boldsymbol{X}_{\mathrm{t}} = [\boldsymbol{x}_{1\mathrm{t}}\ \boldsymbol{x}_{2\mathrm{t}}]$. Because of the symmetry of the TWR, the cascaded channels for Source 2 can be estimated in the same way.

Now we can see that if either the relaying protocol is not modified or other side information (e.g., Gaussian-Kronecker model) is assumed, the sources are only able to estimate the cascaded channels. Individual channels cannot be recovered. Even the channels between the sources and the relay have reciprocal property, i.e., $h_3 = h_1$ and $h_2 = h_4$, there is still a sign ambiguity of recovering h_1 since $p = \alpha h_1^2$. Note that having the CSI of the cascaded channels is enough to detect the messages from the other node. Considering the data phase with the same relaying protocol, the received signal of Source 1 is as follows:

$$\boldsymbol{y}_{1\mathrm{d}} = [\boldsymbol{x}_{1\mathrm{d}}\ \boldsymbol{x}_{2\mathrm{d}}][p\ q]^T + \alpha h_3 \boldsymbol{n}_{\mathrm{rd}} + \boldsymbol{n}_{1\mathrm{d}}, \tag{2.6}$$

where $\boldsymbol{x}_{1\mathrm{d}}$ and $\boldsymbol{x}_{2\mathrm{d}}$ are the messages from the sources and $\boldsymbol{n}_{\mathrm{rd}}$ and $\boldsymbol{n}_{1\mathrm{d}}$ are the noise vectors. Assume p and q are known from the training phase. To detect $\boldsymbol{x}_{2\mathrm{d}}$, Source 1 first subtracts its own signal $\boldsymbol{x}_{1\mathrm{d}}$ (which is known) from the superimposed received signal $\boldsymbol{y}_{1\mathrm{d}}$, then it can detect $\boldsymbol{x}_{2\mathrm{d}}$ normally. Note that the subtraction in the detection is also named self-interference cancellation in the half-duplex TWR literature. To distinguish it from the SIC in FD, this subtraction will be referred to as self-signal removing in this thesis.

Despite the CSI of the cascaded channels is enough for detection, it is worth to estimate the individual channels which are useful in the optimization problems in TWR, e.g., beamforming, relay selection, etc. Approaches to estimate the individual channels can be roughly classified into two categories: designing training schemes to use separate training signals for each individual channel [61–63], and extracting the individual channels by exploiting special structures of the training signal which contains the cascaded channel [64, 65]. In [61], the authors use two non-overlapped subsets of OFDM pilots to transmit training sequences for the two individual channels separately. A training protocol where the relay transmits its own training sequence to estimate the individual channel is used in [62]. The authors in [63] propose a two-stage training protocol to estimate each individual channel in different stages. In contrast to using separate training signals, the authors in [64] assume the Gaussian-Kronecker MIMO channel model and make use of its properties to extract the individual channels from the superimposed training signal. The authors in [65] leverage an algorithm for higher dimension arrays or tensors analysis which generalizes the concept of low-rank decomposition [66, 67] to estimate individual channels.

Other works for channel estimation in half-duplex TWR include optimal training sequence design [63, 68, 69], training schemes in OFDM based TWRs [61, 62, 70–72], and channel estimation for MIMO TWRs [64, 73–75]. All these works focus on designing training schemes compatible with the relaying protocol to take full advantage of the spectrally efficient TWR system, and inspire the training scheme design in FD TWRs.

2.2.2 Channel Estimation in Full-Duplex Relays

Several works propose FD relays and analyze the system performance in the presence of RSI with different criteria, e.g., interference power, outage probability, and

BER [22, 43, 52, 76]. Some of the works assume perfect CSI [22, 52] while others assume imperfect CSI [76], but they do not mention training schemes for FD systems. Though the impact of channel estimation error is studied [32, 77], specific training schemes for FD are not investigated. One may ask why the training schemes for half-duplex relays are not suitable. The reasons are three-fold. First, half-duplex training schemes lose the spectral efficiency provided by FD relaying protocol. The training overhead for half-duplex would be at least twice as that for FD. Second, the relay system has to have the luxury of changing duplex mode between training phase and data phase, which requires more complexity in both hardware and protocols. Last but not least, the estimation needs to include the RSI channel which the half-duplex methods cannot deal with. The CSI of the RSI channel is used to further suppress the SI [54, 78]. There are few works considering the estimation of the RSI channel. Reference [79] proposes two methods for the RSI channel in an AF FD relay system where the destination is equipped with massive MIMO. In the first method the authors consider the case where the RSI channel is estimated by the relay itself, and in the second method the base station estimates the RSI channel. However, in their system model, the RSI is incorporated into the noise term and the ISI caused by the RSI is treated as noise. Consequently, methods in [79] cannot obtain the CSI of RSI for further suppression. In [53], an ML estimator for the RSI channel is investigated and the Cramer-Rao bounds (CRBs) is derived without performance analysis and optimal training design. The time-varying channel estimation in FD is investigated in [80]. The blank of specific training schemes and analysis for FD relays motivates my work in this thesis in which we propose training schemes for FD one-way and two-way relays and analyze the CRB to design the optimal training sequences.

2.3 Residual Self-Interference

2.3.1 Self-Interference Cancellation

Self-interference cancellation is an enabler for FD relay networks. Thus, many recent studies are conducted to approach the issue of SIC from diverse aspects, including propagation domain, analog-circuit domain and digital domain approaches [19]. In propagation domain, physical isolation and directional antennas are used, mainly to block the line-of-sight (LoS) component of SI. For analog-circuit domain approaches, the idea is that the relay estimates the SI channel and subtracts its transmit signal in analog [81, 82]. The estimation error in this process will result in RSI. One natural question is why the subtraction is done in analog or why the relay cannot simply cancel the SIC using digital signal processing to subtract its transmit signal. The main answer is the limited dynamic range of analog-to-digital converters (ADCs). Due to the huge difference in power between the SI and the desired signal, they cannot simultaneously fall into the ADC dynamic range, which makes the simple digital subtraction impossible. Therefore, analog cancellation should reduce the SI for a certain amount to guarantee the desired signal falls into the ADC dynamic range. After the analog cancellation, digital approaches are applied. In these approaches, multiple antennas for transmitting and receiving are adopted at the relay to exploit the potential of extra degrees of freedom for interference cancellation [30, 78, 83]. For more details on SIC approaches, I refer readers to the following references [18, 19]. The combination of these approaches can provide a high attenuation of the SI power. However, the RSI is still quite high compared to the desired received signal, and does not yield good performance when treated as noise. References [19], [35], and [76] report that the power of RSI is about 30 dB higher than the noise floor.

2.3.2 Residual Self-Interference Channel Modeling

The existence of RSI has also been addressed in the literature [19,30,35,52,76,79]. One reason for the presence of RSI is due to the limitation of analog cancellation which suffers from estimation error in the pre-stage [79]. In FD relay systems, there is a pre-stage before the transmission of training and data phases to gather the CSI for the SIC process in later transmission. In the pre-stage, the relay estimates the SI channel and uses the estimates to cancel the self-interference in RF before ADC [81]. The pre-stage estimation error is caused by noise, and time variation of the SI channel. The SI channel consists of an LoS part and a multi-path path part due to scattering from nearby obstacles [35,79]. The LoS part almost remains the same for a relatively long interval and dominates the SI. Thus, using the pre-stage estimates to cancel the SI significantly reduces the power of it. However, the multi-path part changes more often and the estimates are not accurate for it over time. This part can also be seen as an estimation error which results in RSI. The second reason for RSI can be seen from the digital domain when using multiple antennas for both transmitting and receiving at the relay. Reference [30] investigates how to design pre-coding matrices to mitigate the SI and all the degrees of freedom (DoF) offered by antennas are used for the purpose of interference cancellation. However, when multiple antennas are used, beamforming for maximizing the transmission rate can also be considered. Reference [78] jointly designs pre-coding matrices minimizing the self-interference while maximizing the rate. Since part of the DoF is used for improving the rate, the effort of mitigating the self-interference is not as good as the one which uses all the DoF, which also results in RSI. Therefore, there is a trade-off between maximizing the rate and suppressing the self-interference.

An accurate and effective channel model for RSI which captures the features (e.g., the multi-path part of SI, transceiver distortion) in propagation domain and analog-circuit domain is crucial for channel estimation and performance analysis. Since the LoS component of the SI varies very slowly, it can be much reduced by the RF cancellation, which means the multi-path component dominates the RSI in the transmission stage [79, 84]. Under the assumption that the LoS component is largely reduced and the bulk of the interference is from the scattering multi-path components, the RSI channel h_{rr} can be modeled as a complex Gaussian random variable with zero mean and variance σ_{rr}^2 [84]. Moreover, the RSI channel is also assumed to be frequency-flat fading and time-invariant within transmission blocks. The Gaussian model is also used by [78] and [79] for mathematical tractability. In this thesis, we assume that h_{rr} is time-invariant and flat fading in one transmission block and varies from block to block. The Gaussian assumption is used in the simulations to generate realizations of the channels for multiple blocks but not in the derivation of our training scheme and analysis. Different channel models such as Rician model for the self-interference channel before active cancellation [35] can also be adopted. In addition, the signal distortion caused by hardware impediments like the limited dynamic-range of non-ideal amplifiers, oscillators, ADCs, and DACs is considered [31, 33, 85–87] when modeling the RSI channel. However, with sufficient passive self-interference suppression and analog cancellation in RF, the distortion can be ignored [35], which leads to the Gaussian model for the RSI channel mentioned above. The Gaussian model still works when the distortion has to be considered. That is because the distortion is well modeled as additive Gaussian noise terms which can be incorporated into the system noise variance [85].

Chapter 3

CHANNEL ESTIMATION IN HALF-DUPLEX TWO-WAY RELAYS

In this chapter, we investigate the trade-off between high quality estimates and spectrum efficiency in half-duplex TWR through energy allocation. As more power and symbols devoted into training phase, the channel estimates get higher quality, which results in better SNR and an increase in achievable rate. However, the increase in SNR might not compensate the rate loss due to low ratio of data symbols to total symbols. We propose the optimal energy allocation between training phase and data phase in a MIMO TWR system to show how much training and power are needed.

3.1 Channel Estimation in MIMO Two-Way Relays

3.1.1 System Model

We consider a half-duplex TWR with two source nodes and one relay node, as shown in Figure 3.1. The relay uses Amplify-and-Forward (AF) scheme. The protocol of relaying is the two time slots protocol where in the first time slot, Source 1 and Source 2 transmit data to the relay simultaneously; in the second time slot, the relay amplifies and broadcasts its the received signal to both the source nodes. Both sources have M antennas and the relay node has N antennas. We consider the possibility of different number of source antennas M_1 and M_2 later in the sequel. The channels are assumed to be quasi-static flat fading, where they remain constant over $2T$ discrete symbols. The channels from Source 1 to the relay and from Source 2 to relay are denoted by $M \times N$ matrices $\boldsymbol{H}_1$ and $\boldsymbol{H}_2$, respectively. We also assume channel reciprocity holds, i.e., the channels from the relay to Source 1 and the relay to Source

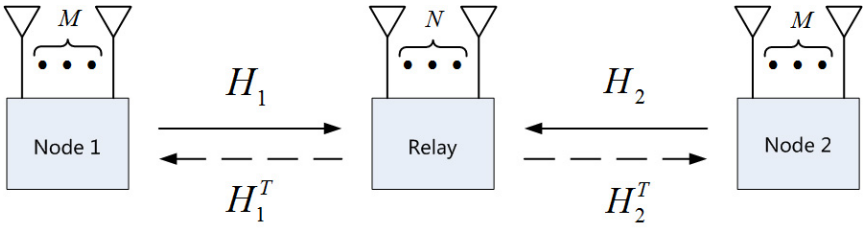

Figure 3.1: System model of the MIMO TWR - both sources have M antennas and the relay node has N antenna in the symmetric case while the two sources have M_1 and M_2 antennas in the asymmetric case.

2 are $\boldsymbol{H}_1^T$ and $\boldsymbol{H}_2^T$ respectively. Both $\boldsymbol{H}_1$ and $\boldsymbol{H}_2$ have zero-mean unit-variance independent complex-Gaussian entries.

The data transmission protocol has two time slots as well. In the first time slot, Source 1 and Source 2 send $T \times M$ matrices simultaneously. The relay scales the superimposed signal by a $N \times N$ diagonal matrix $\boldsymbol{A} = \alpha \boldsymbol{I}$ before broadcasting it in the second time slot. The scale factor α can be chosen as

$$\alpha = \sqrt{\frac{\rho_{\mathrm{R}}}{(\rho_1 + \rho_2 + 1)N}}, \tag{3.1}$$

which satisfies the power constraint ρ_R at the relay.

Because the symmetry of the two source nodes, we can only focus on Source 1. It receives

$$\begin{aligned} \boldsymbol{Y}_1 &= \sqrt{\frac{\rho}{M}} \boldsymbol{S}_1 \boldsymbol{H}_1 \boldsymbol{A} \boldsymbol{H}_1^T + \sqrt{\frac{\rho}{M}} \boldsymbol{S}_2 \boldsymbol{H}_2 \boldsymbol{A} \boldsymbol{H}_1^T + \boldsymbol{Z}_{\mathrm{R}} \boldsymbol{A} \boldsymbol{H}_1^T + \boldsymbol{Z}_1 \\ &= \alpha \sqrt{\frac{\rho}{M}} \boldsymbol{S}_1 \boldsymbol{P} + \alpha \sqrt{\frac{\rho}{M}} \boldsymbol{S}_2 \boldsymbol{Q} + \alpha \boldsymbol{Z}_{\mathrm{R}} \boldsymbol{H}_1^T + \boldsymbol{Z}_1, \end{aligned} \tag{3.2}$$

where we define the cascaded channel matrices to be estimated as $\boldsymbol{P} := \boldsymbol{H}_1 \boldsymbol{H}_1^T$ and $\boldsymbol{Q} := \boldsymbol{H}_2 \boldsymbol{H}_1^T$ for Source 1. Note that while $(\boldsymbol{H}_1, \boldsymbol{H}_2) \rightarrow (\boldsymbol{P}, \boldsymbol{Q})$ is a lossy transformation, $(\boldsymbol{P}, \boldsymbol{Q})$ is sufficient for detection of data from Source 1. The entries of the noise matrices $\boldsymbol{Z}_{\mathrm{R}}$ and $\boldsymbol{Z}_1$ are independent, additive, white, and Gaussian (AWGN) with zero mean and unit variance.

To first review data detection with perfect CSI, if $\boldsymbol{P}$ is known perfectly, Source 1 can cancel out the first term in (3.2) since it knows its own message $\boldsymbol{S}_1$, which is the self-signal removing process. The remaining signal of $\boldsymbol{Y}_1$ after the process, denoted by $\tilde{\boldsymbol{Y}}_1$, is

$$\tilde{\boldsymbol{Y}}_1 = \alpha\sqrt{\frac{\rho}{M}}\boldsymbol{S}_2\boldsymbol{Q} + \alpha\boldsymbol{Z}_{\mathrm{R}}\boldsymbol{H}_1^T + \boldsymbol{Z}_1. \tag{3.3}$$

Then, Source 1 estimates $\boldsymbol{S}_2$ based on $\boldsymbol{Q}$. So in this case, we do not need to know the exact values of $\boldsymbol{H}_1$ and $\boldsymbol{H}_2$ separately, but only need $\boldsymbol{P}$ and $\boldsymbol{Q}$, which are to be estimated at Source 1.

3.1.2 Optimal Training Sequences

We first look at the procedure of Source 1. The procedure of Source 2 is similar and we will discuss it in Section 3.2.2 for the asymmetric case of sources power and number of antennas. The training scheme is composed of the following two phases and each of the phases has two equal length time slots.

1. **Training phase:** In this phase, both sources transmit training symbols to the relay over T_τ symbol intervals at the first time slot, then the relay broadcast the superimposed training signal at the second time slot. The received training signal at Source 1 and the power constraints for the training symbols are

$$\boldsymbol{Y}_{1\tau} = \alpha_\tau\sqrt{\frac{\rho_\tau}{M}}\boldsymbol{S}_{1\tau}\boldsymbol{P} + \alpha_\tau\sqrt{\frac{\rho_\tau}{M}}\boldsymbol{S}_{2\tau}\boldsymbol{Q} + \alpha_\tau\boldsymbol{Z}_{\mathrm{R}\tau}\boldsymbol{H}_1^T + \boldsymbol{Z}_{1\tau}, \tag{3.4}$$

$$\mathrm{tr}(\boldsymbol{S}_{1\tau}\boldsymbol{S}_{1\tau}^H) = MT_\tau,\ \mathrm{tr}(\boldsymbol{S}_{2\tau}\boldsymbol{S}_{2\tau}^H) = MT_\tau,$$

where $\boldsymbol{S}_{i\tau},\ i = 1, 2$ are $T_\tau \times M$ matrices of training symbols sent by Source 1 and Source 2 respectively , ρ_τ is the transmit power of all nodes during the training phase, α_τ is the power scaling factor at the relay in the training phase

and we define the matrices to be estimated as $\boldsymbol{P} := \boldsymbol{H}_1\boldsymbol{H}_1^T$ and $\boldsymbol{Q} := \boldsymbol{H}_2\boldsymbol{H}_1^T$ for Source 1.

2. **Data phase:** In this phase, the length of time slots is T_d. The transmission is the same as the training phase. The received data signal at Source 1 and the power constraints are

$$\boldsymbol{Y}_{1d} = \alpha_d\sqrt{\frac{\rho_d}{M}}\boldsymbol{S}_{1d}\boldsymbol{P} + \alpha_d\sqrt{\frac{\rho_d}{M}}\boldsymbol{S}_{2d}\boldsymbol{Q} + \alpha_d\boldsymbol{Z}_{\mathrm{R}}\boldsymbol{H}_1^T + \boldsymbol{Z}_1, \tag{3.5}$$

$$\mathrm{E}\left[\mathrm{tr}(\boldsymbol{S}_{1d}\boldsymbol{S}_{1d}^H)\right] = MT_d,\ \mathrm{E}\left[\mathrm{tr}(\boldsymbol{S}_{2d}\boldsymbol{S}_{2d}^H)\right] = MT_d,$$

where $\boldsymbol{S}_{id},\ i = 1, 2$, are $T_d \times M$ matrices of data symbols, $T_\tau + T_d = T$, ρ_d is the transmit power during the data phase of all nodes, α_d is the power scaling factor at the relay and $\boldsymbol{Y}_{1d}$ is $T_d \times M$.

To define the MSE, we consider the received signal at the data stage in the presence of channel estimation error. Let $(\hat{\boldsymbol{P}}, \hat{\boldsymbol{Q}})$ be the estimate of $(\boldsymbol{P}, \boldsymbol{Q})$ and $\tilde{\boldsymbol{P}}$ and $\tilde{\boldsymbol{Q}}$ are the residual error of $\boldsymbol{P}$ and $\boldsymbol{Q}$ respectively where $\boldsymbol{P} = \hat{\boldsymbol{P}} + \tilde{\boldsymbol{P}}$, $\boldsymbol{Q} = \hat{\boldsymbol{Q}} + \tilde{\boldsymbol{Q}}$.

Now we write the total MSE of $\boldsymbol{P}$ and $\boldsymbol{Q}$ defined through the Frobenius norm as follows:

$$J = \mathrm{E}\left[\|\tilde{\boldsymbol{Q}}\|_F^2\right] + \mathrm{E}\left[\|\tilde{\boldsymbol{P}}\|_F^2\right] \tag{3.6}$$

$$= \mathrm{E}\left[\|\boldsymbol{Q} - \boldsymbol{V}\boldsymbol{Y}_{1\tau}\|_F^2\right] + \mathrm{E}\left[\|\boldsymbol{P} - \boldsymbol{U}\boldsymbol{Y}_{1\tau}\|_F^2\right], \tag{3.7}$$

where $\boldsymbol{V}$ and $\boldsymbol{U}$ represent the linear transformation of the received signal to estimate $\boldsymbol{Q}$ and $\boldsymbol{P}$.

We can obtain the minimum mean square error (MMSE) estimator $\hat{\boldsymbol{P}}$ through the optimal $\boldsymbol{U}$ which can be found from $\partial J/\partial \boldsymbol{U} = 0$ and is given by

$$\boldsymbol{U}^* = \frac{1}{\alpha_\tau}\sqrt{\frac{M}{\rho_\tau}}\boldsymbol{S}_{1\tau}^H\left(\frac{M}{\rho_\tau}\frac{M\alpha_\tau^2 + 1}{\alpha_\tau^2(M+1)}I_{T_\tau} + \boldsymbol{S}_{1\tau}\boldsymbol{S}_{1\tau}^H + \frac{M}{M+1}\boldsymbol{S}_{2\tau}\boldsymbol{S}_{2\tau}^H\right)^{-1}. \tag{3.8}$$

Similarly, for $\boldsymbol{V}^*$ we have:

$$\boldsymbol{V}^* = \frac{1}{\alpha_\tau}\sqrt{\frac{M}{\rho_\tau}}\boldsymbol{S}_{2\tau}^H\left(\frac{M\alpha_\tau^2+1}{\rho_\tau\alpha_\tau^2}I_{T_\tau} + \boldsymbol{S}_{2\tau}\boldsymbol{S}_{2\tau}^H + \frac{M+1}{M}\boldsymbol{S}_{1\tau}\boldsymbol{S}_{1\tau}^H\right)^{-1}. \tag{3.9}$$

We now discuss how the structure of the training sequences affects the MMSE. After substituting the optimal $\boldsymbol{U}$ and $\boldsymbol{V}$ into (3.7), the variables in (3.7) are $\boldsymbol{S}_{1\tau}$ and $\boldsymbol{S}_{2\tau}$. The training design problem becomes minimizing the MMSE with respect to $\boldsymbol{S}_{1\tau}$ and $\boldsymbol{S}_{2\tau}$:

$$\begin{aligned} &\min_{\boldsymbol{S}_{1\tau},\boldsymbol{S}_{2\tau}} \mathrm{E}\left[\|\tilde{\boldsymbol{Q}}\|_F^2\right] + \mathrm{E}\left[\|\tilde{\boldsymbol{P}}\|_F^2\right], \\ &\text{s.t.} \quad \mathrm{tr}(\boldsymbol{S}_{1\tau}\boldsymbol{S}_{1\tau}^H) = MT_\tau, \\ &\qquad\quad \mathrm{tr}(\boldsymbol{S}_{2\tau}\boldsymbol{S}_{2\tau}^H) = MT_\tau. \end{aligned} \tag{3.10}$$

The following properties of $\boldsymbol{P}$ and $\boldsymbol{Q}$ are used. The second order moment of $\boldsymbol{P}$ and $\boldsymbol{Q}$ required below can be computed from the fourth order moments of the channel matrix which can be obtained since the channel and the noise are assumed to be Gaussian random variables with zero mean and unit variance:

$$\begin{aligned} &\mathrm{E}[\boldsymbol{P}\boldsymbol{P}^H] = (M+1)N\boldsymbol{I}_M, \quad \mathrm{E}[\boldsymbol{Q}\boldsymbol{Q}^H] = MN\boldsymbol{I}_M, \\ &\mathrm{E}[\boldsymbol{P}\boldsymbol{Q}^H] = \boldsymbol{0}, \qquad \mathrm{E}[\boldsymbol{P}\boldsymbol{H}_1^H] = \boldsymbol{0}, \\ &\mathrm{E}[\boldsymbol{P}] = \mathrm{E}[\boldsymbol{Q}] = \boldsymbol{0}, \qquad \mathrm{E}[\boldsymbol{Q}\boldsymbol{H}_1^H] = \boldsymbol{0}. \end{aligned} \tag{3.11}$$

We first calculate $\boldsymbol{R}_{\tilde{\boldsymbol{P}}} = \mathrm{E}[\tilde{\boldsymbol{P}}\tilde{\boldsymbol{P}}^H]$ using the above properties:

$$\begin{aligned} \mathrm{E}[\tilde{\boldsymbol{P}}\tilde{\boldsymbol{P}}^H] &= \mathrm{E}[(\boldsymbol{P} - \boldsymbol{U}\boldsymbol{Y}_{1\tau})(\boldsymbol{P}^H - \boldsymbol{Y}_{1\tau}^H\boldsymbol{U}^H)] \\ &= (M+1)N\left[\boldsymbol{I}_M - \alpha_\tau^2(M+1)N\frac{\rho_\tau}{M}\boldsymbol{S}_{1\tau}^H\boldsymbol{R}_{Y_{1\tau}}^{-1}\boldsymbol{S}_{1\tau}\right], \end{aligned} \tag{3.12}$$

where

$$\begin{aligned} \boldsymbol{R}_{Y_{1\tau}} &= \mathrm{E}[\boldsymbol{Y}_{1\tau}\boldsymbol{Y}_{1\tau}^H] \\ &= \alpha_\tau^2 N\frac{\rho_\tau}{M}(M+1)\boldsymbol{S}_{1\tau}\boldsymbol{S}_{1\tau}^H + \alpha_\tau^2 N\frac{\rho_\tau}{M}M\boldsymbol{S}_{2\tau}\boldsymbol{S}_{2\tau}^H + (\alpha_\tau^2 M+1)N\boldsymbol{I}_{T_\tau}. \end{aligned} \tag{3.13}$$

Similarly,

$$\boldsymbol{R}_{\tilde{\boldsymbol{Q}}} = \mathrm{E}[\tilde{\boldsymbol{Q}}\tilde{\boldsymbol{Q}}^H] = MN\left[\boldsymbol{I}_M - \alpha_\tau^2 N\rho_\tau \boldsymbol{S}_{2\tau}^H \boldsymbol{R}_{Y_{1\tau}}^{-1}\boldsymbol{S}_{2\tau}\right] \quad . \tag{3.14}$$

We have $\mathrm{E}\left[\|\tilde{\boldsymbol{P}}\|_F^2\right] = \mathrm{tr}(\boldsymbol{R}_{\tilde{\boldsymbol{P}}})$ and $\mathrm{E}\left[\|\tilde{\boldsymbol{Q}}\|_F^2\right] = \mathrm{tr}(\boldsymbol{R}_{\tilde{\boldsymbol{Q}}})$. Thus, the objective function in (3.10) becomes

$$\begin{aligned}
&\mathrm{tr}(\boldsymbol{R}_{\tilde{\boldsymbol{P}}}) + \mathrm{tr}(\boldsymbol{R}_{\tilde{\boldsymbol{Q}}}) \\
&= \mathrm{tr}\left((M+1)N\left[\boldsymbol{I}_M - \alpha_\tau^2(M+1)N\frac{\rho_\tau}{M}\boldsymbol{S}_{1\tau}^H\boldsymbol{R}_{Y_{1\tau}}^{-1}\boldsymbol{S}_{1\tau}\right]\right) \\
&\quad + \mathrm{tr}\left(MN\left[\boldsymbol{I}_M - \alpha_\tau^2 N\rho_\tau\boldsymbol{S}_{2\tau}^H\boldsymbol{R}_{Y_{1\tau}}^{-1}\boldsymbol{S}_{2\tau}\right]\right) \\
&= MN\mathrm{tr}\left(\left[\boldsymbol{I}_M - \alpha_\tau^2(M+1)N\frac{\rho_\tau}{M}\boldsymbol{S}_{1\tau}^H\boldsymbol{R}_{Y_{1\tau}}^{-1}\boldsymbol{S}_{1\tau}\right]\right) \\
&\quad + MN\mathrm{tr}\left(\left[\boldsymbol{I}_M - \alpha_\tau^2 N\rho_\tau\boldsymbol{S}_{2\tau}^H\boldsymbol{R}_{Y_{1\tau}}^{-1}\boldsymbol{S}_{2\tau}\right]\right) \\
&\quad + N\mathrm{tr}\left(\boldsymbol{I}_M - \alpha_\tau^2(M+1)\frac{\rho_\tau}{M}\boldsymbol{S}_{1\tau}^H\boldsymbol{R}_{Y_{1\tau}}^{-1}\boldsymbol{S}_{1\tau}\right).
\end{aligned} \tag{3.15}$$

We now want to show that the solution of (3.10) satisfies

$$\begin{aligned}
&\boldsymbol{S}_{1\tau}^H\boldsymbol{S}_{1\tau} = T_\tau\boldsymbol{I}_M, \quad \boldsymbol{S}_{2\tau}^H\boldsymbol{S}_{2\tau} = T_\tau\boldsymbol{I}_M, \\
&\boldsymbol{S}_{1\tau}^H\boldsymbol{S}_{2\tau} = \boldsymbol{0},
\end{aligned} \tag{3.16}$$

and we can see the different number of antennas and different transmit power in each source node do not affect the minimization of MSE through the proof.

Assuming $M \gg 1$, then the second term of (3.15) is negligible. Define $\boldsymbol{S}_\tau = [\boldsymbol{S}_{1\tau} \;\; \boldsymbol{S}_{2\tau}]$, the eigenvalues of $\boldsymbol{S}_\tau^H\boldsymbol{S}_\tau$, denoted by λ_k for $k = 1, 2, \ldots, 2M$, are equal to the eigenvalues of $\boldsymbol{S}_{1\tau}^H\boldsymbol{S}_{1\tau}$ and $\boldsymbol{S}_{2\tau}^H\boldsymbol{S}_{2\tau}$, denoted by λ_{1i} and λ_{2j} for $i = 1, 2, \ldots, M$ and $j = 1, 2, \ldots, M$.

$$
\begin{aligned}
&\mathrm{tr}(\boldsymbol{R}_{\tilde{\boldsymbol{P}}}) + \mathrm{tr}(\boldsymbol{R}_{\tilde{\boldsymbol{Q}}}) \\
&\approx MN\mathrm{tr}(\boldsymbol{I}_{2M} - \alpha_\tau^2 N\rho_\tau \boldsymbol{S}_\tau^H \boldsymbol{R}_{Y_{1\tau}}^{-1} \boldsymbol{S}_\tau) \\
&= MN\mathrm{tr}\left(\boldsymbol{I}_{2M} - \sqrt{\frac{\alpha_\tau^2 N\rho_\tau}{\alpha_\tau^2 M+1}}\boldsymbol{S}_\tau^H(\boldsymbol{I}_{T_\tau} + \frac{\alpha_\tau^2 N\rho_\tau}{\alpha_\tau^2 M+1}\boldsymbol{S}_\tau\boldsymbol{S}_\tau^H)^{-1}\sqrt{\frac{\alpha_\tau^2 N\rho_\tau}{\alpha_\tau^2 M+1}}\boldsymbol{S}_\tau\right) \\
&= MN\mathrm{tr}\left((\boldsymbol{I}_{2M} + \frac{\alpha_\tau^2 N\rho_\tau}{\alpha_\tau^2 M+1}\boldsymbol{S}_\tau^H\boldsymbol{S}_\tau)^{-1}\right) \\
&= \sum_{k=1}^{2M} \frac{1}{1+\frac{\alpha_\tau^2 N\rho_\tau}{\alpha_\tau^2 M+1}\lambda_k} \\
&= \sum_{i=1}^{M} \frac{1}{1+\frac{\alpha_\tau^2 N\rho_\tau}{\alpha_\tau^2 M+1}\lambda_{1i}} + \sum_{j=1}^{M} \frac{1}{1+\frac{\alpha_\tau^2 N\rho_\tau}{\alpha_\tau^2 M+1}\lambda_{2j}}.
\end{aligned} \tag{3.17}
$$

Since the traces of $\boldsymbol{S}_{1\tau}^H\boldsymbol{S}_{1\tau}$ and $\boldsymbol{S}_{2\tau}^H\boldsymbol{S}_{2\tau}$ are fixed, the minimization problem is solved by setting all their eigenvalues equally. Thus $\lambda_{1j} = \lambda_{2j} = T_\tau$ for $i, j = 1, 2, \ldots, 2M$. This means the eigenvalues of $\boldsymbol{S}_\tau^H\boldsymbol{S}_\tau$ are all equal and $\boldsymbol{S}_\tau^H\boldsymbol{S}_\tau = T_\tau I_{2M}$. This shows that (3.16) holds.

This solution means the two training matrices, when concatenated, form a unitary matrix. The training matrices can be simply implemented by choosing $\boldsymbol{S}_\tau = \sqrt{T_\tau}\boldsymbol{I}_{2M}$, a scaled identity matrix. However, this choice requires different power levels to transmit zeros and ones. An alternative way to implement the structure is to choose columns for $\boldsymbol{S}_\tau$ from a Hadamard matrix which is composed of $+1$ and -1 and has orthogonal columns [88]. Thus, the optimal structure is satisfied and transmitting zeros is avoided.

The optimal structure also has a symmetry between nodes Source 1 and Source 2. When looking at Source 2, the two matrices to be estimated is $\boldsymbol{P}' = \boldsymbol{H}_2\boldsymbol{H}_2^T$ and $\boldsymbol{Q}' = \boldsymbol{H}_1\boldsymbol{H}_2^T$, corresponding to $\boldsymbol{S}_{2\tau}$ and $\boldsymbol{S}_{1\tau}$ respectively. The MSE of $\boldsymbol{P}'$ and $\boldsymbol{Q}'$ at Source 2 is minimized by the training choice in (3.16). Thus, the optimal training for

one source is optimal for both, rather than improving the performance for one source at the expense of the performance of the other.

3.2 Allocation Between Training and Data Energy

3.2.1 Symmetric Case of Two Sources

In this subsection we discuss how much power and time should be devoted to the training phase to maximize the average SNR of the data phase. We write the SNR of Source 1 as follows.

$$\bar{\gamma}_1 = \frac{\rho_{2d}\mathrm{E}\left[\|\hat{\boldsymbol{Q}}\|_F^2\right]}{\rho_{2d}\mathrm{E}\left[\|\tilde{\boldsymbol{Q}}\|_F^2\right] + \rho_{1d}\mathrm{E}\left[\|\tilde{\boldsymbol{P}}\|_F^2\right] + M^2(N + 1/\alpha_d^2)}. \tag{3.18}$$

With the optimal structures of the two training sequences, $\bar{\gamma}_1$ can be simplified to a function of power and time by calculating the denominator of (3.18). Substituting $\boldsymbol{S}_{1\tau}$ and $\boldsymbol{S}_{2\tau}$ into (3.15), we have

$$\mathrm{E}\left[\|\tilde{\boldsymbol{P}}\|_F^2\right] = \frac{d_3 MN(M+1)}{d_1 T_\tau (M+1) + d_3}, \tag{3.19}$$

where $d_1 = \alpha_\tau^2 \rho_{1\tau}/M$, $d_2 = \alpha_\tau^2 \rho_{2\tau}/M$ and $d_3 = \alpha_\tau^2 M + 1$. The case of $\mathrm{E}\left[\|\tilde{\boldsymbol{Q}}\|_F^2\right]$ is similar, and given by

$$\mathrm{E}\left[\|\tilde{\boldsymbol{Q}}\|_F^2\right] = \frac{d_3 NM^2}{d_2 T_\tau M + d_3}\ . \tag{3.20}$$

The numerator $\mathrm{E}\left[\|\hat{\boldsymbol{Q}}\|_F^2\right]$ is obtained by using the orthogonal principle of MMSE which implies

$$\mathrm{E}\left[\|\hat{\boldsymbol{Q}}\|_F^2\right] = M^2 N - \mathrm{E}\left[\|\tilde{\boldsymbol{Q}}\|_F^2\right] = \frac{d_2 NM^3 T_\tau}{d_2 T_\tau M + d_3}\ . \tag{3.21}$$

Substituting (3.19), (3.20) and (3.21) into (3.18), we can represent $\bar{\gamma}_1$ as a function of the length and power of the training sequence as

$$\bar{\gamma}_1 = \frac{\rho_{2d} d_2 MT_\tau}{\rho_{2d} d_3 + \rho_{1d}\frac{M+1}{M} d_3 \frac{d_2 T_\tau M + d_3}{d_1 T_\tau (M+1) + d_3} + (1 + \frac{1}{\alpha_d^2 N})(d_2 T_\tau M + d_3)}\ . \tag{3.22}$$

Therefore, the achievable rate at Source 1 is given by

$$\begin{aligned} R_1 &= \mathrm{E}\left[\frac{T_d}{T}\log\left(\det\Big(\boldsymbol{I}+\frac{\alpha_d^2\frac{\rho_d}{M}\hat{\boldsymbol{Q}}^H\hat{\boldsymbol{Q}}}{\sigma_{\tilde{N}}^2}\Big)\right)\right] \\ &= \mathrm{E}\left[\frac{T_d}{T}\log\left(\det\Big(\boldsymbol{I}+\frac{\alpha_d^2\rho_d\sigma_{\hat{\boldsymbol{Q}}}^2}{\sigma_{\tilde{N}}^2}\frac{\bar{\boldsymbol{Q}}^H\bar{\boldsymbol{Q}}}{M}\Big)\right)\right] \\ &= \mathrm{E}\left[\frac{T_d}{T}\log\left(\det\Big(\boldsymbol{I}+\bar{\gamma}_1\frac{\bar{\boldsymbol{Q}}^H\bar{\boldsymbol{Q}}}{M}\Big)\right)\right], \end{aligned} \tag{3.23}$$

where $\bar{\boldsymbol{Q}} = \frac{1}{\sigma_{\hat{\boldsymbol{Q}}}}\hat{\boldsymbol{Q}}$ is the normalized channel with $\sigma_{\hat{\boldsymbol{Q}}}^2 = \mathrm{E}\left[\|\hat{\boldsymbol{Q}}\|_F^2\right]/M$, and $\tilde{N}$ is the equivalent noise which involves the residual error of the channel estimates and the additive noise and is given by

$$\tilde{N} = \alpha_d\sqrt{\frac{\rho_d}{M}}\boldsymbol{S}_{2d}\tilde{\boldsymbol{Q}} + \alpha_d\sqrt{\frac{\rho_d}{M}}\boldsymbol{S}_{1d}\tilde{\boldsymbol{P}} + \alpha_d\boldsymbol{Z}_R\boldsymbol{H}_1^T + \boldsymbol{Z}_1. \tag{3.24}$$

Considering the total energy, we have the following relation of power and time:

$$\rho T = \rho_\tau T_\tau + \rho_d T_d. \tag{3.25}$$

Let β be the ratio of data energy to the total energy, so that

$$\begin{aligned} \rho_\tau T_\tau &= (1-\beta)\rho T, \\ \rho_d T_d &= \beta\rho T. \end{aligned} \tag{3.26}$$

The two sources may have different powers, we consider ξ as the ratio of the power of Source 1 to the total power. Thus,

$$\begin{aligned} \rho_{2d} &= \xi\rho_d, & \rho_{1d} &= (1-\xi)\rho_d, \\ \rho_{2\tau} &= \xi\rho_\tau, & \rho_{1\tau} &= (1-\xi)\rho_\tau. \end{aligned} \tag{3.27}$$

First we consider the symmetric case which means $\xi = 0.5$ and $M_1 = M_2 = M$.

Proposition 1: For any fixed pair of T_τ and T_d, the optimal β the maximizes R_1 can be found in closed form. The closed form can be simplified when the number of antennas is large.

Since the power ρ_τ and ρ_d affect R_1 only through the effective SNR $\bar{\gamma}_1$, maximizing R_1 is equivalent to maximizing $\bar{\gamma}_1$. Substituting (3.26) into (3.22), it becomes a function of β, T_τ, T and ρ:

$$\bar{\gamma}_1 = \frac{a_1\beta^3 + b_1\beta^2 + c_1\beta}{a_2\beta^2 + b_2\beta + c_2}, \tag{3.28}$$

where

$$\begin{aligned}
a_1 &= \frac{\alpha_\tau^4 N^2 \rho^3 T^3 (M+1)}{MT_d}, \\
b_1 &= \frac{-2\alpha_\tau^4 N^2 \rho^3 T^3 (M+1)}{MT_d} - \frac{\alpha_\tau N^2 \rho^2 T^2 (\alpha_\tau^2 M + 1)}{T_d}, \\
c_1 &= a_1 + \frac{\alpha_\tau N^2 \rho^2 T^2 (\alpha_\tau^2 M + 1)}{T_d}, \\
a_2 &= \frac{\alpha_\tau^4 N^2 \rho^2 T^2 (M+1)(1 + 1/(\alpha_d^2 N))}{\alpha_\tau^2 M + 1} - \frac{2\alpha_\tau^2 N \rho^2 T^2 (M+1)}{T_d}, \\
b_2 &= \frac{\rho T M (\alpha_\tau^2 M + 1)}{T_d} - \frac{\alpha_\tau^2 N \rho T (2M+1)(1 + 1/(\alpha_d^2 N))}{M} - a_2, \\
c_2 &= \frac{\alpha_\tau^4 N^2 \rho^2 T^2 (M+1)(1 + 1/(\alpha_d^2 N))}{\alpha_\tau^2 M + 1} + \frac{\alpha_\tau^2 N \rho T (2M+1)(1 + 1/(\alpha_d^2 N))}{M} \\
&\quad + (1 + 1/(\alpha_d^2 N))(\alpha_\tau^2 M + 1).
\end{aligned} \tag{3.29}$$

When T and ρ are fixed, the optimal β that maximizes $\bar{\gamma}_1$ can be found by $\partial\bar{\gamma}_1/\partial\beta = 0$, which yields

$$a_1 a_2 \beta^4 + 2a_1 b_2 \beta^3 + (3a_1 c_2 + b_1 b_2 - c_1 a_2)\beta^2 + 2b_1 c_2 \beta + c_1 c_2 = 0. \tag{3.30}$$

Equation (3.30) shows that the exact solution of the optimal β^* is possible and can be obtained by solving the fourth order equation, analytically or numerically. Though equations (3.22) and (3.30) are derived for node Source 1, in the symmetric case which Source 1 and Source 2 have the same number of antennas and power, they also hold at Source 2. Therefore, β^* is optimal for both sources.

If we consider the case $M \gg 1$, the second term of the denominator of (3.22) becomes $\rho_{1d} d_3$. Thus, (3.28) can be simplified as

$$\begin{aligned}\bar{\gamma}_1 &= \frac{\rho_d d_1 M T_\tau}{2\rho_d d_2 + 2(1 + 1/(\alpha_d^2 N))(d_1 T_\tau M + d_2)} \\ &= \left(\frac{\rho T N \alpha_\tau^2}{4 T_d}\right) \frac{-\beta^2 + \beta}{a_3 \beta + b_3},\end{aligned} \tag{3.31}$$

where

$$\begin{aligned}a_3 &= \frac{(\alpha_\tau^2 M + 1) N}{T_d} - \frac{1}{2}\left(\alpha_\tau^2 N + \frac{\alpha_\tau^2}{\alpha_d^2}\right), \\ b_3 &= \left(1 + \frac{1}{\alpha_d^2 N}\right)\left(\frac{\alpha_\tau^2 M + 1}{\rho T} + \frac{1}{2}\alpha_\tau^2\right) N.\end{aligned} \tag{3.32}$$

Taking $\partial \bar{\gamma}_1 / \partial \beta = 0$ again, we have the quadratic equation

$$a_3 \beta^2 + 2 b_3 \beta - b_3 = 0. \tag{3.33}$$

If $a_3 = 0$, which means $\frac{2(\alpha_\tau^2 M + 1) N}{T_d} = \alpha_\tau^2 N + \frac{\alpha_\tau^2}{\alpha_d^2}$, the optimal power allocation ratio is $\beta^* = \frac{1}{2}$. The total energy is split equally.

If $a_3 \neq 0$, β^* is a root of (3.33), the closed form expression is given as follows.

$$\beta^* = \frac{-b_3 + \sqrt{b_3^2 + a_3 b_3}}{a_3}. \tag{3.34}$$

It can be verified that $b_3^2 + a_3 b_3$ is always greater than zero and this root is between 0 and 1. Thus we have the expression of β that maximizes $\bar{\gamma}_1$ for all the cases.

Through the simplification, equation (3.30) reduces to a quadric equation of β. The simplification is used for getting some intuition about the power allocation from the equations of β and making the computation easier. In Section 3.3 we show that even for small M, (3.16) performs very well, so that practically speaking, $M \gg 1$ is not necessary.

In the point-to-point MIMO system, the power allocation problem only depends on the number of transmit antennas. But in two-way relay systems, the relay is both

a transmitter and a receiver so that the number of antennas in the relay should be considered. For simplicity, we assume high SNR in which case we have $\alpha_\tau^2 = \alpha_d^2 \approx \frac{1}{2N}$. Then (3.34) can be simplified to

$$\beta^* = \frac{-\frac{3(M+2N)}{\rho T} - \frac{3}{2} + (M+2N)\sqrt{\left(\frac{1}{T_d} + \frac{3}{2\rho T}\right)\left(\frac{3}{2\rho T} + \frac{3}{2(M+2N)}\right)}}{\frac{M+2N}{T_d} - \frac{3}{2}}. \tag{3.35}$$

For $a_3 \neq 0$, i.e., $T_d \neq \frac{2}{3}(M+2N)$ is satisfied. From (3.35) we can find that when either $M+2N$ is increased with fixed T_d, β^* will decrease. This shows that with increased number of antennas,either at the source or relay, we should put more energy into the training phase. In contrast, when T_d is increased and M and N are fixed, β^* increases with T_d. Thus, in this case we need to put more energy into the data phase. Note that for estimating the channels in TWRs, we need the length of training sequence satisfies $T_\tau \geq 2M$. Thus the maximum length for the length of data is $T_d \leq T - 2M$.

Equation (3.34) can be used for setting $M = N = 1$, which is the signal antenna case in TWRs. When $\xi = 0.5$ for the symmetric powers for both source, our results of the optimal β^* matches the numerical results provided by [89].

Given the optimal β which is a function of T_d, we now discuss how to choose T_τ and T_d.

Proposition 2: Given the optimal β, R_1 is a monotonically increasing function of T_d. The maximum value of T_d is $T - 2M$.

Let λ be an arbitrary non-zero eigenvalue of $\frac{\bar{\boldsymbol{Q}}^H\bar{\boldsymbol{Q}}}{M}$ ($\lambda > 0$), from (3.23) we have

$$R_1 \geq \frac{M}{T}\mathrm{E}\left[T_d \log(1+\lambda\bar{\gamma}_1)\right]. \tag{3.36}$$

Taking the derivative of (3.36) with respect to T_d yields

$$\frac{\partial R_1}{\partial T_d} \geq \frac{M}{T}\mathrm{E}\left[\log(1+\lambda\bar{\gamma}_1) + \frac{T_d}{1+\bar{\gamma}_1}\frac{\partial\bar{\gamma}_1}{\partial T_d}\right]. \tag{3.37}$$

We discuss the case of $a_3 < 0$. The other cases have similar arguments and the same results. The optimal β that maximizes $\bar{\gamma}_1$ can be obtained by

$$\beta^* = \frac{-b_3 + \sqrt{b_3^2 + a_3 b_3}}{a_3}. \tag{3.38}$$

Substituting (3.38) into (3.31), $\bar{\gamma}_1$ can be rewritten as a function of T_d:

$$\begin{aligned}
\bar{\gamma}_1 &= \frac{\rho T N \alpha_\tau^2}{4M} \cdot \frac{1}{T_d} \cdot \frac{-\beta + 1}{a_3\beta + a_3 + 2b_3} \\
&= \frac{\rho T N \alpha_\tau^2}{4M} \cdot \frac{1}{T_d a_3} \cdot \frac{a_3 + b_3 - \sqrt{b_3^2 + a_3 b_3}}{a_3 + b_3 + \sqrt{b_3^2 + a_3 b_3}} \\
&= \frac{\rho T N \alpha_\tau^2}{4M} \cdot \frac{1}{T_d a_3} \cdot \frac{1 + \frac{b_3}{a_3} + \sqrt{\frac{b_3^2}{a_3^2} + \frac{b_3}{a_3}}}{1 + \frac{b_3}{a_3} - \sqrt{\frac{b_3^2}{a_3^2} + \frac{b_3}{a_3}}} \\
&= \frac{\rho T N \alpha_\tau^2}{4M} \frac{-1}{b_4 T_d - a_4} \cdot \frac{1 - \eta + \sqrt{\eta(\eta - 1)}}{1 - \eta - \sqrt{\eta(\eta - 1)}} \\
&= \frac{\rho T N \alpha_\tau^2}{4M} \frac{1}{b_4 T_d - a_4} (\sqrt{\eta} - \sqrt{\eta - 1})^2,
\end{aligned} \tag{3.39}$$

where $\eta = -b_3/a_3$, $a_4 = \alpha_\tau^2 N + 1$, and $b_4 = 1/M$. From (3.32), we know T_d is involved in η and $\eta > 1$. Thus,

$$\frac{d\eta}{dT_d} = \frac{-a_4 b_3}{(b_4 T_d - a_4)^2}. \tag{3.40}$$

Taking the derivative of $\bar{\gamma}_1$, we have

$$\begin{aligned}
\frac{\partial \bar{\gamma}_1}{\partial T_d} &= \frac{\rho T N \alpha_\tau^2}{4M} \left[\frac{-b_4}{(b_4 T_d - a_4)^2} (\sqrt{\eta} - \sqrt{\eta - 1})^2 \right. \\
&\quad \left. + \frac{1}{b_4 T_d - a_4} \cdot \frac{2\sqrt{\eta(\eta - 1)} - \eta - (\eta - 1)}{\sqrt{\eta(\eta - 1)}} \cdot \frac{d\eta}{dT_d} \right] \\
&= \frac{\rho T N \alpha_\tau^2}{4M} \left[\frac{-b_4}{(b_4 T_d - a_4)^2} (\sqrt{\eta} - \sqrt{\eta - 1})^2 + \frac{a_4 b_3}{(b_4 T_d - a_4)^3} \frac{(\sqrt{\eta} - \sqrt{\eta - 1})^2}{\sqrt{\eta(\eta - 1)}} \right] \\
&= \frac{\rho T N \alpha_\tau^2}{4M} \frac{(\sqrt{\eta} - \sqrt{\eta - 1})^2}{(b_4 T_d - a_4)^2} \left[\frac{a_4 \eta}{T_d} \cdot \frac{1}{\sqrt{\eta(\eta - 1)}} - b_4 \right] \\
&= \frac{\bar{\gamma}_1 b_4}{b_4 T_d - a_4} \left(\frac{a_4 \sqrt{\eta}}{b_4 T_d \sqrt{\eta - 1}} - 1 \right).
\end{aligned} \tag{3.41}$$

Let λ be an arbitrary non-zero eigenvalue of $\frac{\bar{\boldsymbol{Q}}^H\bar{\boldsymbol{Q}}}{M}$ ($\lambda > 0$), we have

$$R_1 \geq \frac{M}{T}\mathrm{E}\Big[T_d \log(1+\lambda\bar{\gamma}_1)\Big]. \tag{3.42}$$

Taking the derivative of (3.42) with respect to T_d yields

$$\begin{aligned}
\frac{\partial R_1}{\partial T_d} &\geq \frac{M}{T}\mathrm{E}\left[\log(1+\lambda\bar{\gamma}_1) + \frac{T_d}{1+\bar{\gamma}_1}\frac{\partial\bar{\gamma}_1}{\partial T_d}\right] \\
&= \frac{M}{T}\mathrm{E}\left[\log(1+\lambda\bar{\gamma}_1) - \frac{\lambda\bar{\gamma}_1}{1+\lambda\bar{\gamma}_1}\frac{b_4T_d}{b_4T_d-a_4}\left(1-\frac{a_4\sqrt{\eta}}{b_4T_d\sqrt{\eta-1}}\right)\right] \qquad (3.43)\\
&\geq \frac{M}{T}\mathrm{E}\left[\log(1+\lambda\bar{\gamma}_1) - \frac{\lambda\bar{\gamma}_1}{1+\lambda\bar{\gamma}_1}\right], \qquad (3.44)
\end{aligned}$$

where

$$0 < \frac{b_4T_d}{b_4T_d-a_4}\left(1-\frac{a_4\sqrt{\eta}}{b_4T_d\sqrt{\eta-1}}\right) < 1. \tag{3.45}$$

The left inequality can be shown by substituting all the coefficients into the middle term of (3.45). Note that we discuss the case of $a_3 < 0$. Thus, $b_4T_d - a_4 = -T_da_3 > 0$ and $T_d > 2M$. Then

$$\frac{a_4\sqrt{\eta}}{b_4T_d\sqrt{\eta-1}} = \sqrt{\frac{2M}{T_d}}\cdot\sqrt{\frac{2M+\rho T/3}{T_d+\rho T/3}} < 1. \tag{3.46}$$

To prove the right inequality, one can upper bound the middle term of (3.45) by replacing $\sqrt{\eta-1}$ with $\sqrt{\eta}$:

$$\begin{aligned}
&\frac{b_4T_d}{b_4T_d-a_4}\left(1-\frac{a_4\sqrt{\eta}}{b_4T_d\sqrt{\eta-1}}\right) \\
&< \frac{b_4T_d}{b_4T_d-a_4}\left(1-\frac{a_4\sqrt{\eta}}{b_4T_d\sqrt{\eta}}\right) = \frac{b_4T_d}{b_4T_d-a_4}\left(1-\frac{a_4}{b_4T_d}\right) = 1. \qquad (3.47)
\end{aligned}$$

Therefore, (3.44) holds.

Assuming $x = \lambda\bar{\gamma}_1$, it can be proved that $\log(1+x) - \frac{x}{1+x} \geq 0$ for all $x \geq 0$. Therefore, $\partial R_1/\partial T_d \geq 0$ and R_1 is a monotonically increasing function of T_d. To maximize R_1, T_d should be chosen as its maximum value. Note that to obtain

meaningful estimates of the channels, $T_\tau \geq 2M$ is required in the TWR system to ensure as many measurements as unknowns. Therefore, the choice of $T_\tau = 2M$ and $T_d = T - 2M$ maximizes R_1.

3.2.2 Asymmetric Case of Two Sources

For the asymmetric case, as the sources have different power and number of antennas, the formulas for the effective SNRs at the two sources are different. Let M_1 and M_2 be the number of antennas for Source 1 and Source 2 respectively. In this case, it cannot be guaranteed that the optimal β for one source is still optimal for the other, and there is a trade-off between the two sources. We consider to maximize the smaller one of the two SNRs. The effective SNRs for Source 1 and Source 2 are $\bar{\gamma}_1$ and $\bar{\gamma}_2$ respectively, and are given by

$$\bar{\gamma}_1 = \left(\frac{\rho T N \alpha_\tau^2}{T_d M_2}\right) \frac{\xi^2(-\beta^2+\beta)}{a_{31}\beta + b_{31}}, \tag{3.48}$$

$$\bar{\gamma}_2 = \left(\frac{\rho T N \alpha_\tau^2}{T_d M_1}\right) \frac{(1-\xi)^2(-\beta^2+\beta)}{a_{32}\beta + b_{32}}, \tag{3.49}$$

where

$$\begin{aligned}
a_{31} &= \frac{\alpha_\tau^2 N + 1}{T_d} - \frac{\xi}{M_2}\left(\alpha_\tau^2 N + \frac{\alpha_\tau^2}{\alpha_d^2}\right), \\
b_{31} &= \left(1 + \frac{1}{\alpha_d^2 N}\right)\left(\frac{\alpha_\tau^2 N + 1}{\rho T} + \frac{\xi}{M_2}\alpha_\tau^2 N\right), \\
a_{32} &= \frac{\alpha_\tau^2 N + 1}{T_d} - \frac{1-\xi}{M_1}\left(\alpha_\tau^2 N + \frac{\alpha_\tau^2}{\alpha_d^2}\right), \\
b_{32} &= \left(1 + \frac{1}{\alpha_d^2 N}\right)\left(\frac{\alpha_\tau^2 N + 1}{\rho T} + \frac{1-\xi}{M_1}\alpha_\tau^2 N\right).
\end{aligned} \tag{3.50}$$

The parameter $\xi \in (0,1)$ represents the power imbalance of the two sources, which can be related to the location of the relay and it is assumed fixed. The optimal ratio that maximizes $\bar{\gamma}_i$ is

$$\beta_i^* = \frac{-b_{3i} + \sqrt{b_{3i}^2 + a_{3i} b_{3i}}}{a_{3i}}, \tag{3.51}$$

where $i = 1, 2$. Both of the two SNRs are functions of β. Our optimization problem becomes

$$\beta^* = \arg\max_{\beta} \min\{\bar{\gamma}_1, \bar{\gamma}_2\}. \tag{3.52}$$

Define $f(\beta) = \bar{\gamma}_1 - \bar{\gamma}_2$, we have the following proposition.

Proposition 3: When $M_1 = M_2$, if $\xi > 0.5$, $f(\beta)$ is a concave function of β and $f(\beta) > 0$ for $\beta \in (0, 1)$. Thus $\min\{\bar{\gamma}_1, \bar{\gamma}_2\} = \bar{\gamma}_2$ and $\beta^* = \beta_2^*$. If $\xi < 0.5$, $f(\beta)$ is a convex function of β and $f(\beta) < 0$ for $\beta \in (0, 1)$. Thus $\min\{\bar{\gamma}_1, \bar{\gamma}_2\} = \bar{\gamma}_1$ and $\beta^* = \beta_1^*$.

Proof: We have $a_{31}\beta + b_{31} > 0$ and $a_{32}\beta + b_{32} > 0$ for $\beta \in (0, 1)$ and $a_{31} + b_{31} = a_{32} + b_{32}$. Taking the second order derivative of $f(\beta)$ and after some manipulations, we have

$$f''(\beta) = 2\left(\frac{\rho T N \alpha_\tau^2}{M_1 T_d}\right)(a_{31} + b_{31}) \times \frac{b_{32}(1-\xi)^2(a_{31}\beta + b_{31})^3 - b_{31}\xi^2(a_{32}\beta + b_{32})^3}{(a_{31}\beta + b_{31})^3(a_{32}\beta + b_{32})^3}. \tag{3.53}$$

All the parts in (3.53) are positive except the numerator of the fraction. Substituting (3.50) into the numerator and applying difference of cubes formula on it, its sign is determined by the factor $1 - 2\xi$. When $\xi > 0.5$, which means Source 2 has the larger power, then $f''(\beta)$ is negative and $f(\beta)$ is a concave function for $\beta \in (0, 1)$. Moreover, we have $f(0) = 0$ and $f(1) = 0$. Thus $f(\beta) > 0$ in $(0, 1)$. If $\xi < 0.5$, with the same argument, $f(\beta)$ is a convex function and $f(\beta) < 0$ for $\beta \in (0, 1)$. The optimal β^* can be calculated by (3.51).

3.3 Numerical Results

We choose $T = 256$ and $\rho = 10$ dB in our simulations. In Figure 3.2 we fix $T_d = 192$ and simulate $\bar{\gamma}_1$ with different number of antennas for the symmetric case. We also illustrate the approximation of $\bar{\gamma}_1$ calculated by (3.31) for $(M, N) = (4, 4)$. The results show that the $\bar{\gamma}_1$ through Monte Carlo simulation almost overlaps with

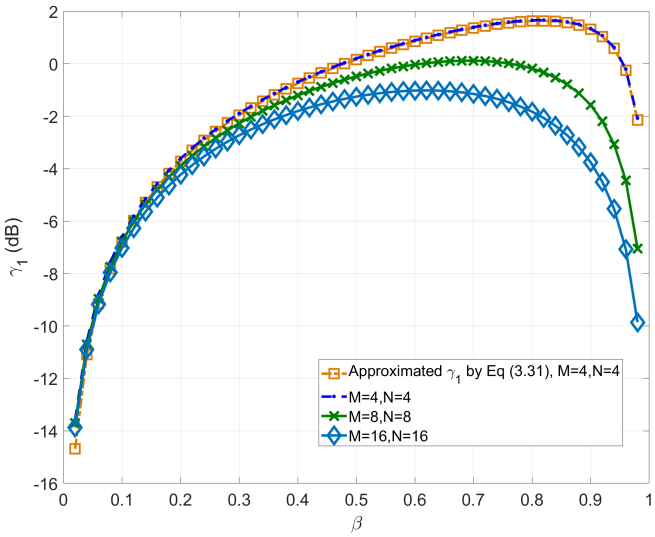

Figure 3.2: Effect of number of antennas on optimal β - when the number of antennas increases, either at the source or at the relay, β^* decreases, which means more energy should be devoted to the training.

the approximation. Figure 3.2 also shows when the number of antennas increases, either at the source or at the relay, β^* decreases as we inferred from (3.35). Thus, more energy should be devoted to the training for large number of antennas.

Figure 3.3 shows the achievable rate as a function of T_d with different choices of β for the symmetric case. We choose $M = N = 8$. When the optimal β is used, the rate is a monotonically increasing function of T_d and reaches its maximum value at $T_d = T - 2M$. We also simulate the rate for fixed $\beta = 0.5$ and for $\beta = T_d/T$ in which case $\rho_\tau = \rho_d$ always holds. The results for these two cases achieve inferior performance compared to the optimal β.

3.4 Conclusion

In this chapter, we propose a power allocation method in the presence of channel estimation in MIMO TWR. We optimize the ratio of training-versus-data for both the symmetric and asymmetric cases. In the symmetric case, with $M_1 = M_2$ and

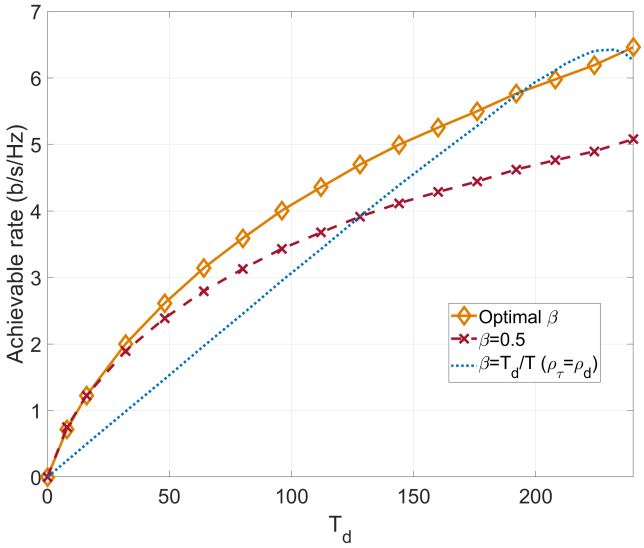

Figure 3.3: Achievable rate as a function of T_d with different choices of β - with the optimal β, the rate is a monotonically increasing function of T_d and reaches its maximum value at $T_d = T - 2M$. The rate for fixed $\beta = 0.5$ and for $\beta = T_d/T$ achieve inferior performance compared to the optimal β.

$\xi = 0.5$, the optimal β can be found by solving a fourth order equation, which is further reduced to a quadratic equation when the number of antennas at the sources grows large. Data time is set to its maximum value $T_d = T - 2M$ since the achievable rate is a monotonically increasing function of T_d. In the asymmetric case, we show that the difference of two average SNRs is a concave or convex function for $\beta \in (0, 1)$, depending on ξ, enabling the maximization of the minimum of $\bar{\gamma}_1$ and $\bar{\gamma}_2$.

Chapter 4

CHANNEL ESTIMATION IN FULL-DUPLEX TWO-WAY RELAYS

In this chapter, we focus on analyzing the channel estimation problem in a TWR system with an FD relay helping to exchange data between two FD capable devices in the presence of RSI. Though the channel estimation can be done by making the training phase working in half-duplex mode, it is more spectrally efficient to estimate the channels in FD mode. Moreover, as mentioned in Section 2.3.2, the RSI still exists after active self-interference cancellation (SIC) at the relay and makes the overall end-to-end channel an inter-symbol-interference (ISI) channel [52, 76]. Therefore, simply treating the RSI as noise does not yield good performance. To improve the performance, the estimation and equalization of the ISI channel parameters are needed. Thus, we estimate the RSI in the destination node to enable cancellation of the interference of the system further, through equalization.

We propose a novel one-block training scheme and two baseline schemes to estimate the RSI channel at both sources in an amplify-and-forward (AF) TWR system. The one-block training scheme uses one transmission block to keep the training phase relaying protocol consistent with the data phase. An ML estimator is derived to estimate the RSI channel as well as the individual channels. A popular quasi-Newton method, the Broyden-Fletcher-Goldfarb-Shanno (BFGS) algorithm [90], is used to numerically solve the ML estimator. Zero-forcing estimation is used for initialization to improve the accuracy and reduce the complexity of the ML estimator.

As a baseline, we also propose a multi-block training scheme in which the traditional least squares (LS) channel estimation method is used. A half-duplex transmission protocol is needed in this training phase to make the received signal linear in the

RSI channel. In addition, the cross-correlation method for estimating the ISI channel is also considered for comparison. The two baseline schemes estimate the same channel parameters as the one-block scheme does. The CRBs for both training schemes are derived respectively to assess the fundamental limits of each training scheme.

4.1 System Model

We consider a system with two sources and a relay in between, with no direct link, as shown in Figure 4.1. The sources and the relay are equipped with two antennas, one serving as a receive antenna while the other one a transmit antenna. The AF scheme is adopted at the relay. To operate this scheme in the FD mode, the relay receives the current symbols while it amplifies and forwards the previously received symbols. The channel coefficients between Source 1 and the relay, and Source 2 and the relay are $h_{1\mathrm{r}}$ and $h_{2\mathrm{r}}$, respectively. The reverse channels between the relay and the two sources are $h_{\mathrm{r}1}$ and $h_{\mathrm{r}2}$. Without loss of generality, we assume the forward and reverse channels between a source and the relay are different (i.e., we do not assume the channels are reciprocal, which also could be handled with some modifications). The four individual channels above are complex Gaussian, independent, with zero means and unit variance. They are also assumed to be time invariant across multiple blocks. The noise at both sources and the relay are assumed to be complex Gaussian with zero mean and variance σ_{v}^2. Perfect synchronization is assumed in our system. The methods for synchronization in half-duplex can be extended to FD [91] and used in conjunction without methods.

In our system model, the relay estimates the SI channel in the pre-stage which is explained in Section 2.3.2 and uses the estimates to cancel the SI in the following transmission. The RSI channel which is due to the pre-stage estimation error can be modeled as a flat fading channel [30, 52]. Let h_{rr}, h_{11}, h_{22} be the RSI channels

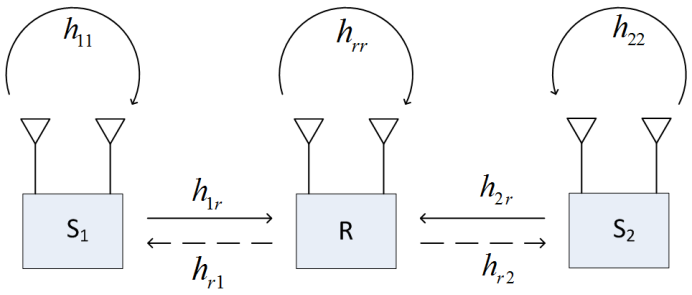

Figure 4.1: Full-duplex two-way relays - the sources and the relay are equipped with two antennas, one serving as a receive antenna while the other one a transmit antenna. The FD relay receives the current symbols while it amplifies and forwards the previously received symbols.

between the two antennas at the relay and source nodes. They are with zero means and variance $\sigma^2_{\text{rr}}, \sigma^2_{11}, \sigma^2_{22}$ respectively which capture the inaccuracy of SIC in the pre-stage. The RSI power, which is related to the transmit power of the relay, is not small enough to be treated as noise, and often higher than the desired signal power. Moreover, it makes the overall end-to-end channel an ISI channel in the AF relay even when the channels on all links are flat fading. The channel state information (CSI) of the RSI channel is needed for equalizers to alleviate the ISI at the receiver.

4.2 One-Block Training Scheme

In this section, we propose the one-block training scheme for FD transmission training and compare it with the multi-block training scheme which is proposed in the following section. The one-block scheme consists of only one transmission block consisting of N symbols during training and the multi-block scheme consists of four blocks that have a total of N symbols. One block in our scheme means one transmission phase that either the source or the relay node transmits its training sequence without changing the transmission protocol. In the one-block scheme, we consider the transmission from Source 1 to Source 2 : Source 1 transmits its training sequence (and the relay forwards) for the whole training. No nodes change their training pro-

tocols and thus this training scheme is considered as one block. In contrast, in the multi-block scheme, in the first block Source 1 transmits its training sequence. Then in the second block Source 1 stops and the relay transmits what it received in the previous block. In the third block the relay transmits its own training data and in the fourth block the relay transmits what it received in the third block. Hence the transmission protocol changes multiple times during training. Each time it changes is a different block during training. The overhead due to training, which is the total training length, is one block length for the one-block scheme and four blocks for the multi-block scheme. In the comparison of the two schemes, we fix the training overhead, which leads to different block lengths for the two schemes. The one-block scheme has N symbols per block, and the multi-block scheme has $N/4$ symbols per block that totals N symbols during training.

4.2.1 The Training Phase

In the training phase, we extend to FD the two time slots relaying protocol for half-duplex in which two sources transmit their signals to the relay simultaneously in the first time slot and the relay broadcasts its received signal in the second time slot. In FD mode, the transmission of the two sources and the broadcast of the relay happens in the same symbol interval. The relay receives the current signal while continuing to transmit its received signal in the previous symbol interval. For the purpose of training, the relay adds its own training sequence to its received signal, scales the processed signal to satisfy the power constraint, then it transmits the scaled signal. The sources also transmit and receive together. At symbol interval n, the relay receives

$$y_{\mathrm{r}}[n] = h_{1\mathrm{r}}x_1[n] + h_{2\mathrm{r}}x_2[n] + h_{\mathrm{rr}}t_{\mathrm{r}}[n] + v_{\mathrm{r}}[n], \tag{4.1}$$

where $x_1[n]$ and $x_2[n]$ are the training sequences sent by Source 1 and Source 2 respectively. Let P_{s} be the transmit power of both sources. Thus, the training sequences satisfy $|x_1[n]|^2 = |x_2[n]|^2 = P_{\mathrm{s}}$. The term $t_{\mathrm{r}}[n]$ is the transmit signal of the relay and thus $h_{\mathrm{rr}}t_{\mathrm{r}}[n]$ is RSI term due to the broadcast of the previous received signal at the relay in the previous time slot. The noise term is $v_{\mathrm{r}}[n] \sim \mathcal{CN}(0, \sigma_v^2)$. The relay adds its own training sequence $x_{\mathrm{r}}[n]$ satisfying $|x_{\mathrm{r}}[n]|^2 = P_{\mathrm{s}}$ and scales the processed signal. Without loss of generality, we assume that there is a one-symbol delay for the relay to forward its received symbols, which is due to the SIC processing. The transmit signal of the relay therefore is

$$t_{\mathrm{r}}[n] = \alpha(y_{\mathrm{r}}[n-1] + x_{\mathrm{r}}[n-1]), \tag{4.2}$$

where α is a power scaling factor used to satisfy the power constraint at the relay. At Source 1, the received symbol at time n is

$$\begin{aligned} y_1[n] &= h_{\mathrm{r1}}t_{\mathrm{r}}[n] + h_{11}x_1[n] + v_1[n] && (4.3)\\ &= \sum_{k=1}^{\infty} \theta^{(k-1)} \left(px_1[n-k] + qx_2[n-k] + dx_{\mathrm{r}}[n-k]\right) \\ &\quad + h_{11}x_1[n] + \sum_{k=1}^{\infty} d\theta^{(k-1)}v_{\mathrm{r}}[n-k] + v_1[n], && (4.4) \end{aligned}$$

where we define $p := \alpha h_{\mathrm{r1}}h_{1\mathrm{r}}$, $q := \alpha h_{\mathrm{r1}}h_{2\mathrm{r}}$, $d := \alpha h_{\mathrm{r1}}$, and $\theta := \alpha h_{\mathrm{rr}}$ for simplicity. The recursive form of (4.4) is obtained by substituting (4.1) and (4.2) in (4.3). Due to the feedback in the SI link θ at the relay, the overall channel in (4.4) is a single pole infinite impulse response (IIR) channel which causes ISI. Moreover, the effective noise is colored with correlations that depend on the pole. The impulse response for $x_1[n]$ is $p[k] := p\theta^{k-1}$, and for $x_2[n]$ is $q[k] = q\theta^{k-1}$, $k = 1, 2, \cdots$.

The power scaling factor α is chosen to keep the system stable and guarantee finite relay transmit power. The relay transmit power is calculated as

$$\mathrm{E}[t_{\mathrm{r}}[n]t_{\mathrm{r}}^{*}[n]] = \alpha^2 \sum_{k=1}^{\infty} (\alpha^2 |h_{\mathrm{rr}}|^2)^{(k-1)} \left(P_{\mathrm{s}} |h_{1\mathrm{r}}|^2 + P_{\mathrm{s}} |h_{2\mathrm{r}}|^2 + P_{\mathrm{s}} + \sigma_{\mathrm{v}}^2 \right) \tag{4.5}$$

$$= \alpha^2 \frac{P_{\mathrm{s}} |h_{1\mathrm{r}}|^2 + P_{\mathrm{s}} |h_{2\mathrm{r}}|^2 + P_{\mathrm{s}}}{1 - \alpha^2 |h_{\mathrm{rr}}|^2}. \tag{4.6}$$

By solving $\mathrm{E}[t_{\mathrm{r}}[n]t_{\mathrm{r}}^{*}[n]] \leq P_{\mathrm{r}}$, α should satisfy $\alpha^2 < 1/|h_{\mathrm{rr}}|^2$ [50]. However, in a channel estimation scenario, the instantaneous CSI is not available. We can choose α to satisfy a long term condition which is $\alpha^2 < 1/\mathrm{E}[|h_{\mathrm{rr}}|^2] = 1/\sigma_{rr}^2$, and σ_{rr}^2 can be obtained at the pre-stage. Therefore, we choose the power scaling factor as

$$\alpha^2 = \frac{P_{\mathrm{r}}}{3P_{\mathrm{s}} + P_{\mathrm{r}}\sigma_{\mathrm{rr}}^2 + \sigma_{\mathrm{v}}^2} \quad . \tag{4.7}$$

where P_{r} is the maximum transmit power of the relay. With this power scaling factor, the average RSI power is $P_{\mathrm{r}}\sigma_{\mathrm{rr}}^2$. We can also setup a fixed, pre-defined gain margin to prevent the instantaneous $|h_{\mathrm{rr}}|$ value from exceeding the constraint.

We define L as the effective length of the overall channel impulse response in where most of the energy, e.g. 99%, is contained [52]. Thus, a block based transmission can be adopted with a guard time of L symbol intervals in which the sources keep silent to avoid inter-block interference. Without loss of generality, we assume the block length N is far greater than L, so the rate loss due to the guard time is negligible. We can now rewrite (4.4) for block transmission. For the mth block, the nth received symbol is

$$\begin{aligned} y_1^{(m)}[n] = \sum_{k=1}^{\infty} \theta^{(k-1)} \Big(& p x_1[(m-1)(N+L) + n - k] + q x_2[(m-1)(N+L) + n - k] \\ & + d x_{\mathrm{r}}[(m-1)(N+L) + n - k] \Big) + h_{11} x_1[(m-1)(N+L) + n] \\ & + \sum_{k=1}^{\infty} d\theta^{(k-1)} v_{\mathrm{r}}[(m-1)(N+L) + n - k] + v_1[(m-1)(N+L) + n], \end{aligned} \tag{4.8}$$

for $n = 0, 1, 2, \cdots, N + L$, and $m = 1, 2, \cdots$, and $x_1[n] = x_2[n] = x_{\mathrm{r}}[n] = 0$ for $n = N + 1, \cdots, N + L$. With the last L symbols of every block being zero, there is no inter-block interference, which allow us to drop the block index henceforth.

To write the output of the system in vector form, we relate the following vectors

$$\begin{aligned}
\boldsymbol{x}_1 &= [x_1[0], \cdots, x_1[N-1]]^T, \\
\boldsymbol{x}_2 &= [x_2[0], \cdots, x_2[N-1]]^T, \\
\boldsymbol{x}_{\mathrm{r}} &= [x_{\mathrm{r}}[0], \cdots, x_{\mathrm{r}}[N-1]]^T, \\
\boldsymbol{y}_1 &= [y_1[1], \cdots, y_1[N]]^T,
\end{aligned}$$

as follows:

$$\boldsymbol{y}_1 = p\boldsymbol{H}_\theta \boldsymbol{x}_1 + q\boldsymbol{H}_\theta \boldsymbol{x}_2 + d\boldsymbol{H}_\theta \boldsymbol{x}_{\mathrm{r}} + d\boldsymbol{H}_\theta \boldsymbol{v}_{\mathrm{r}} + h_{11}\boldsymbol{J}^{\mathrm{u}} \boldsymbol{x}_1 + \boldsymbol{v}_1, \tag{4.9}$$

where $\boldsymbol{J}^{\mathrm{u}}$ is an $N \times N$ upshift matrix given by a Toeplitz matrix with the first column $[0, 0, \cdots, 0]^T$ and the first row $[0, 1, 0, \cdots, 0]$, and $\boldsymbol{H}_\theta$ is an $N \times N$ Toeplitz matrix with the first row $[1, 0, \cdots, 0]$ and the first column $[1, \theta, \theta^2, \cdots, \theta^{L-1}, 0, \cdots, 0]^T$. Note that the last L guard time symbols of every block are discarded so that the lengths of the input and the output vector are N.

The data phase uses the same protocol as the training phase. The only difference is the relay does not add its own signal when forwarding its received overlapped signal. The received data signal at Source 1 is

$$\boldsymbol{y}_{1\mathrm{d}} = p\boldsymbol{H}_\theta \boldsymbol{x}_{1\mathrm{d}} + q\boldsymbol{H}_\theta \boldsymbol{x}_{2\mathrm{d}} + d\boldsymbol{H}_\theta \boldsymbol{v}_{\mathrm{rd}} + h_{11}\boldsymbol{J}^{\mathrm{u}} \boldsymbol{x}_{1\mathrm{d}} + \boldsymbol{v}_{1\mathrm{d}}, \tag{4.10}$$

where $\mathrm{E}\left[|x_{1\mathrm{d}}[n]|^2\right] = \mathrm{E}\left[|x_{2\mathrm{d}}[n]|^2\right] = P_{\mathrm{s}}$.

4.2.2 Maximum Likelihood Estimator

In this section, we derive the ML estimator for Source 1 but it is similar for Source 2 due to symmetry. For data detection and better performance, not only the

two cascaded channels $h_{\mathrm{r}1}h_{1\mathrm{r}}$ and $h_{\mathrm{r}1}h_{2\mathrm{r}}$ are needed, but also the colored noise needs be whitened. The whitening of the noise requires Source 1 to have the knowledge of the RSI channel at the relay and the individual channels, either via relay feedback or estimating them by itself. Due to the impracticality of the feedback channel, Source 1 will estimate the RSI channel as well as the individual channels in our approach, which needs the relay to send its own training sequence.

Letting the relay transmit leads to a loss of simplicity at the AF relay by adding the capability of sampling process to it, in contrast of doing the AF in analog. However, there are reasons to have the sampling process at the relay. In FD mode, the relay needs to perform SIC which is assumed to be done in the pre-stage and results in the RSI. The SIC cannot be done only by analog means; digital domain methods such as time domain cancellation through estimating the SI channel and SI suppression using MIMO are also used to get enough attenuation [19]. Thus, sampling is already necessary at the relay for reasons other than channel training.

From (4.9), channel parameters p, q, θ, d, and h_{11} are complex unknown parameters to be estimated. We define $\boldsymbol{\omega} = [p_x, p_y, q_x, q_y, \theta_x, \theta_y, d_x, d_y, h_{11x}, h_{11y}]^T$ as the parameter vector, where p_x and p_y are the real and the imaginary part for p respectively and similar to the other complex parameters. We separate the real and imaginary parts because BFGS algorithm optimizes with respect to real parameters. Given $\boldsymbol{\omega}$, the mean and the covariance matrix of $\boldsymbol{y}_1$ are given by

$$\boldsymbol{\mu} = \mathrm{E}[\boldsymbol{y}_1] = p\boldsymbol{H}_\theta \boldsymbol{x}_1 + q\boldsymbol{H}_\theta \boldsymbol{x}_2 + d\boldsymbol{H}_\theta \boldsymbol{x}_{\mathrm{r}} + h_{11}\boldsymbol{J}^{\mathrm{u}}\boldsymbol{x}_1, \tag{4.11}$$

$$\boldsymbol{C} = |d|^2\sigma_{\mathrm{v}}^2 \boldsymbol{H}_\theta \boldsymbol{H}_\theta^H + \sigma_{\mathrm{v}}^2 \boldsymbol{I}_N. \tag{4.12}$$

Thus, the likelihood function of $\boldsymbol{y}_1$ is

$$p(\boldsymbol{y}_1; \boldsymbol{\omega}) = \frac{1}{\pi^N |\boldsymbol{C}|} \exp\left(-(\boldsymbol{y}_1 - \boldsymbol{\mu})^H \boldsymbol{C}^{-1} (\boldsymbol{y}_1 - \boldsymbol{\mu})\right), \tag{4.13}$$

where $|\boldsymbol{C}|$ denotes the determinant of matrix $\boldsymbol{C}$. The corresponding log-likelihood function is

$$\log p(\boldsymbol{y}_1; \boldsymbol{\omega}) = -N \log \pi - \log |\boldsymbol{C}| - (\boldsymbol{y}_1 - \boldsymbol{\mu})^H \boldsymbol{C}^{-1} (\boldsymbol{y}_1 - \boldsymbol{\mu}). \tag{4.14}$$

Maximizing the likelihood function is equivalent to minimizing the last two terms in (4.14). Let $f(\boldsymbol{\omega})$ denote our objective function, then we have

$$f(\boldsymbol{\omega}) = \log |\boldsymbol{C}| + (\boldsymbol{y}_1 - \boldsymbol{\mu})^H \boldsymbol{C}^{-1} (\boldsymbol{y}_1 - \boldsymbol{\mu}). \tag{4.15}$$

The ML estimator is given by

$$\hat{\boldsymbol{\omega}} = \arg\min_{\boldsymbol{\omega}} \ f(\boldsymbol{\omega}). \tag{4.16}$$

The objective function is not jointly convex with respect to $\boldsymbol{\omega}$. To solve the problem numerically, we use the BFGS algorithm, which is a popular quasi-Newton method. The BFGS is guaranteed to converge to a local minimum no matter whether the objective function is convex or not [92]. Also, the BFGS often needs less steps to converge than the gradient descent method [90], and thus is more efficient.

The parameters in $\boldsymbol{\omega}$ are optimized with different step sizes rather than optimizing $\boldsymbol{\omega}$ as a whole since they have different scales. For example d_x and θ_x are related to the relay-to-source channel and the RSI channel receptively. The gain of RSI channel is far smaller than that of the channel between nodes. So it is better to use different stepsizes when optimizing them. The algorithm takes the estimates of the real and imaginary part as the initial values. Due to the non-convexity, the algorithm might be trapped in a local minimum that is far from the optimal solution. Thus, it is necessary to initialize properly, which will be discussed in the following subsection. Backtracking line search is used to determinate the stepsize in the update process. The gradients needed in the BFGS method are derived in Appendix A. They are taken with respect to real parameters which are the elements in $\boldsymbol{\omega}$.

4.2.3 *Initialization*

We use zero-forcing (ZF) estimation method to initialize the BFGS method. The first five received symbols at Source 1 are taken to estimate h_{11}, p, q, d, and θ. The five symbols used are

$$y_1[0] = h_{11}x_1[0] + v_1[0], \tag{4.17}$$

$$y_1[i] = \sum_{k=1}^{i} \theta^{k-1}(px_1[i-k] + qx_2[i-k] + dx_{\mathrm{r}}[i-k]) + h_{11}x_1[i] + \sum_{k=1}^{i} d\theta^{k-1}v_{\mathrm{r}}[i-k] + v_1[i]. \tag{4.18}$$

We obtain the estimate of h_{11} first by the following.

$$\hat{h}_{11} = \frac{y_1[0]}{x_1[0]}. \tag{4.19}$$

Define $\tilde{y}_1[i] = y[i] - \hat{h}_{11}x_1[i]$ and we may design the the training symbols to make it easier to estimate the other four parameters. Let $x_1[0] = x_1[1]$, $x_2[0] = x_2[1]$, and $x_{\mathrm{r}}[0] = x_{\mathrm{r}}[1]$. With ZF method, the noise is ignored. We can estimate θ by using $\tilde{y}_1[1]$ and $\tilde{y}_1[2]$:

$$\hat{\theta} = \frac{\tilde{y}_1[2] - \tilde{y}_1[1]}{y_1[1]}. \tag{4.20}$$

Let $\tilde{y}'_1[1] = \tilde{y}_1[1] - \hat{\theta}y[i-1]$ for $i = 2, 3, 4$. Then, the estimator of p, q, and d are

$$\begin{bmatrix} \\ \hat{p} \\ \\ \hat{q} \\ \\ \hat{d} \\ \\ \end{bmatrix} = \begin{bmatrix} \\ x_1[1] & x_2[1] & x_{\mathrm{r}}[1] \\ \\ x_1[2] & x_2[2] & x_{\mathrm{r}}[2] \\ \\ x_1[3] & x_2[3] & x_{\mathrm{r}}[3] \\ \\ \end{bmatrix}^{-1} \begin{bmatrix} \\ \tilde{y}'_1[2] \\ \\ \tilde{y}'_1[3] \\ \\ \tilde{y}'_1[4] \\ \\ \end{bmatrix}, \tag{4.21}$$

which provides an exact estimate in the absence of noise. We may design the symbols of $x_1[n]$, $x_2[n]$, and $x_{\mathrm{r}}[n]$ that are involved in the coefficient matrix of (4.21) to guarantee the matrix is invertible.

The ZF initialization provides a starting point close to the optimal solution, which not only reduces the number of iterations for convergence compared to random initialization, but also reduces the likelihood that the algorithm will trap in a local minimum far from the optimal solution.

4.2.4 BFGS Algorithm

After we obtain all the required inputs of the algorithm, it is summarized as the following:

Initialize: $\boldsymbol{x}^0_{\{p\}} \triangleq \left[\hat{p}_x^T\ \hat{p}_y^T\right]^T$, $\boldsymbol{x}^0_{\{q\}} \triangleq \left[\hat{q}_x^T\ \hat{q}_y^T\right]^T$,$\boldsymbol{x}^0_{\{d\}} \triangleq [\hat{d}_x\ \hat{d}_y]^T$,
$\boldsymbol{x}^0_{\{\theta\}} \triangleq [\hat{\theta}_x\ \hat{\theta}_y]^T$, $\boldsymbol{x}^0_{\{h_{11}\}} \triangleq [\hat{h}_{11x}\ \hat{h}_{11y}]^T$.

Repeat until convergence for $i \geq 1$:

Step 1: $\boldsymbol{x}_0^{(i)} = \boldsymbol{x}_{\{p\}}^{(i-1)}$, $\boldsymbol{B}_0^{-1} = \boldsymbol{I}_2$

Step 2: Repeat until convergence for k: (BFGS)

1. Obtain a search direction $\boldsymbol{p}_k = -\boldsymbol{B}_k^{-1}\nabla f(\boldsymbol{x}_k^{(i)})$.
2. Find stepsize α_k by backtracking linesearch,
   then update $\boldsymbol{x}_{k+1}^{(i)} = \boldsymbol{x}_k^{(i)} + \alpha_k \boldsymbol{p}_k$.
3. Set $\boldsymbol{s}_k = \alpha_k \boldsymbol{p}_k$, $\boldsymbol{v}_k = \nabla f(\boldsymbol{x}_{k+1}^{(i)}) - \nabla f(\boldsymbol{x}_k^{(i)})$
4. Update the inverse Hessian approximation by
   $\boldsymbol{B}_{k+1}^{-1} = \boldsymbol{B}_k^{-1} + \frac{(\boldsymbol{s}_k^T\boldsymbol{v}_k + \boldsymbol{v}_k^T\boldsymbol{B}_k^{-1}\boldsymbol{v}_k)\boldsymbol{s}_k\boldsymbol{s}_k^T}{(\boldsymbol{s}_k^T\boldsymbol{v}_k)^2} - \frac{\boldsymbol{B}_k^{-1}\boldsymbol{v}_k\boldsymbol{s}_k^T + \boldsymbol{s}_k\boldsymbol{v}_k^T\boldsymbol{B}_k^{-1}}{\boldsymbol{s}_k^T\boldsymbol{v}_k}$

Step 3: Obtain the converged result $\boldsymbol{x}_{\{h\}}^{(i)} = \boldsymbol{x}_k^{(i)}$

Step 4: Repeat **Step 1** to **Step 3** for q, d, h_{11}, and θ with $\boldsymbol{x}_0^{(i)} = \boldsymbol{x}_{\{q\}}^{(i-1)}$,$\boldsymbol{x}_0^{(i)} = \boldsymbol{x}_{\{d\}}^{(i-1)}$, $\boldsymbol{x}_0^{(i)} = \boldsymbol{x}_{\{h_{11}\}}^{(i-1)}$, and $\boldsymbol{x}_0^{(i)} = \boldsymbol{x}_{\{\theta\}}^{(i-1)}$ respectively

There are three inputs of the algorithm: (i) received training data from (4.9), (ii) gradients of the real part and imaginary part of the parameters which are derived in Appendix A (from (A.3) to (A.10)), and (iii) the initialization of the parameters which can be obtained from (4.19) and (4.21) in Section 4.2.3. For each parameter in $\boldsymbol{\omega}$, after the initial values are given, it is optimized by BFGS algorithm when the other parameters are fixed. The five parameters are optimized alternatively, which is the iteration controlled by i. The results of the iteration will be used as initial values for the next iteration.

The BFGS algorithm is guaranteed to converge to a local minimum point because it is a descent algorithm. This is the case in our setup as explained next. In Step 2.4, BFGS algorithm updates the inverse Hessian approximation matrix which approximates the true Hessian to reduce complexity. The corresponding equation to update the Hessian approximation matrix is given by

$$\boldsymbol{A}_{k+1} = \boldsymbol{A}_k + \frac{\boldsymbol{v}_k \boldsymbol{v}_k^T}{\boldsymbol{v}_k^T \boldsymbol{s}_k} - \frac{(\boldsymbol{A}_k \boldsymbol{s}_k)(\boldsymbol{A}_k \boldsymbol{s}_k)^T}{\boldsymbol{s}_k^T \boldsymbol{A}_k \boldsymbol{s}_k}. \tag{4.22}$$

This is a rank-two update which ensures the Hessian approximation matrix is positive definite [92, Sec. 8.3.5]. The positive definite property implies that the search direction $\boldsymbol{p}_k = -\boldsymbol{A}_k^{-1} \nabla f(\boldsymbol{x}_k^{(i)})$ is a descent direction. Thus, the algorithm is guaranteed to converge to a minimum. However, for non-convex objective functions, the convergence point may be a local minimum that is not optimal. To avoid this, we use ZF estimates of the parameters to initialize the algorithm as mentioned above.

The complexity consists of the evaluation of three parts: (i) The calculation of gradients, (ii) line search, and (iii) the approximate inverse-Hessian matrix update. For the gradients of (4.15), the calculation is dominated by the matrix inversion of the covariance matrix $\boldsymbol{C}$ which has complexity of $O(N^3)$, where N is the length of the

training length. For large N, $\boldsymbol{C}$ asymptotically becomes to a Toeplitz matrix. The complexity of inverting a positive definite Toeplitz matrix is $O(N \log^2 N)$. The line search step requires the calculation of (4.15) which also includes the matrix inversion. Thus line search has the same complexity as the gradients step. The approximate inverse-Hessian matrix update has the complexity of $O(n^2)$ where n is the number of parameters to be estimated, i.e. the length of ω which is 10. The complexity of this update does not scale with N since $n = 10$ is a constant. Therefore, the total complexity of the BFGS algorithm in one iteration is $O(N \log^2 N)$ for large N. Moreover, based on our observation in the simulation, the algorithm with zero-forcing initialization converges at an average of about 3 iterations, which is 2 less iterations than random initialization. This also reduces the complexity of the algorithm.

4.3 Baseline Schemes

In this section we provide two baseline schemes for comparison. One is the multi-block training scheme which works similar to half-duplex training. The other is the conventional cross-correlation channel estimation method for ISI channel.

To compare to the proposed one-block training scheme, we propose another training scheme that takes multiple transmission blocks in the training. We discuss how the traditional LS method is applied in the FD system. The training phase adopts a relay protocol similar to half-duplex which is different from the protocol of the data phase. We still do not assume any feedback channel here. The training consists of four phases. In phase 1, the two sources transmit their training sequences $\boldsymbol{x}_{1\mathrm{t}}$ and $\boldsymbol{x}_{2\mathrm{t}}$ with length N_1 simultaneously. Meanwhile, the two sources receive what they transmit. The relay only receives in this phase. The received signals at Source 1 and

the relay are $\boldsymbol{y}_{P1}$ and $\boldsymbol{y}_{\mathrm{r}}$. We have

$$\boldsymbol{y}_{\mathrm{P1}} = h_{11}\boldsymbol{x}_{1\mathrm{t}} + \boldsymbol{v}_{\mathrm{P11}}, \tag{4.23}$$

$$\boldsymbol{y}_{\mathrm{r}} = h_{1\mathrm{r}}\boldsymbol{x}_{1\mathrm{t}} + h_{2\mathrm{r}}\boldsymbol{x}_{2\mathrm{t}} + \boldsymbol{v}_{\mathrm{P1r}}. \tag{4.24}$$

The RSI channel h_{11} can be estimated by Source 1 itself. Phase 1 costs one-block time which has N_1 symbols.

In phase 2, the relay scales the received signal from phase 1, then transmits this processed signal. The two sources only receive the signal from the relay. The received signal at Source 1 is

$$\boldsymbol{y}_{\mathrm{P2}} = \alpha_1 h_{\mathrm{r1}}\boldsymbol{y}_{\mathrm{r}} + \boldsymbol{n}_{\mathrm{P21}} = p_{\mathrm{m}}\boldsymbol{x}_{1\mathrm{t}} + q_{\mathrm{m}}\boldsymbol{x}_{2\mathrm{t}} + d_{\mathrm{m}}\boldsymbol{v}_{\mathrm{P1r}} + \boldsymbol{v}_{\mathrm{P21}}, \tag{4.25}$$

where $p_{\mathrm{m}} = \alpha_1 h_{\mathrm{r1}} h_{1\mathrm{r}}$, $q_{\mathrm{m}} = \alpha_1 h_{\mathrm{r1}} h_{2\mathrm{r}}$, $d_{\mathrm{m}} = \alpha_1 h_{\mathrm{r1}}$ and $\alpha_1 = \sqrt{P_{\mathrm{r}}/(2P_{\mathrm{s}}+1)}$.

Through $\boldsymbol{y}_{\mathrm{P2}}$, Source 1 can estimate two cascaded channels. Phase 2 takes another N_1 symbols. In the first two phases the relay works in half-duplex mode. The sources only do FD at phase 1. Since the training sequence in Phase 2 depends on Phase 1, the time cost of Phase 2 is also N_1 symbols

From the above two phases, the only unknown channel to Source 1 is the RSI channel h_{rr} at the relay. If a feedback channel from the relay to Source is possible, in phase 3 the relay could transmit and receive its own training signal and estimate h_{rr}, then feedback its estimates to the sources, which is more easier to operate. However, we do not assume feedback channels due to practical reasons. Therefore, the relay needs to transmit training signal that contains h_{rr} to the sources. Assuming the training sequence sent by the relay is $\boldsymbol{x}_{\mathrm{rt}}$ with length N_2, the relay transmits it to the sources in phase 3. The received signal is

$$\boldsymbol{y}_{\mathrm{P3}} = h_{\mathrm{r1}}\boldsymbol{x}_{\mathrm{rt}} + \boldsymbol{v}_{\mathrm{P3}}. \tag{4.26}$$

In this phase h_{r1} can be estimated at the source. At the same time, the relay receives its transmitted signal which will be used in the last phase.

In Phase 4, the relay transmits its received signal from the previous phase, and we have

$$\boldsymbol{y}_{\mathrm{P4}} = h_{\mathrm{r1}}\theta\boldsymbol{x}_{\mathrm{rt}} + \alpha_2 h_{\mathrm{r1}}\boldsymbol{v}_{\mathrm{P3r}} + \boldsymbol{v}_{P4}, \tag{4.27}$$

where $\theta = \alpha_2 h_{\mathrm{rr}}$ and $\alpha_2 = \sqrt{P_{\mathrm{r}}/(P_{\mathrm{r}}\sigma_{\mathrm{rr}}^2 + 1)}$.

Source 1 is able to estimate the individual channel h_{r1} through $\boldsymbol{y}_{\mathrm{P3}}$ and then recover the other individual channels. The estimate of θ can be obtained by using $\boldsymbol{y}_{\mathrm{P4}}$. Phase 3 and Phase 4 cost another two transmission blocks with block length N_2. If we assume $N_1 = N_2 = N/4$, then the training overhead of the multi-block scheme is the same as that of the one-block scheme. Both estimators achieve estimating the individual channels and the RSI channel at each source node.

The estimators are given as follows.

$$\hat{h}_{11} = \left(\boldsymbol{x}_{1\mathrm{t}}^H\boldsymbol{x}_{1\mathrm{t}}\right)^{-1}\boldsymbol{x}_{1\mathrm{t}}^H\boldsymbol{y}_{\mathrm{P1}}, \qquad [\hat{p}\ \hat{q}]^T = \left(\boldsymbol{X}_{\mathrm{rt}}^H\boldsymbol{X}_{\mathrm{rt}}\right)^{-1}\boldsymbol{X}_{\mathrm{rt}}^H\boldsymbol{y}_{\mathrm{P2}}, \tag{4.28}$$

$$\hat{h}_{\mathrm{r1}} = \left(\boldsymbol{x}_{\mathrm{rt}}^H\boldsymbol{x}_{\mathrm{rt}}\right)^{-1}\boldsymbol{x}_{\mathrm{rt}}^H\boldsymbol{y}_{\mathrm{P3}}, \qquad \hat{\theta} = \left(\boldsymbol{x}_{\mathrm{rt}}^H\boldsymbol{x}_{\mathrm{rt}}\right)^{-1}\boldsymbol{x}_{\mathrm{rt}}^H\boldsymbol{y}_{\mathrm{P4}}/\hat{h}_{\mathrm{r1}}, \tag{4.29}$$

where $\boldsymbol{X}_{\mathrm{rt}} = [\boldsymbol{x}_{1\mathrm{t}}\ \boldsymbol{x}_{2\mathrm{t}}]$.

The multi-block scheme is not a bandwidth efficient scheme since it works in half-duplex mode. However, it has some advantages. First, with the switch between the half-duplex and FD, linear estimator such as LS and MMSE can be applied for channel estimation, in which case we do not need to design special estimators for the system. Second, when the block length in the multi-block scheme is the same as it in one-block scheme, the MSE performance is better than the one-block scheme. Thus, in the multi-block scheme the MSE is improved at the cost of bandwidth.

Another baseline scheme is the correlation method. Using the same signal model in (4.9), the cross-correlation method for ISI channel can also be applied by treating

the taps as different parameters. By using training sequences which has an autocorrelation function that is approximately a delta function, the estimator can be obtained by doing the cross-correlation between the received signal and the training sequences. The parameters $\boldsymbol{\xi}_{\text{ISI}} = [p, q, d, h_{11}, \theta_1, \cdots, \theta_{L-1}]^T$, where $\theta_i = \theta^i$ but is treated as different parameters, can be estimated. We directly use the estimate of θ_1 as the final estimates of θ without investigating the the relationship between the channel taps.

4.4 Cramer-Rao Bounds and Analysis of the Fisher Information

4.4.1 Cramer-Rao Bounds for One-Block Training Scheme

The Cramer-Rao bound is used to evaluate the fundamental limits of each training scheme. We obtain the Fisher information matrix (FIM) through the second order derivative of the likelihood function. We use complex derivatives [93] to find the FIM. We define $\boldsymbol{\xi} = [p\ q\ \theta\ d\ h_{11}]^T$, which has the same parameters as $\boldsymbol{\omega}$, except each entry is a complex variable. The FIM is given by

$$\boldsymbol{\Gamma}(\boldsymbol{\xi}) = \mathrm{E}\left[\frac{\partial f}{\partial \boldsymbol{\xi}^*}\frac{\partial f}{\partial \boldsymbol{\xi}^T}\right]. \tag{4.30}$$

The (m,n)th element of $\boldsymbol{\Gamma}$ is given by

$$\Gamma_{mn} = \frac{\partial \boldsymbol{\mu}^H}{\partial \xi_m^*}\boldsymbol{C}^{-1}\frac{\partial \boldsymbol{\mu}}{\partial \xi_n} + \mathrm{tr}\left(\boldsymbol{C}^{-1}\frac{\partial \boldsymbol{C}}{\partial \xi_m^*}\boldsymbol{C}^{-1}\frac{\partial \boldsymbol{C}}{\partial \xi_n}\right). \tag{4.31}$$

We first begin with the diagonal elements of the FIM. For p and q, we have

$$\Gamma_{11} = \frac{\partial \boldsymbol{\mu}^H}{\partial p^*}\boldsymbol{C}^{-1}\frac{\partial \boldsymbol{\mu}}{\partial p} + \mathrm{tr}\left(\boldsymbol{C}^{-1}\frac{\partial \boldsymbol{C}}{\partial p^*}\boldsymbol{C}^{-1}\frac{\partial \boldsymbol{C}}{\partial p}\right) = \boldsymbol{x}_1^H \boldsymbol{H}_\theta^H \boldsymbol{C}^{-1}\boldsymbol{H}_\theta \boldsymbol{x}_1, \tag{4.32}$$

$$\Gamma_{22} = \boldsymbol{x}_2^H \boldsymbol{H}_\theta^H \boldsymbol{C}^{-1}\boldsymbol{H}_\theta \boldsymbol{x}_2. \tag{4.33}$$

Both $\boldsymbol{\mu}$ and $\boldsymbol{C}$ contains θ, so

$$\begin{aligned}\Gamma_{33} &= \frac{\partial \boldsymbol{\mu}^H}{\partial \theta^*}\boldsymbol{C}^{-1}\frac{\partial \boldsymbol{\mu}}{\partial \theta} + \mathrm{tr}\left(\boldsymbol{C}^{-1}\frac{\partial \boldsymbol{C}}{\partial \theta^*}\boldsymbol{C}^{-1}\frac{\partial \boldsymbol{C}}{\partial \theta}\right) \\ &= (p\boldsymbol{x}_1 + q\boldsymbol{x}_2 + d\boldsymbol{x}_{\mathrm{r}})^H \boldsymbol{B}_\theta^H \boldsymbol{C}^{-1}\boldsymbol{B}_\theta(p\boldsymbol{x}_1 + q\boldsymbol{x}_2 + d\boldsymbol{x}_{\mathrm{r}}) \\ &+ |d|^4\sigma_{\mathrm{n}}^4 \mathrm{tr}\left(\boldsymbol{C}^{-1}\boldsymbol{H}_\theta\boldsymbol{B}_\theta^H\boldsymbol{C}^{-1}\boldsymbol{B}_\theta\boldsymbol{H}_\theta^H\right), \end{aligned} \tag{4.34}$$

where $\boldsymbol{B}_\theta = \frac{\partial \boldsymbol{H}_\theta}{\partial \theta}$ is also an $N \times N$ Toeplitz matrix given by the first column $[0, 1, 2\theta, \cdots, (L-1)\theta^{L-2}, 0, \cdots, 0]^T$ and the first row $[0, 0, \cdots, 0]$. For d, it is similar to the case of θ since it appears in both $\boldsymbol{\mu}$ and $\boldsymbol{C}$,

$$\begin{aligned}\Gamma_{44} &= \frac{\partial \boldsymbol{\mu}^H}{\partial d^*}\boldsymbol{C}^{-1}\frac{\partial \boldsymbol{\mu}}{\partial d} + \mathrm{tr}\left(\boldsymbol{C}^{-1}\frac{\partial \boldsymbol{C}}{\partial d^*}\boldsymbol{C}^{-1}\frac{\partial \boldsymbol{C}}{\partial d}\right) \\ &= \boldsymbol{x}_{\mathrm{r}}^H\boldsymbol{H}_\theta^H\boldsymbol{C}^{-1}\boldsymbol{H}_\theta\boldsymbol{x}_{\mathrm{r}} + |d|^2\sigma_{\mathrm{n}}^4\mathrm{tr}\left(\boldsymbol{C}^{-1}\boldsymbol{H}_\theta\boldsymbol{H}_\theta^H\boldsymbol{C}^{-1}\boldsymbol{H}_\theta\boldsymbol{H}_\theta^H\right), \end{aligned} \tag{4.35}$$

and last for h_{11},

$$\Gamma_{55} = \frac{\partial \boldsymbol{\mu}^H}{\partial h_{11}^*}\boldsymbol{C}^{-1}\frac{\partial \boldsymbol{\mu}}{\partial h_{11}} + \mathrm{tr}\left(\boldsymbol{C}^{-1}\frac{\partial \boldsymbol{C}}{\partial h_{11}^*}\boldsymbol{C}^{-1}\frac{\partial \boldsymbol{C}}{\partial h_{11}}\right) = \boldsymbol{x}_1^H(\boldsymbol{J}^{\mathrm{u}})^H\boldsymbol{J}^{\mathrm{u}}\boldsymbol{x}_1. \tag{4.36}$$

Other elements are given in Appendix B. We focus on these diagonal elements because we will analyze how the channel parameters affect the Fisher information in Section 4.4.2.

The CRBs are given by the diagonal elements of inverse of the FIM such that

$$CRB_{\boldsymbol{\xi}} = \mathrm{tr}\left(\boldsymbol{\Gamma}^{-1}\right). \tag{4.37}$$

In particular, $CRB_p = [\boldsymbol{\Gamma}^{-1}]_{11}$, $CRB_q = [\boldsymbol{\Gamma}^{-1}]_{22}$, $CRB_\theta = [\boldsymbol{\Gamma}^{-1}]_{33}$, $CRB_d = [\boldsymbol{\Gamma}^{-1}]_{44}$, and $CRB_{h_{11}} = [\boldsymbol{\Gamma}^{-1}]_{55}$ where $[\boldsymbol{A}]_{mn}$ denotes the (m, n)th element of matrix $\boldsymbol{A}$.

We also derive the CRBs for the multiple transmission blocks training case in Appendix B for comparison with the CRBs of the one-block training scheme.

4.4.2 Analysis of the Fisher Information

In this subsection, we anaylze the Fisher information for the one-block training scheme by using asymptotic properties of Toeplitz matrices [94] to see how the channel parameters and transmit powers affect the estimation, in the regime where the training length N is large. To analyze the asymptotic behavior of the Toeplitz matrix, $\boldsymbol{H}_\theta$ will be used. Define a function

$$t(\lambda) = \sum_{k=0}^{\infty} t_k e^{j\lambda k}, \tag{4.38}$$

where t_k are the elements of the first column of the $N \times N$ Toeplitz matrix $\boldsymbol{T}_N$. Thus, we can use the function $t(\lambda)$ to represent the matrix. We denote the matrix as $\boldsymbol{T}_N(t(\lambda))$. In our system, $t_k = \theta^k$ for $k = 0, \cdots, L-1$ and otherwise $t_k = 0$. We show that $\boldsymbol{H}_\theta$ and $\boldsymbol{T}_N(t(\lambda))$ are asymptotically equivalent. First, since both $\boldsymbol{H}_\theta$ and $\boldsymbol{T}_N(t(\lambda))$ are banded Toeplitz matrices, their strong norms (operator norms) are bounded. Secondly, from the definition of $\boldsymbol{T}_N(t(\lambda))$, we have $\lim_{N\to\infty} ||\boldsymbol{H}_\theta - \boldsymbol{T}_N(t(\lambda))|| = 0$, where $||\boldsymbol{A}||$ denotes the weak norm (Hilbert-Schmidt norm) of matrix $\boldsymbol{A}$. With the two conditions above, we can say that $\boldsymbol{H}_\theta$ and $\boldsymbol{T}_N(t(\lambda))$ are asymptotically equivalent [94]. Therefore, we will write $\boldsymbol{H}_\theta = \boldsymbol{T}_N(t(\lambda))$ which will be understood to hold for asymptotically large N. We have the following expression for $t(\lambda)$.

$$t(\lambda) = \sum_{k=0}^{L-1} \theta^k e^{j\lambda k} = \frac{1-\theta^L e^{jL\lambda}}{1-\theta e^{j\lambda}} = \frac{1}{1-\theta e^{j\lambda}}, \tag{4.39}$$

where $\theta^L \approx 0$ by our assumption of channel energy in Section 4.2.1. The covariance matrix $\boldsymbol{C}$ is

$$\boldsymbol{C} = |d|^2 \sigma_{\mathrm{v}}^2 \boldsymbol{T}_N(t(\lambda)) \boldsymbol{T}_N(t^*(\lambda)) + \sigma_{\mathrm{v}}^2 \boldsymbol{I}_N. \tag{4.40}$$

Without loss of generality, we set $\sigma_{\mathrm{v}}^2 = 1$. According to the asymptotic properties of Toeplitz matrices [94], the product of two Toeplitz matrices and the inverse of

a Toeplitz matrix are Toeplitz matrices asymptotically, which can be expressed as follows.

$$\boldsymbol{C} = |d|^2 \boldsymbol{T}_N(|t(\lambda)|^2) + \boldsymbol{I}_N = \boldsymbol{T}_N(|d|^2|t(\lambda)|^2 + 1), \tag{4.41}$$

$$\boldsymbol{C}^{-1} = \boldsymbol{T}_N\left(\frac{1}{|d|^2|t(\lambda)|^2 + 1}\right). \tag{4.42}$$

Theorem 1: The Fisher information of the cascaded channel p is an increasing function of the absolute value of the RSI channel h_{rr}, a decreasing function of the relay transmit power P_{r} and the individual channel h_{r1}, and an increasing function of the source transmit power P_{s} asymptotically when the length of training goes to infinity with fixed training energy.

Proof. The Fisher information of the cascaded channel p in the one-block training scheme from (4.32) is

$$\Gamma_{11} = \boldsymbol{x}_1^H \boldsymbol{H}_\theta^H \boldsymbol{C}^{-1} \boldsymbol{H}_\theta \boldsymbol{x}_1 = \boldsymbol{x}_1 \boldsymbol{T}_N(t(\lambda)) \boldsymbol{T}_N\left(\frac{1}{|d|^2|t(\lambda)|^2 + 1}\right) \boldsymbol{T}_N(t^*(\lambda)) \boldsymbol{x}_1 \tag{4.43}$$

$$= \boldsymbol{x}_1 \boldsymbol{T}_N\left(\frac{|t(\lambda)|^2}{|d|^2|t(\lambda)|^2 + 1}\right) \boldsymbol{x}_1 \leq \eta_{\max} ||\boldsymbol{x}||^2, \tag{4.44}$$

where $\eta_{\max}$ is the maximum eigenvalue of $\boldsymbol{T}_N\left(\frac{|t(\lambda)|^2}{|d|^2|t(\lambda)|^2+1}\right)$. When $N \to \infty$, we have

$$\eta_{\max} = \max_{\lambda} \frac{|t(\lambda)|^2}{|d|^2|t(\lambda)|^2 + 1} = \max_{\lambda} \frac{1}{|d|^2 + |1 - \theta e^{j\lambda}|^2} = \frac{1}{|d|^2 + \left|1 - |\theta|\right|^2}, \tag{4.45}$$

with λ equals to the minus phase of θ. Therefore, the Fisher information can be expressed in terms of the channel parameters and power scaling factor α,

$$\Gamma_{11} = \frac{E_{\mathrm{t}}}{\alpha^2 |h_{\mathrm{r1}}|^2 + \left|1 - \alpha |h_{\mathrm{rr}}|\right|^2}, \tag{4.46}$$

where $E_{\mathrm{t}} = ||\boldsymbol{x}_1||^2$ is the training energy and is kept to be a constant.

From the derivation of α to keep the stability of the system in Section 4.2.1, we conclude that $\mathrm{E}[|\theta|^2] = \alpha^2 \mathrm{E}[|h_{\mathrm{rr}}|^2] < 1$. Proper α can be chosen by using fixed gain

margin to satisfy this condition. Thus $|\theta| < 1$ and $|h_{\mathrm{rr}}|$ has a constraint related to α. Therefore, for a constant α, Γ_{11} is an increasing function of $|h_{\mathrm{rr}}|$. It is also a decreasing function of α. Since α grows with P_{r} and decreases with P_{s}, Γ_{11} is a decreasing function of P_{r}, and an increasing function of P_{s}. □

Theorem 1 shows large value of the RSI channel gain increases the Fisher information of the cascaded channel and makes it easier to estimate. On the other hand, Γ_{11} is a decreasing function of α, we can say that increasing P_{r} does not help to estimate the cascaded channel but increasing P_{s} does.

Theorem 2: The Fisher information of the RSI channel h_{rr} is an increasing function of $|h_{\mathrm{rr}}|$, the absolute values of both the cascaded channels, and the power scaling factor α asymptotically when the length of training goes to infinity with fixed training energy.

Proof. Define $\boldsymbol{B}_\theta = \boldsymbol{T}_N(g(\lambda))$ where $g(\lambda) = \frac{e^{j\lambda}}{(1-\theta e^{j\lambda})^2}$. Function $g(\lambda)$ is obtained similarly to $t(\lambda)$ by using the sum of a geometric sequence and $\theta^L \approx 0$. Then, from (4.34), the Fisher information of the RSI channel can be represented by Toeplitz matrices as

$$\begin{aligned}\Gamma_{33} &= (p\boldsymbol{x}_1 + q\boldsymbol{x}_2 + d\boldsymbol{x}_{\mathrm{r}})^H \boldsymbol{T}_N\left(\frac{|g(\lambda)|^2}{|d|^2|t(\lambda)|^2+1}\right)(p\boldsymbol{x}_1 + q\boldsymbol{x}_2 + d\boldsymbol{x}_{\mathrm{r}}) \\ &\quad + |d|^4 \mathrm{tr}\left(\boldsymbol{T}_N\left(\frac{|g(\lambda)|^2|t(\lambda)|^2}{(|d|^2|t(\lambda)|^2+1)^2}\right)\right) \qquad (4.47) \\ &\leq \left(|p|^2||\boldsymbol{x}_1||^2 + |q|^2||\boldsymbol{x}_2||^2 + |d|^2||\boldsymbol{x}_{\mathrm{r}}||^2\right)\max_\lambda\left(\frac{|g(\lambda)|^2}{|d|^2|t(\lambda)|^2+1}\right) \\ &\quad + |d|^4\frac{1}{2\pi}\int_0^{2\pi}\frac{|g(\lambda)|^2|t(\lambda)|^2}{(|d|^2|t(\lambda)|^2+1)^2}\mathrm{d}\lambda. \qquad (4.48)\end{aligned}$$

For the first term in (4.52), the maximum value is $\frac{1}{|1-|\theta||^2(|d|^2+|1-|\theta||^2)}$. The second term comes from the asymptotic property of Toeplitz matrix that the trace of it is equal to the integration of the function that characterized it. Simplifying the integral we

have

$$\int_0^{2\pi} \frac{|g(\lambda)|^2|t(\lambda)|^2}{(|d|^2|t(\lambda)|^2+1)^2}\mathrm{d}\lambda = \int_0^{2\pi} \frac{1}{|1-\theta e^{j\lambda}|^2(|d|^2+|1-\theta e^{j\lambda}|^2)^2}\mathrm{d}\lambda. \tag{4.49}$$

In the FD TWR system, we assume $P_{\mathrm{r}} \gg P_{\mathrm{s}}$ since P_{s} is the received power at the relay which incorporates the pathloss. Thus $\alpha^2 \gg 1$. Note that $|\theta| < 1$, we have $|d^2| = \alpha^2|h_{\mathrm{r1}}|^2 \gg |1-\theta e^{j\lambda}|^2$. We can approximately calculate the integral as

$$\frac{1}{2\pi}\int_0^{2\pi} \frac{1}{|1-\theta e^{j\lambda}|^2(|d|^2+|1-\theta e^{j\lambda}|^2)^2}\mathrm{d}\lambda \tag{4.50}$$

$$\approx \frac{1}{2\pi}\int_0^{2\pi} \frac{1}{|1-\theta e^{j\lambda}|^2|d|^4}\mathrm{d}\lambda = \frac{1}{|d|^4}\frac{1}{(|\theta|+1)\big||\theta|-1\big|}. \tag{4.51}$$

The Fisher information of the RSI channel θ becomes

$$\Gamma_{33} = \frac{\alpha^2 E_t(|h_{\mathrm{r1}}h_{1\mathrm{r}}|^2+|h_{\mathrm{r1}}h_{2\mathrm{r}}|^2+|h_{\mathrm{r1}}|^2)}{\big|1-\alpha|h_{\mathrm{rr}}|\big|^2(\alpha^2|h_{\mathrm{r1}}|^2+|1-\alpha|h_{\mathrm{rr}}||^2)} + \frac{1}{(\alpha|h_{\mathrm{rr}}|+1)\big|\alpha|h_{\mathrm{rr}}|-1\big|}. \tag{4.52}$$

□

Γ_{33} is an increasing function of α so that increasing P_{r} helps to estimate h_{rr} while increasing P_{s} does not. Γ_{33} is also a function of $|h_{\mathrm{rr}}|$ and it increases with growing $|h_{\mathrm{rr}}|$. That means larger RSI channel will make itself easier to estimate. Lastly, Γ_{33} is an increasing function of channel gains between sources and relay, thus large channel gains increase the accuracy of the estimate of h_{rr}.

Theorem 3: The Fisher information of the individual channel h_{r1} is an increasing function of the absolute value of the RSI channel h_{rr}, a decreasing function of the power scaling factor α, and a decreasing function of the absolute value of h_{r1} asymptotically when the length of training goes to infinity with fixed training energy.

Proof. Similar to the above two proofs, for the relay to source channel h_{r1}, we have

$$\Gamma_{44} = \frac{E_t}{\alpha^2|h_{\mathrm{r1}}|^2+\big|1-\alpha|h_{\mathrm{rr}}|\big|^2} + + \frac{1}{(\alpha|h_{\mathrm{rr}}|+1)\big|\alpha|h_{\mathrm{rr}}|-1\big|}. \tag{4.53}$$

The first term of (4.53) is the same as (4.46). The second term is similar to the second term in (4.52) and can be obtained by using (4.49) to (4.51). □

The affects of RSI channel and α to estimating $h_{\mathrm{r}1}$ are the same to the cascaded channel case. However the Fisher information of $h_{\mathrm{r}1}$ contains itself so that it will be harder to estimate the channel when it has large absolute value.

4.4.3 Exploiting the Structure of the Related Channel Taps

To show the advantage of exploiting the channel structure created by the RSI feedback, we compare the Fisher information of the RSI channel θ corresponding to two channel assumptions in one-block training scheme. In the first case, the structure of geometric sequence ISI channel taps is considered, while in the other case the channel taps are treated as different parameters (not necessarily a geometric sequence). We will show that exploiting the channel structure has larger Fisher information than treating the taps as different parameters.

We first look at the Fisher information of treating the taps as different parameters. The parameter vector for this case is defined by $\boldsymbol{\xi}_{\mathrm{ISI}} = [p, q, d, h_{11}, \theta_1, \cdots, \theta_{L-1}]^T$, where θ_i are independent channel taps. The Fisher information of p, q, d, and h_{11} are the same as the Fisher information of exploiting the channel structure. Let the partial derivative of $\boldsymbol{H}_\theta$ with respect to θ_1 be $\boldsymbol{D}_1 = \frac{\partial \boldsymbol{H}_\theta}{\partial \theta_1} = \boldsymbol{J}^{\mathrm{d}}$. $\boldsymbol{D}_1$ is also a Toeplitz matrix and thus we have $\boldsymbol{D}_1 = \boldsymbol{T}_N(e^{j\lambda})$. The Fisher information for θ_1 is similar to (4.34) which is

$$\begin{aligned}\Gamma_{\theta_1} &= (p\boldsymbol{x}_1 + q\boldsymbol{x}_2 + d\boldsymbol{x}_{\mathrm{r}})^H \boldsymbol{D}_1^H \boldsymbol{C}^{-1} \boldsymbol{D}_1 (p\boldsymbol{x}_1 + q\boldsymbol{x}_2 + d\boldsymbol{x}_{\mathrm{r}}) \\ &\quad + |d|^4 \sigma_{\mathrm{n}}^4 \mathrm{tr}\left(\boldsymbol{C}^{-1} \boldsymbol{H}_\theta \boldsymbol{D}_1^H \boldsymbol{C}^{-1} \boldsymbol{D}_1 \boldsymbol{H}_\theta^H\right). \end{aligned} \tag{4.54}$$

Theorem 4: With designed training sequences, the Fisher information of θ is greater than that of θ_1 by Γ_{diff} which can be approximated in closed form, when training length goes to infinity.

Proof. The difference of the two Fisher information is

$$\begin{aligned}\Gamma_{\text{diff}} &= \Gamma_{33} - \Gamma_{\theta_1} \\ &= \underbrace{(p\boldsymbol{H}_\theta \boldsymbol{x}_1 + q\boldsymbol{H}_\theta \boldsymbol{x}_2 + d\boldsymbol{x}_{\text{r}})^H \boldsymbol{T}_N \left(\frac{|g(\lambda)|^2 - 1}{|d|^2|t(\lambda)|^2 + 1} \right) (p\boldsymbol{H}_\theta \boldsymbol{x}_1 + q\boldsymbol{H}_\theta \boldsymbol{x}_2 + d\boldsymbol{x}_{\text{r}})}_{\Gamma_{\text{a}}} \\ &\quad + \underbrace{|d|^4 \text{tr} \left(\boldsymbol{T}_N \left(\frac{|t(\lambda)|^2(|g(\lambda)|^2 - 1)}{(|d|^2|t(\lambda)|^2 + 1)^2} \right) \right)}_{\Gamma_{\text{b}}}. \end{aligned} \tag{4.55}$$

For the first term of (4.55), we have

$$\Gamma_{\text{a}} \leq \left(|p|^2 ||\boldsymbol{x}_1||^2 + |q|^2 ||\boldsymbol{x}_2||^2 + |d|^2 ||\boldsymbol{x}_{\text{r}}||^2 \right) \max_{\lambda} \left(\frac{|g(\lambda)|^2 - 1}{|d|^2|t(\lambda)|^2 + 1} \right) \tag{4.56}$$

$$= \left(|p|^2 ||\boldsymbol{x}_1||^2 + |q|^2 ||\boldsymbol{x}_2||^2 + |d|^2 ||\boldsymbol{x}_{\text{r}}||^2 \right) \frac{1 - (1 - |\theta|)^4}{|d|^2(1 - |\theta|^2) + (1 - |\theta|^4)}. \tag{4.57}$$

The equality holds when the training sequence is the eigenvector corresponding to the maximum eigenvalue of $\boldsymbol{T}_N \left(\frac{|g(\lambda)|^2 - 1}{|d|^2|t(\lambda)|^2 + 1} \right)$ which is given by [55, 94]

$$\boldsymbol{x}_{\text{t}} = \frac{1}{\sqrt{N}} [1, e^{j2\pi}, e^{j4\pi} \cdots, e^{j2\pi(N-1)}]^T. \tag{4.58}$$

Note that $|\theta| < 1$, therefore, by choosing the training sequence, the first term of the difference is greater than zero.

For the second term, first we calculate

$$\frac{1}{2\pi} \int_0^{2\pi} |g(\lambda)|^2 \text{d}\lambda = \left(\frac{1 + |\theta|^2}{(1 - |\theta|^2)^3} \cdot \text{sign}(1 - |\theta|^2) \right). \tag{4.59}$$

The integration in Γ_{b} can be approximated by using integration by parts and the results from (4.49) to (4.51) and (4.59), we have

$$\begin{aligned}\Gamma_{\text{b}} &= \frac{1 - |1 - \theta|^4}{|1 - \theta|^4(|\theta| + 1)\big||\theta| - 1\big|} - \frac{1}{2\pi} \int_0^{2\pi} (|g(\lambda)|^2)' \frac{1}{|1 - \theta e^{j\lambda}|^2} \text{d}\lambda \\ &= \frac{1 - |1 - \theta|^4}{|1 - \theta|^4(|\theta| + 1)\big||\theta| - 1\big|} - \frac{1}{2\pi} \int_0^{2\pi} \frac{-4|\theta| \sin\lambda}{|1 - \theta e^{j\lambda}|^8} \qquad (4.60) \\ &= \frac{1 - |1 - \theta|^4}{|1 - \theta|^4(|\theta| + 1)\big||\theta| - 1\big|}, \qquad (4.61)\end{aligned}$$

where the second term in (4.60) is zero since it is an odd function over $[0, 2\pi]$. $\Gamma_{\mathrm{b}} > 0$ for $|\theta| < 1$. Thus, $\Gamma_{\mathrm{diff}} = \Gamma_{\mathrm{a}} + \Gamma_{\mathrm{b}} > 0$. □

The Fisher information of related channel taps is larger than independent channel taps, regardless of estimators so that exploiting the structure arising from the RSI channel increases its Fisher information.

4.5 Numerical Results

In our simulations, we first setup a set of parameters and keep it unchanged for all the training schemes. We set the relay power $P_r = 40$ dB and the RSI variance $\sigma^2_{\mathrm{rr}} = -20$ dB. If the original SI channel has unit variance, then the RSI variance σ^2_{rr} represents the ability of self-interference cancellation to reduce the interference power. We first simulate the MSEs of estimates of the channels to show the performance of the ML estimator in the one-block training scheme with training length $N = 100$. Figure 4.2 shows the MSEs of different channel parameters. For the cascaded channel, we plot the MSE of $h_{\mathrm{cas}} = h_{\mathrm{r1}}h_{\mathrm{1r}} = p/\alpha$ which is the channel without power scaling factors for comparison with other schemes. The other cascaded channel q/α is omitted since it has a symmetric position to p/α and similar results. In Figure 4.2 and 4.3, h_{r1} represents the individual channel from the relay to Source 1, and h_{rr} and h_{11} are the RSI channels in the relay and Source 1 respectively. The MSEs are compared with the CRBs obtained by (4.32) to (4.36). It can be observed that there is a gap between MSE and CRB because the block length which is also the overhead in the one-block scheme N is not large enough. Since the ML estimator is asymptotic efficient, i.e. achieves the CRB as N goes to infinity [93], we expect this gap to close for large N.

The MSEs and CRBs for the two baseline methods are also simulated. Figure 4.3 shows the performance of the LS estimator in the multi-block training scheme. Here we set $N_1 = N_2 = 100$ which means this scheme has the same training block length as

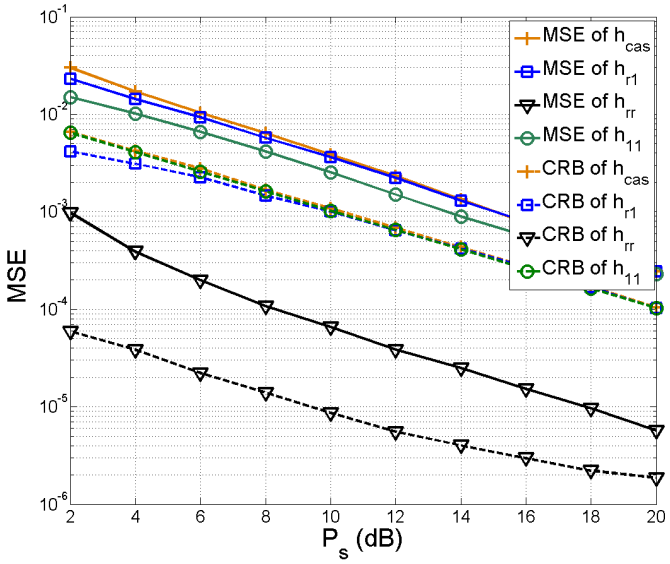

Figure 4.2: MSE of the one-block training scheme - the MSEs are compared with the CRBs. In the figure, h_{r1} represents the individual channel from the relay to Source 1, and h_{rr} and h_{11} are the RSI channels in the relay and Source 1 respectively.

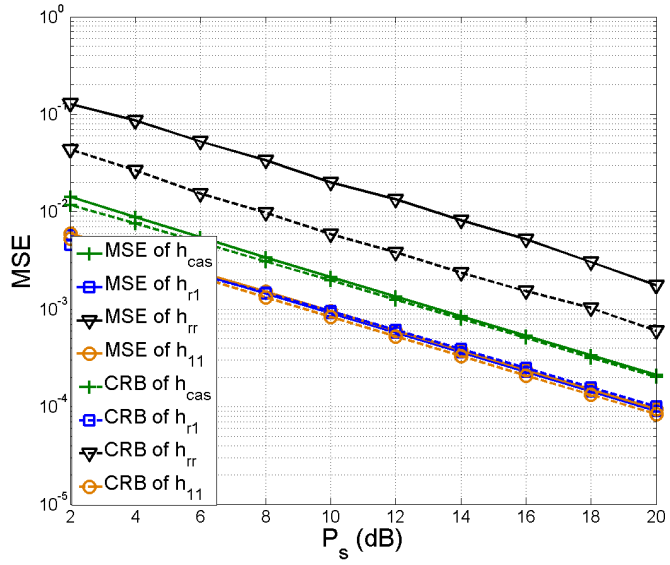

Figure 4.3: MSE of the multiple-block training scheme - the MSE of the LS estimator in the multi-block training scheme is simulated. To keep a fair comparison, we set the training block length and the power of the relay as same as those in one block training scheme.

the one block training scheme. To keep a fair comparison, the training power of the relay in the multi-block training is $P_{\mathrm{r}} = P_{\mathrm{s}}$, same as the one-block training scheme.

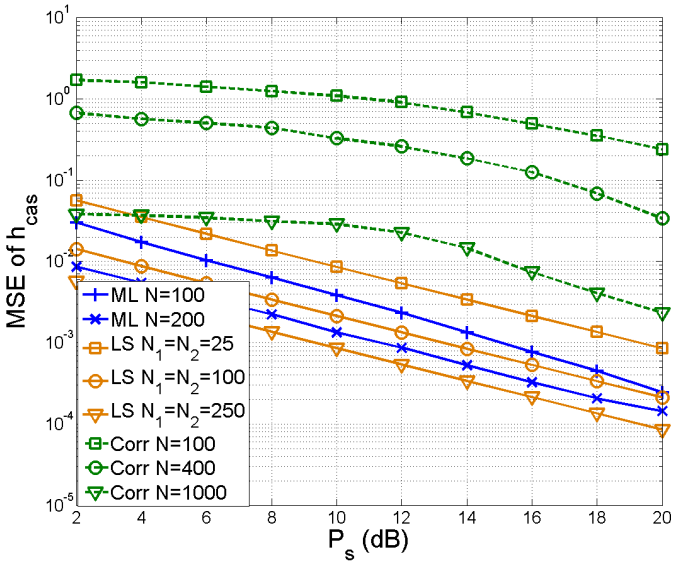

Figure 4.4: MSE performance comparison of different training schemes - if the overhead of training is kept the same, the one-block training scheme has better performance than the other schemes.

In Figure 4.4, the MSE performance of the cascaded channel h_{cas} for different training schemes are compared. If the overhead of training is kept the same, which means the $N_1 = N_2 = N/4$, the one-block training scheme has better performance than the multi-block training, and the cross-correlation method. However, the multi-block training scheme outperforms the one-block training scheme when the training block lengths, which is fixed, of both schemes are the same. This is expected since the LS estimator keeps the same transmit power as the ML estimator for both nodes but takes four times the transmit time for training. When the overhead increases, all the schemes have lower MSEs.

The CRBs of the RSI channel h_{rr} for different schemes are shown in Figure 4.5. The MSE of h_{rr} for the cross-correlation method is also shown in this figure. The cross-correlation method has large gap between the MSE and CRB because the autocorrelation function of the training sequence is not a perfect delta function with limited training length. The CRBs with and without exploiting the structure of re-

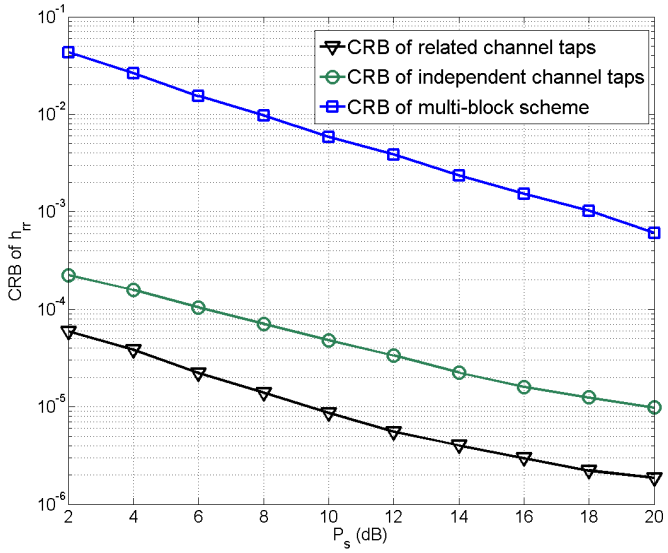

Figure 4.5: Comparison of CRBs of h_{rr} for different training schemes - the one-block training scheme exploits the structure of related channel taps while the others do not. Exploiting the structure has lower CRB than treating the taps as different parameters in one-block training scheme.

lated channel taps are also compared. Exploiting the structure has lower CRB than treating the taps as different parameters in one-block training scheme. We also see that the CRB of the multi-block training scheme is higher than those of one-block training scheme when overhead is fixed.

In Figure 4.6, we compare the Fisher information calculated by (4.46), (4.52), and (4.53) and that from simulation results. The Fisher information $\Gamma_{11}, \Gamma_{33}, \Gamma_{44}$ are for the cascaded channel h_{cas}, RSI channel h_{rr}, and the individual channel h_{r1} in the one-block training scheme respectively. The figure shows Γ_{11} and Γ_{44} decreases while Γ_{33} increases with increasing $|h_{r1}|$, which verifies Theorem 1 to 3. We can conclude from Figure 4.6 that large gain of the individual channel helps to estimate the individual channel and it does not help to estimate the cascaded channel and the RSI channel. We set training length as $N = 100$ in this simulation. There is a gap between the simulated Fisher information and the analytical one since the analytical

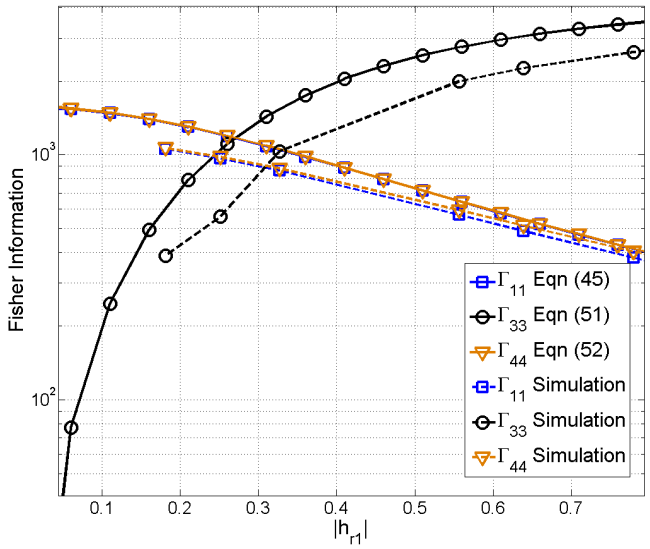

Figure 4.6: Fisher information vs. $|h_{\mathrm{r}1}|$ - the analytical results and the simulated results which verify Theorem 1 to 3 are compared. Large gain of the individual channel helps to estimate the individual channel and it does not help to estimate the cascaded channel and the RSI channel.

Fisher information expression is obtained in the asymptotic regime when N is large. For Γ_{11} and Γ_{44} the gaps are negligible and for Γ_{33} the gap is within a factor of 1.3.

The difference in Fisher information of exploiting the channel structure versus treating the taps as individual variables, which is Γ_{diff}, is also simulated and compared to that calculated from (4.57) and (4.61) in Figure 4.7. When using $N = 100$ in the simulation, the gap between the theory and simulation for the difference in Fisher information is around a factor of 1.6, illustrating the usefulness of (4.57) and (4.61). From the simulation we observe that the analysis of the asymptotic behavior of the Fisher information is close to the simulation results. Figure 4.7 verifies Theorem 4 which asserts that taking the channel structure into account is always better than treating the taps as individual variables when estimating the RSI channel. Figure 4.7 also shows increasing P_{r} helps to estimate the RSI channel which is concluded in Theorem 3.

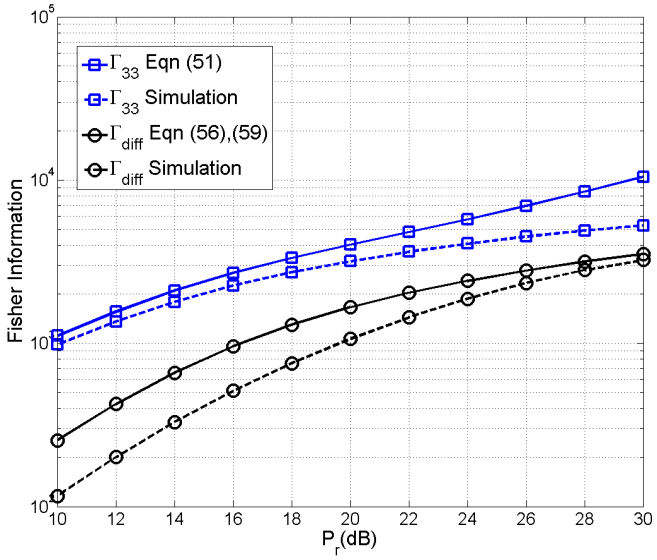

Figure 4.7: Difference in the Fisher information - the difference in Fisher information between exploiting the channel structure and treating the taps as individual variables is simulated. The results verify Theorem 4 and assert that taking the channel structure into account is always better than treating the taps as individual variables when estimating the RSI channel.

To illustrate the benefit of canceling RSI at the receiver by using the estimates of θ, BER performance with different detectors are simulated. We implemented two detectors: (i) an equalizer using Viterbi algorithm which uses the full information of channel taps, (ii) a matched filer with the strongest channel tap. In this simulation, estimated CSI are used. We also simulate the effect of noise whitening. Figure 4.8 shows the comparison of BER of the two detectors with a fixed relay power $P_{\mathrm{r}} = 40$ dB. Define the signal to interference ratio at relay as

$$\mathrm{SIR}_{\mathrm{r}} = \frac{\mathrm{E}\left[|h_{1\mathrm{r}}x_{1\mathrm{d}}[n] + h_{2\mathrm{r}}x_{2\mathrm{d}}[n]|^2\right]}{t_{\mathrm{rd}}[n]} = \frac{2P_{\mathrm{s}}}{P_{\mathrm{r}}\sigma_{\mathrm{rr}}^2}. \tag{4.62}$$

Note that σ_{rr}^2 is the variance of the RSI after the self-interference cancellation at the relay. Since P_{s} actually represents the power of the source transmit signal arriving at the relay, according to the data reported in [19] and [35], it could be much smaller than the self-interference power from the relay itself, even after some method of

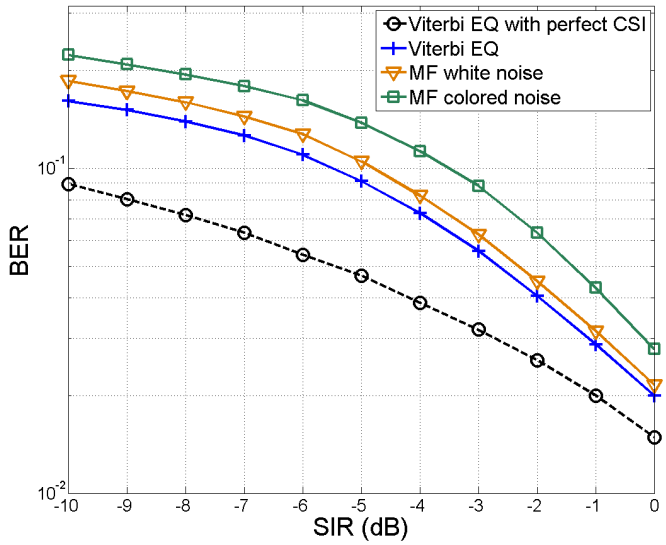

Figure 4.8: BER performance for different detectors - a Viterbi equalizer which uses the full CSI is compared to an MF detector which only uses the CSI of the strongest channel tap. The Viterbi equalizer outperforms the MF detector in low SIR regime, which shows benefit of estimating the RSI channel at the receiver.

cancellation. This case become more severe when the FD transceiver is a base station. Thus SIR_r can be negative in dB scale. Figure 4.8 shows the BER performance for different detectors. For the whitened noise case, the Viterbi equalizer outperforms the matched filter detector by about 1.5 dB in this important low SIR regime showing that the ISI due to the RSI cannot be ignored. This advantage decreases with increasing SIR since the RSI becomes lower. There is also a gap of about 1dB between the two matched filter detectors with and without noise whitening. Thus, whitening the noise not only limits the maximum signal power but also improves the BER. It shows one advantage of estimating the individual channel rather than only estimating the cascaded channel. However, when SIR_r increases, the gap between the equalizer and matched filter decreases since RSI becomes rather small and the ISI effect can be ignored.

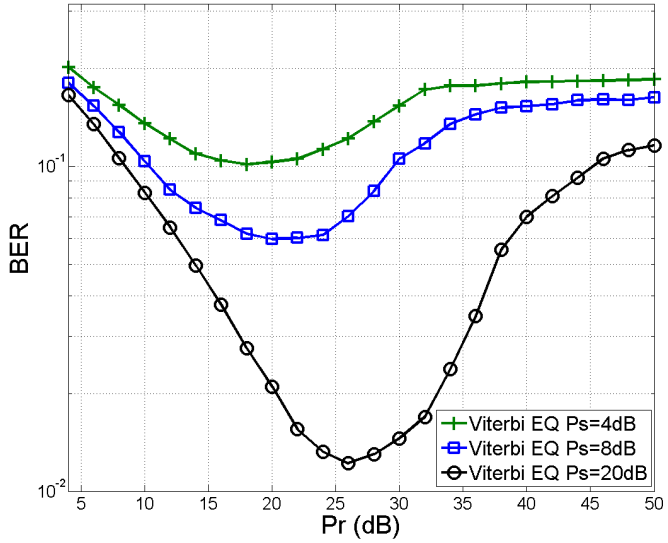

Figure 4.9: BER performance for different combinations of P_{r} and P_{s} - increasing P_{s} always helps to improve the BER but increasing P_{r} does not; BER first decreases and then increases since the RSI also increases with P_{r}.

Figure 4.9 shows the BER performance varying with P_{r}. For a fixed P_{s}, the BER first reduces and then goes up with increasing P_{r}. The destination source will have high SNR when the relay transmits with large P_{r} so increasing it helps to improve the BER performance. However, continuing to increase P_{r} results in worse BER because the RSI power is also related to P_{r} and the desired signal is overwhelmed by interference when P_{r} is too large. On the other hand, for a fixed P_{r}, increasing P_{s} always reduces the BER because the $\mathrm{SIR}_{\mathrm{r}}$ is proportional to P_{s}. In summary, increasing P_{s} always helps to improve the BER but increasing P_{r} does not; BER first decreases and then increases since the RSI also increases with P_{r}.

4.6 Conclusion

The one-block training schemes and two baselines for FD TWR are proposed in this chapter to obtain the CSI in the presence of RSI. With one-block training scheme, an ML estimator is derived to estimate the cascaded channel, individual

channel as well as the RSI channel simultaneously. The BFGS algorithm is used in the calculation of the ML estimator. The initialization and convergence of the algorithm are also discussed. The two baselines including the multi-block training scheme with LS estimator and the cross-correlation method are proposed for comparison. The CRBs for the three schemes are derived. By using the asymptotic properties of Toeplitz matrices, how the channel parameters and transmit powers affect the Fisher information is analyzed. We also showed analytically that the Fisher information of exploiting the structure of the channel taps is greater than that of treating the taps as individual variables.

Chapter 5

CHANNEL ESTIMATION IN FULL-DUPLEX ONE-WAY RELAYS

In this chapter, we consider an AF FD one-way relay system with only the relay working in FD mode. The RSI in the relay propagates to the destination, creating an end-to-end ISI channel. We further cancel the RSI at the destination by estimating the RSI channel and applying equalization. The one-way relay system model is simpler than the TWR model which is more analytic when considering the effect of RSI. In the previous chapter we analyze the Fisher information while in this chapter we further analyze the CRB in closed-form expression. We are able to minimize the CRB and find the optimal training sequence. Besides, we also extend our training method to the case when the channels between nodes are frequency-selective and the case of multiple relay systems.

5.1 System Model

We consider a system consisting of a source, a relay, and a destination, without any direct link between the source and the destination, as shown in Figure 5.1. AF relaying protocol is adopted. The relay uses two antennas, one receiving the current symbol while the other one amplifying and forwarding the previously received symbol, to operate in FD mode. The channel coefficients between the source and the relay, and the relay and the destination are h_{sr} and h_{rd} respectively. The two channels between nodes are assumed to be flat fading modeled by independent complex Gaussian random variable with zero means and variances σ_{sr}^2, σ_{rd}^2, respectively. A separate pre-stage is assumed to gather the information of the SI channel to perform analog and digital cancellation methods in the next transmission stage [19, 79]. Dur-

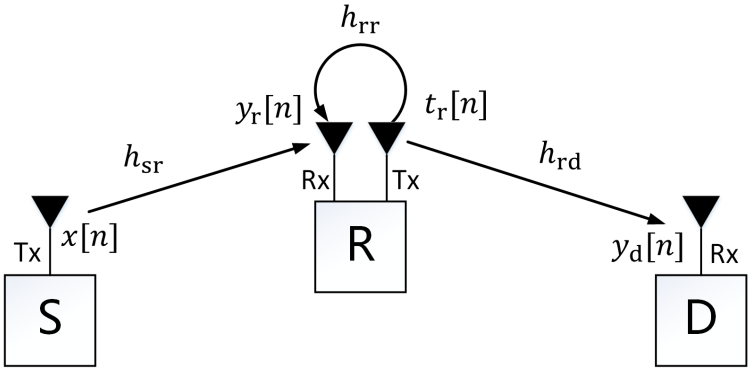

Figure 5.1: An FD one-way relay system - the system consists of a source, a relay, and a destination. The FD relay uses two antennas, one receiving the current symbol while the other one amplifying and forwarding the previously received symbol.

ing the transmission, the SI is reduced in RF with analog cancellation methods until the RSI power falls in the ADC dynamic range, and then is further suppressed by digital methods. However, despite these suppression methods, the RSI is still present at the destination. We consider the RSI as the residual (error) through either analog cancellation only or analog-plus-digital cancellation. The non-zero residual is an unavoidable result of the SIC. Even though the LoS component is largely canceled, the RSI power is still not small enough to be treated as noise, and is often higher than the desired signal power [19, 35]. Moreover, the RSI makes the overall end-to-end channel an ISI channel at the AF relay, even when the channels on all links are flat fading. Thus, estimating the RSI at the destination is needed for equalizers to alleviate the ISI at the destination receiver. In our system model, we assume that $h_{\rm rr}$ is time-invariant and flat fading in one transmission block and varies from block to block. The Gaussian assumption is used in the simulations to generate realizations of the channels for multiple blocks but not in the derivation of our training scheme and analysis.

We assume the processing delay for the relay to forward its received symbols is τ_0 which is an integer multiple of the symbol duration T_s, i.e., $\tau_0 = mT_s$, $m = 1, 2, \cdots$.

The processing delay τ_0 is a deterministic system parameter and can be known at the system design level once the hardware and the SIC approaches are chosen. We can introduce an artificial additional processing delay to make τ_0 an integer multiple of the symbol duration if it is not. With the synchronized signal, the resulting discrete-time equivalent channel model is sparse with zero coefficients and can simplify the analysis. Let the transmit signal at the relay be $t_{\mathrm{r}}[n] = \alpha y_{\mathrm{r}}[n-m]$ where α is a real and positive power scaling factor. We will discuss the choices of it later in this section. At the destination, the received symbol at the nth time interval is

$$\begin{aligned} y_{\mathrm{d}}[n] &= h_{\mathrm{rd}} t[n] + n_{\mathrm{d}}[n] = h_{\mathrm{rd}}(\alpha y_{\mathrm{r}}[n-m]) + n_{\mathrm{d}}[n] \\ &= \sum_{k=1}^{\infty} h\theta^{k-1} x[n-km] + \sum_{k=1}^{\infty} d\theta^{k-1} n_{\mathrm{r}}[n-km] + n_{\mathrm{d}}[n] \quad n = 0, 1, \cdots, \end{aligned} \tag{5.1}$$

where $y_{\mathrm{r}}[n] = h_{\mathrm{sr}} x[n] + \alpha h_{\mathrm{rr}} y_{\mathrm{r}}[n-m] + n_{\mathrm{r}}[n]$ is the nth received symbol at the relay. $x[n]$ is the transmit signal of the source and satisfies $E\big[|x[n]|^2\big] = P_{\mathrm{s}}$ where P_{s} is the transmit power of the source and incorporates the path loss. For brevity, we define $d := \alpha h_{\mathrm{rd}}$, $h := \alpha h_{\mathrm{sr}} h_{\mathrm{rd}}$ and $\theta := \alpha h_{\mathrm{rr}}$. Noise terms $n_{\mathrm{r}}[n]$ and $n_{\mathrm{d}}[n]$ are complex Gaussian with zero mean and variance σ_{r}^2 and σ_{d}^2 respectively. If there is no RSI, the effective end-to-end channel h is the overall channel for the system. However, the SI link θ forms a feedback at the relay, which makes the overall channel a single pole infinite impulse response (IIR) channel and causes ISI. Additionally, the effective noise at the destination is colored with correlations that depend on the pole. The overall IIR channel has channel taps $[\underbrace{h, 0, \cdots, 0}_{m \text{ terms}}, \underbrace{h\theta, 0, \cdots, 0}_{m \text{ terms}}, h\theta^2, 0, \cdots]^T$. We can see that m only affects the position of the non-zero coefficients, which means that m has no effect on calculating the gradients in Section 5.2.2. Moreover, in Section 5.3.2, the zero coefficients have no contribution to (5.28) which is the key component in the CRB analysis. Thus, assuming $m = 1$ is without loss of generality.

The SIC at the relay should be such that $|\theta| < 1$ is possible with proper choice of α. Such α keeps the system stable and guarantees finite average relay transmit power. The average relay transmit power is calculated as

$$\mathrm{E}[t_{\mathrm{r}}[n]t_{\mathrm{r}}^{*}[n]] = \alpha^2 \sum_{k=1}^{\infty} (\alpha^2 |h_{\mathrm{rr}}|^2)^{(k-1)} \left(P_{\mathrm{s}}|h|^2 + \sigma_{\mathrm{r}}^2\right) = \alpha^2 \frac{P_{\mathrm{s}}|h|^2 + \sigma_{\mathrm{r}}^2}{1 - \alpha^2 |h_{\mathrm{rr}}|^2}. \tag{5.2}$$

Define P_{r} as the maximum relay transmit power. The condition for the stability of the system is given by [50]

$$\mathrm{E}[t_{\mathrm{r}}[n]t_{\mathrm{r}}^{*}[n]] \leq P_{\mathrm{r}}, \tag{5.3}$$

where the expectation in (5.3) is with respect to the noise. By solving (5.3), α should satisfy $\alpha^2|h_{\mathrm{rr}}|^2 = |\theta|^2 < 1$. However, in a channel estimation scenario, the expectation value of h_{rr} is used instead of its instantaneous value in α. We can choose α to satisfy a long term condition $\mathrm{E}[\alpha^2|h_{\mathrm{rr}}|^2] < 1$ which leads to $\alpha^2\sigma_{\mathrm{rr}}^2 < 1$. Using the variance of the RSI channel instead of its realizations is a common problem in AF FD relays since the RSI is considered as the residual error which cannot be further estimated after all the self-interference cancellation approaches. Note that RSI channel realization might exceed some threshold. If that happens, α can be adjusted to make the relay transmit with its maximum power. This will lead to clipping and distortions but not instability. In addition, the clipping case happens with small probability since the RSI channel has small variance [19] which limits the dynamic range of the realizations. To further reduce the clipping probability, a fixed power margin between the relay gain power and the maximum power can be made on α to increase the threshold. Therefore, we do not incorporate these distortions in our system model and analysis. Thus, α first normalizes the received signal power, then amplifies the signal power to P_{r}. Such an α is given by

$$\alpha^2 = \frac{P_{\mathrm{r}}}{P_{\mathrm{s}} + P_{\mathrm{r}}\sigma_{\mathrm{rr}}^2 + \sigma_{\mathrm{r}}^2} \quad . \tag{5.4}$$

Since the non-zero coefficients θ^{k-1} at the kth taps of the IIR channel decrease in amplitude with increasing tap index k, we can assume that most of the energy (e.g. 99%) is contained in a finite length of the overall channel impulse response [52]. Define L as the effective length of the overall impulse response which is $h[k] := h\theta^k, k = 0, \cdots, L-1$. Thus, we use a block-based transmission with a guard time of L symbol intervals to avoid inter-block interference [54]. At the receiver, it receives $N+L$ symbols and discards the last L symbols. Without loss of generality, the block length N is assumed to be far greater than L, so the rate loss due to the guard time is negligible. With the effective length L and block-based transmission, we can truncate the IIR channel.

Let $\boldsymbol{H}_\theta$ be the matrix form of the channel in one block, which is given by an $N \times N$ Toeplitz matrix with first column $[1, \theta, \theta^2, \cdots, \theta^{L-1}, 0, \cdots, 0]^T$ and first row $[1, 0, \cdots, 0]$. We rewrite the output in terms of $\boldsymbol{x} := [x[0], \cdots, x[N-1]]^T$ and $\boldsymbol{y} := [y_{\mathrm{d}}[1], \cdots, y_{\mathrm{d}}[N]]^T$ as:

$$\boldsymbol{y} = h\boldsymbol{H}_\theta \boldsymbol{x} + d\boldsymbol{H}_\theta \boldsymbol{n}_{\mathrm{r}} + \boldsymbol{n}_{\mathrm{d}}, \tag{5.5}$$

where $\boldsymbol{n}_{\mathrm{r}}$ and $\boldsymbol{n}_{\mathrm{d}}$ are noise vectors composed of independent samples from the same distribution as $n_{\mathrm{r}}[n]$ and $n_{\mathrm{d}}[n]$ respectively. As can be seen from the matrix expression, $h\boldsymbol{H}_\theta$ is the overall channel and the sum of the last two terms in (5.5) is the colored noise. Thus, the overall channel becomes an ISI channel. In (5.5), we assume distortion of the signal caused by hardware impediment is negligible due to sufficient passive self-interference suppression and analog cancellation in RF [35]. However, if the distortion has to be considered, (5.5) does not change because the distortion can be incorporated as part of the noise. To be specific, the distortion from the transmitter and the receiver are incorporated into the colored noise term $d\boldsymbol{H}_\theta \boldsymbol{n}_{\mathrm{r}}$ and additive noise term $\boldsymbol{n}_{\mathrm{d}}$ respectively [85]. Since we have explicitly labeled the noise variances

of $\boldsymbol{n}_{\mathrm{r}}$ and $\boldsymbol{n}_{\mathrm{d}}$ as σ_{r}^2 and σ_{d}^2 respectively, the incorporation of the distortion can be captured by modifying the noise variance values.

5.2 Channel Estimation

5.2.1 Maximum Likelihood Formulation

We now derive the ML estimator of h and θ for a given training sequence $\boldsymbol{x}$. We are only interested in h and θ since knowing them is enough for detection and equalization. In (5.5) we have three parameters h, θ and d. The coefficients of the desired signal $\boldsymbol{x}$ is $h\boldsymbol{H}_\theta$ which only contain h and θ while d appears in the colored noise term $d\boldsymbol{H}_\theta\boldsymbol{n}_{\mathrm{r}}$. When detecting $\boldsymbol{x}$, d is not necessary. For example, at high SNR, a zero-forcing detector can be used which is obtained by using h and θ to calculate the inverse of $h\boldsymbol{H}_\theta$. We set d as a nuisance parameter and integrate out the nuisance parameter from the likelihood function which is an established method [93] to deal with it in the likelihood function. We have

$$p(\boldsymbol{y}|h,\theta) = \int p(\boldsymbol{y}|h,\theta,d)p(d)\mathrm{d}d. \tag{5.6}$$

Since $p(\boldsymbol{y}|h,\theta,d)$ and $p(d)$ are Gaussian distributed, it is shown in Appendix C that the distribution of $p(\boldsymbol{y}|h,\theta)$ is also Gaussian with mean and covariance matrix

$$\boldsymbol{\mu} = h\boldsymbol{H}_\theta, \tag{5.7}$$

$$\boldsymbol{C} = \alpha^2\sigma_{\mathrm{r}}^2\boldsymbol{H}_\theta\boldsymbol{H}_\theta^H + \sigma_{\mathrm{d}}^2\boldsymbol{I}_N. \tag{5.8}$$

Therefore, the likelihood function of $\boldsymbol{y}$ is

$$p(\boldsymbol{y}|h,\theta) = \frac{1}{\pi^N|\boldsymbol{C}|}\exp\left(-(\boldsymbol{y}-\boldsymbol{\mu})^H\boldsymbol{C}^{-1}(\boldsymbol{y}-\boldsymbol{\mu})\right), \tag{5.9}$$

where $|\boldsymbol{C}|$ denotes the determinant of matrix $\boldsymbol{C}$. The corresponding log-likelihood function is [93]

$$\log p(\boldsymbol{y}|h,\theta) = -N\log\pi - \log|\boldsymbol{C}| - (\boldsymbol{y}-\boldsymbol{\mu})^H\boldsymbol{C}^{-1}(\boldsymbol{y}-\boldsymbol{\mu}). \tag{5.10}$$

Maximizing (5.10) is equivalent to minimizing the last two terms of it. Let f denote our objective function.

$$f(h,\theta) = \log|\boldsymbol{C}| + (\boldsymbol{y}-\boldsymbol{\mu})^H\boldsymbol{C}^{-1}(\boldsymbol{y}-\boldsymbol{\mu}). \tag{5.11}$$

The ML estimator is given by

$$\{\hat{h},\hat{\theta}\} = \arg\min_{h,\theta}\big\{\log|\boldsymbol{C}| + (\boldsymbol{y}-\boldsymbol{\mu})^H\boldsymbol{C}^{-1}(\boldsymbol{y}-\boldsymbol{\mu})\big\}. \tag{5.12}$$

Note that the two parameters are complex. We denote $h = h_x + jh_y$ where h_x and h_y are the real part and imaginary part of h respectively and j is the imaginary unit. Similarly we have $\theta = \theta_x + j\theta_y$. Before we solve the ML estimator, we will simplify the objective function to express it in terms of only one complex parameter θ. First we take derivative of f with respect to h,

$$\frac{\partial f}{\partial h} = -\boldsymbol{y}^H\boldsymbol{C}^{-1}\boldsymbol{H}_\theta\boldsymbol{x} + h^*\boldsymbol{x}^H\boldsymbol{H}_\theta^H\boldsymbol{C}^{-1}\boldsymbol{H}_\theta\boldsymbol{x}. \tag{5.13}$$

Setting the derivative to 0 we have

$$h = (\boldsymbol{x}^H\boldsymbol{H}_\theta^H\boldsymbol{C}^{-1}\boldsymbol{H}_\theta\boldsymbol{x})^{-1}\boldsymbol{x}^H\boldsymbol{H}_\theta^H\boldsymbol{C}^{-1}\boldsymbol{y}. \tag{5.14}$$

We can substitute (5.14) into (5.11) to eliminate h.

The objective function is not convex with respect to θ. To solve the problem numerically, we use the BFGS algorithm [92], which is a popular quasi-Newton method. Note that the constraint $|\theta| < 1$ is imposed to ensure stability in (5.1). Euclidean projection is further applied to $\hat{\theta}$ to ensure that $|\hat{\theta}| < 1$ so that the estimates conform with the stability assumption. Because the algorithm can only deal with real valued parameters, the real and imaginary parts are optimized separately.

5.2.2 BFGS algorithm

We use the BFGS algorithm which is also used in [54] to solve the ML estimator in a different two-way relay context. The algorithm needs the gradients of f with respect to θ_x and θ_y. We derive the gradients in Appendix D. A linear MMSE estimator is used to initialize the BFGS algorithm, which helps the algorithm to converge faster and to reduce the possibility of trapping in a local minimum. We now elaborate on the initialization before we provide the details of the BFGS algorithm.

Pairs of received samples can be used for linear MMSE estimation even though the received samples $\boldsymbol{y}$ are not linear in the desired parameters h and θ. We take two received symbols $y_{\mathrm{d}}[2]$ and $y_{\mathrm{d}}[3]$ to estimate h and θ. For estimating h, the second received symbol at the destination is used, which is

$$y_{\mathrm{d}}[2] = hx[1] + dn_{\mathrm{r}}[1] + n_{\mathrm{d}}[2]. \tag{5.15}$$

The linear MMSE estimator $\hat{h}_0$ is given by [93, Sec. 12.3]

$$\hat{h}_0 = \frac{\alpha^2\sigma_{\mathrm{sr}}^2\sigma_{\mathrm{rd}}^2 x^*[1]y_{\mathrm{d}}[2]}{\alpha^2\sigma_{\mathrm{sr}}^2\sigma_{\mathrm{rd}}^2|x[1]|^2 + \alpha^2\sigma_{\mathrm{rd}}^2\sigma_{\mathrm{r}}^2 + \sigma_{\mathrm{d}}^2}. \tag{5.16}$$

Let $\tilde{h}_0$ be the residual estimation error of h, i.e. $h = \hat{h}_0 + \tilde{h}_0$. Thus, $\tilde{h}_0$ is a random variable with zero mean and variance $\sigma_{\tilde{h}_0}^2$ which is given by

$$\sigma_{\tilde{h}_0}^2 = \frac{\alpha^2\sigma_{\mathrm{sr}}^2\sigma_{\mathrm{rd}}^2(\alpha^2\sigma_{\mathrm{rd}}^2\sigma_{\mathrm{r}}^2 + \sigma_{\mathrm{d}}^2)}{\alpha^2\sigma_{\mathrm{sr}}^2\sigma_{\mathrm{rd}}^2|x[1]|^2 + \alpha^2\sigma_{\mathrm{rd}}^2\sigma_{\mathrm{r}}^2 + \sigma_{\mathrm{d}}^2}. \tag{5.17}$$

After having $\hat{h}_0$, we can estimate θ. First we use $\hat{h}_0$ to remove the known part $\hat{h}_0 x[2]$ in $y_{\mathrm{d}}[3]$. The remaining signal of $y_{\mathrm{d}}[3]$ is as follows:

$$y'_{\mathrm{d}}[3] = \hat{h}_0\theta x[1] + \tilde{h}_0\theta x[1] + \tilde{h}_0 x[2] + hdn_{\mathrm{r}}[1] + dn_{\mathrm{r}}[2] + n_{\mathrm{d}}[3]. \tag{5.18}$$

The linear MMSE estimator of θ is

$$\hat{\theta}_0 = \frac{\hat{h}_0\alpha^2\sigma_{\mathrm{rr}}^2 x^*[1]y'_{\mathrm{d}}[3]}{\hat{h}_0^2\alpha^2\sigma_{\mathrm{rr}}^2|x[1]|^2 + \sigma_{\tilde{h}_0}^2|x[2]|^2 + \sigma_{\tilde{h}_0}^2\alpha^2\sigma_{\mathrm{rr}}^2|x[1]|^2 + \alpha^4\sigma_{\mathrm{sr}}^2\sigma_{\mathrm{rd}}^4\sigma_{\mathrm{r}}^2 + \alpha^2\sigma_{\mathrm{rd}}^2\sigma_{\mathrm{r}}^2 + \sigma_{\mathrm{d}}^2}. \tag{5.19}$$

Though we only make use of one training symbol in the above linear MMSE method, it is possible to extend the method to use multiple symbols, in which case a special training sequence with $L-1$ zeros followed by one symbol is transmitted, where L is the effective length of the channel impulse response.

We now provide the BFGS algorithm which uses the initialization explained above, and the gradients in Appendix D.

Initialize: $\boldsymbol{z}_0 \triangleq [\hat{\theta}_x \ \hat{\theta}_y]^T$, $\boldsymbol{A}_0^{-1} = \boldsymbol{I}_{2\times 2}$.

Repeat until convergence for k: (BFGS)

1. Obtain a search direction $\boldsymbol{p}_k = -\boldsymbol{A}_k^{-1}\nabla f(\boldsymbol{z}_k)$.
2. Find stepsize λ_k by backtracking linesearch, then update $\boldsymbol{z}_{k+1} = \boldsymbol{z}_k + \lambda_k \boldsymbol{p}_k$.
3. Set $\boldsymbol{s}_k = \lambda_k \boldsymbol{p}_k$, $\boldsymbol{v}_k = \nabla f(\boldsymbol{z}_{k+1}) - \nabla f(\boldsymbol{z}_k)$
4. Update the inverse Hessian approximation by

$\boldsymbol{A}_{k+1}^{-1} = \boldsymbol{A}_k^{-1} + \frac{(\boldsymbol{s}_k^T\boldsymbol{v}_k + \boldsymbol{v}_k^T\boldsymbol{A}_k^{-1}\boldsymbol{v}_k)\boldsymbol{s}_k\boldsymbol{s}_k^T}{(\boldsymbol{s}_k^T\boldsymbol{v}_k)^2} - \frac{\boldsymbol{A}_k^{-1}\boldsymbol{v}_k\boldsymbol{s}_k^T + \boldsymbol{s}_k\boldsymbol{v}_k^T\boldsymbol{A}_k^{-1}}{\boldsymbol{s}_k^T\boldsymbol{v}_k}$

Obtain the converged result $\boldsymbol{z}_k$ and construct the estimate $\hat{\theta}$ from it.

If $|\hat{\theta}| > 1$, $\hat{\theta} = \hat{\theta}/|\hat{\theta}|$ (Euclidean projection).

After the initial values are input, the complex parameter θ is optimized by the BFGS algorithm. The iteration is controlled by the index k. The results of one iteration will be used as initial values for the next iteration. Let $\hat{\theta}$ be the estimate of θ and is obtained from $\boldsymbol{z}_k$. In particular, there is a constraint $|\theta| < 1$ on θ. We use Euclidean projection, which in this case is a vector normalization, to keep $\hat{\theta}$ in its valid region. If the result of $\hat{\theta}$ is a point outside of the valid region, Euclidean projection maps the outside point to its nearest valid point. The BFGS algorithm is able to converge since it uses the Hessian approximation matrix to update the search direction. The positive definite property of the Hessian approximation matrix implies

a descent search direction, which guarantees convergence [92]. However, due to the non-convexity of the objective function, the algorithm might be trapped in a local minimum. To avoid this, we use MMSE estimates of the parameters to initialize the algorithm as mentioned above.

The complexity of the algorithm is dominated by the matrix inversion of the covariance matrix $\boldsymbol{C}$ in the calculation of the gradients and the objective function (5.11). For large training length N, $\boldsymbol{C}$ asymptotically becomes to a positive definite Toeplitz matrix. The complexity of inverting it is $O(N \log^2 N)$ [93]. The approximate inverse-Hessian matrix update only depends on the number of parameters to be estimate but not on N. Therefore, the total complexity of the BFGS algorithm in one iteration is $O(N \log^2 N)$ for large N. Moreover, the algorithm with linear MMSE initialization converges faster than random initialization based on our observation in the simulation. Thus, our initialization method also helps to reduce the complexity of the algorithm.

5.3 Optimal Training Sequences

5.3.1 Cramer-Rao Bounds

The CRB is derived not only to show the accuracy of the estimates but also to act as a metric when designing the training sequences. Differentiating the log-likelihood function $\log p(\boldsymbol{y}|h, \theta)$ twice, we can obtain the Fisher information matrix (FIM). Let $\boldsymbol{\xi} = [h\ \theta]^T$ be the vector of parameters. The FIM is given by

$$\boldsymbol{\Gamma}(\boldsymbol{\xi}) = \mathrm{E}\left[\frac{\partial \log p}{\partial \boldsymbol{\xi}^*}\frac{\partial \log p}{\partial \boldsymbol{\xi}^T}\right]. \tag{5.20}$$

The (m, n) element of $\boldsymbol{\Gamma}$ is given by

$$\Gamma_{mn} = \frac{\partial \boldsymbol{\mu}^H}{\partial \xi_m^*}\boldsymbol{C}^{-1}\frac{\partial \boldsymbol{\mu}}{\partial \xi_n} + \mathrm{tr}\left(\boldsymbol{C}^{-1}\frac{\partial \boldsymbol{C}}{\partial \xi_m^*}\boldsymbol{C}^{-1}\frac{\partial \boldsymbol{C}}{\partial \xi_n}\right), \tag{5.21}$$

where ξ_m is the mth element of $\boldsymbol{\xi}$. Thus we have

$$\Gamma_{11} = \frac{\partial \boldsymbol{\mu}^H}{\partial h^*} \boldsymbol{C}^{-1} \frac{\partial \boldsymbol{\mu}}{\partial h} + \mathrm{tr}\left(\boldsymbol{C}^{-1} \frac{\partial \boldsymbol{C}}{\partial h^*} \boldsymbol{C}^{-1} \frac{\partial \boldsymbol{C}}{\partial h} \right) = \boldsymbol{x}^H \boldsymbol{H}_\theta^H \boldsymbol{C}^{-1} \boldsymbol{H}_\theta \boldsymbol{x}. \tag{5.22}$$

Similarly,

$$\begin{aligned} \Gamma_{22} &= \frac{\partial \boldsymbol{\mu}^H}{\partial \theta^*} \boldsymbol{C}^{-1} \frac{\partial \boldsymbol{\mu}}{\partial \theta} + \mathrm{tr}\left(\boldsymbol{C}^{-1} \frac{\partial \boldsymbol{C}}{\partial \theta^*} \boldsymbol{C}^{-1} \frac{\partial \boldsymbol{C}}{\partial \theta} \right) \\ &= |h|^2 \boldsymbol{x}^H \boldsymbol{B}_\theta^H \boldsymbol{C}^{-1} \boldsymbol{B}_\theta \boldsymbol{x} + \alpha^4 \sigma_{\mathrm{r}}^4 \mathrm{tr}\left(\boldsymbol{C}^{-1} \boldsymbol{H}_\theta \boldsymbol{B}_\theta^H \boldsymbol{C}^{-1} \boldsymbol{B}_\theta \boldsymbol{H}_\theta^H \right). \end{aligned} \tag{5.23}$$

Since $\boldsymbol{C}$ is not a function of h,

$$\Gamma_{12} = \frac{\partial \boldsymbol{\mu}^H}{\partial h^*} \boldsymbol{C}^{-1} \frac{\partial \boldsymbol{\mu}}{\partial \theta} = h \boldsymbol{x}^H \boldsymbol{H}_\theta^H \boldsymbol{C}^{-1} \boldsymbol{B}_\theta \boldsymbol{x}, \tag{5.24}$$

$$\Gamma_{21} = \frac{\partial \boldsymbol{\mu}^H}{\partial \theta^*} \boldsymbol{C}^{-1} \frac{\partial \boldsymbol{\mu}}{\partial h} = h^* \boldsymbol{x}^H \boldsymbol{B}_\theta^H \boldsymbol{C}^{-1} \boldsymbol{H}_\theta \boldsymbol{x}. \tag{5.25}$$

The CRB is given by the trace of the inverse of $\boldsymbol{\Gamma}$, which is $CRB_{\boldsymbol{\xi}} = \mathrm{tr}(\boldsymbol{\Gamma}^{-1})$. In particular, the CRBs for each parameter are the diagonal elements of the inverse FIM. Since $\boldsymbol{\Gamma}$ is a 2 by 2 complex matrix, we can find its inverse by calculating its determinant and adjoint. The determinant is $|\boldsymbol{\Gamma}| = \Gamma_{11}\Gamma_{22} - \Gamma_{12}\Gamma_{21}$. Therefore, the CRBs are given by

$$CRB_h = \Gamma_{22}/|\boldsymbol{\Gamma}|, \tag{5.26}$$

$$CRB_\theta = \Gamma_{11}/|\boldsymbol{\Gamma}|. \tag{5.27}$$

5.3.2 Training Sequence Design via the CRB

In this subsection, we analyze the CRB by using theorems for inverses, products, and eigenvalues of Toeplitz matrices derived in [94] about asymptotic behavior of Toeplitz matrix eigenvalues. The CRB is minimized in the regime where the training length N is large. We show that the optimal training sequence that minimizes the CRB is sinusoidal and we characterize the frequency of this sinusoidal. The key idea behind this is that circulant matrices have sinusoidal eigenvectors and the Toeplitz

matrices in the CRB expression can be well approximated by circulant matrices for large N.

To analyze the asymptotic behavior of Toeplitz matrices, we define an $N \times N$ Toeplitz matrix $\boldsymbol{T}_N$ whose elements t_k satisfy $\sum_{k=-\infty}^{\infty} |t_k| < \infty$. According to [94], $\boldsymbol{T}_N$ is equivalent to a circulant matrix as $N \to \infty$, and can be expressed as $\boldsymbol{T}_N(t(\lambda))$ where $t(\lambda) = \sum_{k=-\infty}^{\infty} t_k e^{j\lambda k}$. Now we show that $\boldsymbol{H}_\theta$ is asymptotically equivalent to $\boldsymbol{T}_N(t(\lambda))$. First, since both $\boldsymbol{H}_\theta$ and $\boldsymbol{T}_N(t(\lambda))$ are banded Toeplitz matrices [94, Sec. 4.3], their strong norms (operator norms) are bounded. Secondly, let $t_k = \theta^k$ for $k = 0, \cdots, L-1$ and otherwise $t_k = 0$, we have $\lim_{N\to\infty} ||\boldsymbol{H}_\theta - \boldsymbol{T}_N(t(\lambda))|| = 0$, where $||\boldsymbol{A}||$ denotes the weak norm (Hilbert-Schmidt norm) of matrix $\boldsymbol{A}$. With the two conditions above, we can say that $\boldsymbol{H}_\theta$ and $\boldsymbol{T}_N(t(\lambda))$ are asymptotically equivalent [94, Sec. 2.3]. Therefore, we will write $\boldsymbol{H}_\theta = \boldsymbol{T}_N(t(\lambda))$ which will be understood to hold for asymptotically large N and thus the asymptotic properties which are introduced later can be applied to analyze the CRB. We have the following expression for $t(\lambda)$,

$$t(\lambda) = \sum_{k=0}^{L-1} \theta^k e^{j\lambda k} = \frac{1 - |\theta|^L}{1 - \theta e^{j\lambda}} = \frac{1}{1 - \theta e^{j\lambda}}, \tag{5.28}$$

where the assumption of channel energy $|\theta|^L \approx 0$ is used. The covariance matrix $\boldsymbol{C}$ is

$$\boldsymbol{C} = \alpha^2 \sigma_{\mathrm{r}}^2 \boldsymbol{T}_N(t(\lambda)) \boldsymbol{T}_N(t^*(\lambda)) + \sigma_{\mathrm{d}}^2 \boldsymbol{I}_N. \tag{5.29}$$

Without loss of generality, we set $\sigma_{\mathrm{r}}^2 = \sigma_{\mathrm{d}}^2 = 1$. According to [94], the product of two Toeplitz matrices is a Toeplitz matrix asymptotically, as well as the inverse of a Toeplitz matrix. Thus we have

$$\boldsymbol{C} \approx \alpha^2 \boldsymbol{T}_N(|t(\lambda)|^2) + \boldsymbol{I}_N = \boldsymbol{T}_N(\alpha^2 |t(\lambda)|^2 + 1), \quad \boldsymbol{C}^{-1} \approx \boldsymbol{T}_N\left(\frac{1}{\alpha^2 |t(\lambda)|^2 + 1}\right). \tag{5.30}$$

The Fisher information of the source-relay-destination channel h is

$$\Gamma_{11} = \boldsymbol{x}^H \boldsymbol{H}_\theta^H \boldsymbol{C}^{-1} \boldsymbol{H}_\theta \boldsymbol{x} = \boldsymbol{x}^H \boldsymbol{T}_N(t^*(\lambda)) \boldsymbol{T}_N \left(\frac{1}{\alpha^2 |t(\lambda)|^2 + 1} \right) \boldsymbol{T}_N(t(\lambda)) \boldsymbol{x} \tag{5.31}$$

$$\approx \boldsymbol{x}^H \boldsymbol{T}_N \left(\frac{|t(\lambda)|^2}{\alpha^2 |t(\lambda)|^2 + 1} \right) \boldsymbol{x} = \frac{|t(\lambda)|^2}{\alpha^2 |t(\lambda)|^2 + 1} ||\boldsymbol{x}||^2, \tag{5.32}$$

where $\frac{|t(\lambda)|^2}{\alpha^2 |t(\lambda)|^2 + 1}$ is the eigenvalue of $\boldsymbol{T}_N \left(\frac{|t(\lambda)|^2}{\alpha^2 |t(\lambda)|^2 + 1} \right)$ and depends on λ. Similarly, we can denote $\boldsymbol{B}_\theta = \boldsymbol{T}_N(g(\lambda))$ where $g(\lambda) = \frac{e^{j\lambda}}{(1 - \theta e^{j\lambda})^2}$ is the derivative of $t(\lambda)$ with respect to θ. The Fisher information of the RSI channel can be represented by Toeplitz matrices as

$$\Gamma_{22} = |h|^2 \boldsymbol{x}^H \boldsymbol{B}_\theta^H \boldsymbol{C}^{-1} \boldsymbol{B}_\theta \boldsymbol{x} + \alpha^4 \mathrm{tr} \left(\boldsymbol{C}^{-1} \boldsymbol{H}_\theta \boldsymbol{B}_\theta^H \boldsymbol{C}^{-1} \boldsymbol{B}_\theta \boldsymbol{H}_\theta^H \right) \tag{5.33}$$

$$\approx |h|^2 \boldsymbol{x}^H \boldsymbol{T}_N \left(\frac{|g(\lambda)|^2}{\alpha^2 |t(\lambda)|^2 + 1} \right) \boldsymbol{x} + \alpha^4 \mathrm{tr} \left(\boldsymbol{T}_N \left(\frac{|g(\lambda)|^2 |t(\lambda)|^2}{(\alpha^2 |t(\lambda)|^2 + 1)^2} \right) \right) \tag{5.34}$$

$$= |h|^2 \frac{|g(\lambda)|^2}{\alpha^2 |t(\lambda)|^2 + 1} ||\boldsymbol{x}||^2 + \alpha^4 \frac{||\boldsymbol{x}||^2}{2\pi P_\mathrm{s}} \int_0^{2\pi} \frac{|g(\lambda)|^2 |t(\lambda)|^2}{(\alpha^2 |t(\lambda)|^2 + 1)^2} \mathrm{d}\lambda. \tag{5.35}$$

We can simplify the first term in (5.35) similarly to Γ_{11}. The second term comes from the fact that the trace of Toeplitz matrices is equal to the integral of the function of λ that characterizes it [94]. Simplifying this integral we have

$$\int_0^{2\pi} \frac{|g(\lambda)|^2 |t(\lambda)|^2}{(\alpha^2 |t(\lambda)|^2 + 1)^2} \mathrm{d}\lambda = \int_0^{2\pi} \frac{1}{|1 - \theta e^{j\lambda}|^2 (\alpha^2 + |1 - \theta e^{j\lambda}|^2)^2} \mathrm{d}\lambda. \tag{5.36}$$

In our FD relay system, we assume $P_\mathrm{r} \gg P_\mathrm{s}$ since P_s is the transmit power at the source which incorporates the path loss. Thus $\alpha^2 \gg 1$. Note that since $|\theta| < 1$, we have $\alpha^2 \gg |1 - \theta e^{j\lambda}|^2$. We can approximate the integral as

$$\begin{aligned} &\frac{1}{2\pi} \int_0^{2\pi} \frac{1}{|1 - \theta e^{j\lambda}|^2 (\alpha^2 + |1 - \theta e^{j\lambda}|^2)^2} \mathrm{d}\lambda \\ &\approx \frac{1}{2\pi} \int_0^{2\pi} \frac{1}{|1 - \theta e^{j\lambda}|^2 \alpha^4} \mathrm{d}\lambda = \frac{1}{\alpha^4} \frac{1}{(|\theta| + 1)\big||\theta| - 1\big|}. \end{aligned} \tag{5.37}$$

Therefore, the Fisher information of the RSI channel θ becomes

$$\Gamma_{22} = \frac{|h|^2 |g(\lambda)|^2}{\alpha^2 |t(\lambda)|^2 + 1} ||\boldsymbol{x}||^2 + \frac{1}{P_\mathrm{s}(|\theta| + 1)\big||\theta| - 1\big|} ||\boldsymbol{x}||^2. \tag{5.38}$$

Similarly, we can represent Γ_{12} and Γ_{21} as

$$\Gamma_{12} = h\boldsymbol{x}^H \boldsymbol{B}_\theta^H \boldsymbol{C}^{-1} \boldsymbol{H}_\theta \boldsymbol{x} \approx \boldsymbol{x}^H \boldsymbol{T}_N \left(\frac{ht(\lambda)g^*(\lambda)}{\alpha^2 t(\lambda)|^2 + 1} \right) \boldsymbol{x}, \tag{5.39}$$

$$\Gamma_{21} = h^*\boldsymbol{x}^H \boldsymbol{H}_\theta^H \boldsymbol{C}^{-1} \boldsymbol{B}_\theta \boldsymbol{x} \approx \boldsymbol{x}^H \boldsymbol{T}_N \left(\frac{h^*t^*(\lambda)g(\lambda)}{\alpha^2 |t(\lambda)|^2 + 1} \right) \boldsymbol{x}. \tag{5.40}$$

To calculate the CRB, we need the product of Γ_{12} and Γ_{21} which is

$$\Gamma_{12}\Gamma_{21} = |h|^2 \frac{p^2(\lambda)}{(\alpha^2|t(\lambda)|^2 + 1)^2} ||\boldsymbol{x}||^4. \tag{5.41}$$

where $p(\lambda) = \frac{1}{2}[t^*(\lambda)g(\lambda) + t(\lambda)g^*(\lambda)]$. Function $p(\lambda)$ is the real part of $t^*(\lambda)g(\lambda)$ and it shows that only the symmetric part of the Toeplitz matrix affects the product. Thus, the CRB of θ is

$$CRB_\theta = \frac{\Gamma_{11}}{\Gamma_{11}\Gamma_{22} - \Gamma_{12}\Gamma_{21}} = \frac{1}{\Gamma_{11}\Gamma_{22} - \Gamma_{12}\Gamma_{21}} \boldsymbol{x}^H \boldsymbol{T}_N \left(\frac{|t(\lambda)|^2}{\alpha^2|t(\lambda)|^2 + 1} \right) \boldsymbol{x}. \tag{5.42}$$

Minimizing (5.42) is to find a eigenvalue of $\boldsymbol{T}_N(\frac{|t(\lambda)|^2}{\alpha^2|t(\lambda)|^2+1})$ which depends on λ. Note that the term $\Gamma_{11}\Gamma_{22} - \Gamma_{12}\Gamma_{21}$ also depends on λ, the minimization of (5.42) is only through λ and the optimal training sequence is the corresponding eigenvector. Since $\boldsymbol{T}_N(\frac{|t(\lambda)|^2}{\alpha^2|t(\lambda)|^2+1})$ is asymptotically equivalent to a circulant matrix, the eigenvector is sinusoidal. Plug (5.32), (5.38), and (5.41) into (5.42),

$$\begin{aligned} CRB_\theta &= \frac{1}{||\boldsymbol{x}||^2} \frac{|t(\lambda)|^2(\alpha^2|t(\lambda)|^2 + 1)}{|h|^2|t(\lambda)|^2|g(\lambda)|^2 + A|t(\lambda)|^2(\alpha^2|t(\lambda)|^2 + 1) - |h|^2|p(\lambda)|^2} \\ &\triangleq \frac{1}{||\boldsymbol{x}||^2} F(\lambda), \end{aligned} \tag{5.43}$$

where $A = (P_{\mathrm{s}}(|\theta| + 1)\big||\theta| - 1\big|)^{-1}$. To find the frequency of the sinusoidal training sequence, we minimize the $F(\lambda)$ in (5.43) with $\lambda \in [0, 2\pi]$. Simplifying $F(\lambda)$ we have

$$F(\lambda) = \frac{\alpha^2 + |1 - \theta e^{j\lambda}|^2}{\frac{|h|^2}{|1-\theta e^{j\lambda}|^2} + A(\alpha^2 + |1 - \theta e^{j\lambda}|^2) - \frac{1}{4}|h|^2 \frac{(\mathrm{Re}[e^{j\lambda} - \theta^*])^2}{|1-\theta e^{j\lambda}|^4}}. \tag{5.44}$$

Let $z = |1 - \theta e^{j\lambda}|^2$ and $z \in [(1 - |\theta|^2), (1 + |\theta|)^2]$. Substitute it into $F(\lambda)$, we have

$$G(z) = \frac{\alpha^2 + z}{\frac{|h|^2}{z} + A(\alpha^2 + z) - \frac{|h|^2}{4z^2} \left(\frac{(1+|\theta|^2-z)\theta_x}{2|\theta|^2} + \sqrt{1 - \frac{(1+|\theta|^2-x)^2}{4|\theta|^2}} \frac{\theta_y}{|\theta|} - \theta_x \right)^2}, \tag{5.45}$$

where θ_x and θ_y are the real and imaginary parts of θ respectively.

The optimal solution that minimizes $F(\lambda)$ can be found by numerically solving $G'(z) = 0$ which can be rewritten as a polynomial in z with highest order 8. The coefficients of the polynomial are given in Appendix E. Note that $z \in [(1-|\theta|^2), (1+\theta)^2]$, so that the two endpoints of the interval are also candidates for the optimal solution in case that the only solution to $G'(z) = 0$ is a saddle point or there is no solution in the interval. After we get all the candidates (of which there are a maximum of 8), we are able to substitute each of them into $G(z)$ to find the one that minimizes the function. Since the Toeplitz matrices asymptotically behave equivalently to circulant matrices according to Lemma 4.2 in [94], the same way for circulant matrices can be used to find the corresponding eigenvector for Toeplitz matrices. Assume the solution that minimizes CRB_θ is λ^*, the corresponding optimal training sequence is given by $\frac{1}{\sqrt{N}}[1, \cdots, e^{j2\pi k\lambda^*}, \cdots, e^{j2\pi(N-1)\lambda^*}]^T$ for $k = 0, \cdots, N-1$.

The CRB for h can be also derived the same way as the CRB of θ,

$$CRB_h = \frac{1}{||\boldsymbol{x}||^2} \frac{|h|^2|g(\lambda)|^2(\alpha^2|t(\lambda)|^2+1) + A(\alpha^2|t(\lambda)|^2+1)^2}{|h|^2|t(\lambda)|^2|g(\lambda)|^2 + A|t(\lambda)|^2(\alpha^2|t(\lambda)|^2+1) - |h|^2|p(\lambda)|^2}. \tag{5.46}$$

It can also be minimized by finding the roots of a polynomial. Note that when minimizing the CRB for θ, it is not guaranteed that the CRB of h is minimized as well. However, we can minimize the sum of CRBs of θ and h if both parameters are considered, also through polynomial rooting.

The optimal training sequence depends on both of the channel h and θ through λ. In practice, we do not have the information of h and θ until the first training sequence is sent. We can apply an adaptive training method where the optimal training sequence is designed by using estimates obtained from its previous training sequence. In what follows we show through an approximation that the minimizer of (5.45) only weakly depends on h.

5.3.3 Low Complexity Approximation

The optimal solution can be found by minimizing the CRB numerically via finding the polynomial roots. However, the complexity can be reduced by a certain approximation which we now describe. This provides an approximately optimal and practical solution for the problem. Assume $|\theta|$ is small, so that the value of x is very close to 1. Then we can have the following approximation

$$\left(\frac{(1+|\theta|^2-z)\theta_x}{2|\theta|^2}+\sqrt{1-\frac{(1+|\theta|^2-z)^2}{4|\theta|^2}}\frac{\theta_y}{|\theta|}-\theta_x\right)^2 \approx 1\ . \tag{5.47}$$

Thus,

$$G(z) \approx \frac{\alpha^2+z}{\frac{|h|^2}{z}+A(\alpha^2+z)-\frac{|h^2|}{4z^2}}\ . \tag{5.48}$$

Solving $G'(x)=0$ is equivalent to solving the following equation:

$$8|h^2|z^3+(4\alpha^2-3)|h|^2z^2-2\alpha^2|h|^2z=0. \tag{5.49}$$

Equation (5.49) shows that h does not affect the solution of $G'(z)=0$. One can verify that none of the three real roots of (5.49) is in the valid interval of z which is $[(1-|\theta|)^2,(1+|\theta|)^2]$. Note that $G(z)$ is an increasing function since $|h|^2>0$. Therefore the approximately optimal solution is the left endpoint of the interval i.e. $z=(1-|\theta|)^2$. Thus, $\lambda=-\angle\theta$ where $\angle$ represents the phase of a complex number. Moreover, the channel $|h|$ does not affect the solution of z, so that the training sequence for estimating θ only depends on θ and not $|h|$, making it easier to implement than the optimal training sequence. The normalized corresponding training sequence is given by $\frac{1}{\sqrt{N}}[1,\cdots,e^{j2\pi k\lambda_1^*},\cdots,e^{j2\pi(N-1)\lambda_1^*}]^T$ for $k=0,\cdots,N-1$ where λ_1^* minimizes (5.48).

5.4 Frequency-Selective Channels

In this section, we extend our channel estimation method to the case where the channels between nodes are frequency-selective fading. We show that our training method and CRB calculation can be extended to this case based on our analysis of the basic one-way relay system.

We assume the source-to-relay and relay-to-destination channels are frequency-selective fading with channel taps

$$\begin{aligned} \boldsymbol{h}_{\mathrm{sr}} &= [h_{\mathrm{sr}}[1], h_{\mathrm{sr}}[2], \cdots, h_{\mathrm{sr}}[L_1]], \\ \boldsymbol{h}_{\mathrm{rd}} &= [h_{\mathrm{rd}}[1], h_{\mathrm{rd}}[2], \cdots, h_{\mathrm{rd}}[L_2]], \end{aligned} \tag{5.50}$$

respectively. Therefore, with block based transmission, the channel matrix for the source-to-relay channel $\boldsymbol{H}_{\mathrm{sr}}$ is an $N \times N$ Toeplitz matrix with the first column $[\boldsymbol{h}_{\mathrm{sr}}^T, 0, \cdots, 0]^T$ and the first row $[1, 0, 0, \cdots, 0]$. For the relay-to-destination channel, the channel matrix $\boldsymbol{H}_{\mathrm{rd}}$ is also an $N \times N$ Toeplitz matrix with the first column $[\boldsymbol{h}_{\mathrm{rd}}^T, 0, \cdots, 0]^T$ and the first row $[1, 0, 0, \cdots, 0]$. The received signal for the training phase is similar to (5.5) and becomes

$$\boldsymbol{y}_{\mathrm{f}} = \alpha_{\mathrm{f}} \boldsymbol{H}_{\mathrm{rd}} \boldsymbol{H}_{\theta} \boldsymbol{H}_{\mathrm{sr}} \boldsymbol{x} + \alpha_{\mathrm{f}} \boldsymbol{H}_{\mathrm{rd}} \boldsymbol{H}_{\theta} \boldsymbol{n}_{\mathrm{r}} + \boldsymbol{n}_{\mathrm{d}}, \tag{5.51}$$

where α_{f} is the new power scaling factor for the frequency-selective channel given by

$$\alpha_{\mathrm{f}}^2 = \frac{P_{\mathrm{r}}}{P_{\mathrm{s}}(\sum_{i=1}^{L_1} \sigma_{\mathrm{sr}i}^2) + P_{\mathrm{r}}\sigma_{\mathrm{rr}}^2 + \sigma_{\mathrm{r}}^2} \quad . \tag{5.52}$$

where $\sigma_{\mathrm{sr}i}^2$ is the variance of the ith source-to-relay channel tap. The overall channel is $\alpha_{\mathrm{f}} \boldsymbol{H}_{\mathrm{rd}} \boldsymbol{H}_{\theta} \boldsymbol{H}_{\mathrm{sr}}$ in the frequency-selective case instead of $h\boldsymbol{H}_{\theta}$ for flat fading.

To extend our training method, we can use the theorem for products of Toeplitz matrices which is explained in Section 5.3.2 to approximate the overall channel matrix as a Toeplitz matrix. According to the theorem, when the training length is large,

the product of two Toeplitz matrices is still a Toeplitz matrix and the elements of the product can be determined by the elements of the two matrices. Similar to the way we define $\boldsymbol{H}_\theta = \boldsymbol{T}_N(t(\lambda))$ for large N, we can define $\boldsymbol{H}_{\rm sr} = \boldsymbol{T}_N(q(\lambda))$ and $\boldsymbol{H}_{\rm rd} = \boldsymbol{T}_N(p(\lambda))$, where $q(\lambda) = \sum_{k=0}^{L_1-1} h_{\rm sr}[k+1]e^{j\lambda k}$ and $p(\lambda) = \sum_{k=0}^{L_2-1} h_{\rm rd}[k+1]e^{j\lambda k}$. Thus, the overall channel matrix is

$$\boldsymbol{H}_{\rm f} = \boldsymbol{H}_{\rm rd}\boldsymbol{H}_\theta\boldsymbol{H}_{\rm sr} = \alpha_{\rm f}\boldsymbol{T}_N(p(\lambda))\boldsymbol{T}_N(t(\lambda))\boldsymbol{T}_N(q(\lambda)) \approx \alpha_{\rm f}\boldsymbol{T}_N(p(\lambda)t(\lambda)q(\lambda)). \quad (5.53)$$

$\boldsymbol{H}_{\rm f}$ is also a Toeplitz matrix. Assume the elements in its first column are $h_{\rm f}[k]$ for $k = 1, 2, \cdots, N$, we have

$$h_{\rm f}[k] = \alpha_{\rm f}\frac{1}{2\pi}\int_0^{2\pi} p(\lambda)t(\lambda)q(\lambda)e^{-jk\lambda}{\rm d}\lambda. \quad (5.54)$$

The parameters to be estimated are $h_{\rm f}[k]$ for $k = 1, 2, \cdots, L_{\rm f}$ where $L_{\rm f} = L_1+L_2+L-2$. Assume $\boldsymbol{\xi}_{\rm f} = [h_{\rm f}[1], \cdots, h_{\rm f}[L_{\rm f}]]^T$, our ML estimator can be extended to estimate $\boldsymbol{\xi}_{\rm f}$ by the following. First $h_{\rm f}[1]$ has the same position as h in (5.12). Then using $h_{\rm f}[i+1]$ replace θ^i in (5.12). Thus, our ML method can be applied to estimate the overall channel even in the frequency-selective setup.

The Fisher information for the frequency-selective can be obtained similarly to the flat fading case by using

$$\Gamma^{\rm (f)}_{mn} = \frac{\partial\boldsymbol{\mu}_{\rm f}^H}{\partial\xi_{{\rm f}m}^*}\boldsymbol{C}_{\rm f}^{-1}\frac{\partial\boldsymbol{\mu}_{\rm f}}{\partial\xi_{{\rm f}n}} + {\rm tr}\left(\boldsymbol{C}_{\rm f}^{-1}\frac{\partial\boldsymbol{C}_{\rm f}}{\partial\xi_{{\rm f}m}^*}\boldsymbol{C}_{\rm f}^{-1}\frac{\partial\boldsymbol{C}_{\rm f}}{\partial\xi_{{\rm f}n}}\right), \quad (5.55)$$

where $\boldsymbol{\mu}_{\rm f} = \boldsymbol{H}_{\rm f}\boldsymbol{x}$ and $\boldsymbol{C}_{\rm f} = \alpha_{\rm f}^2\sigma_{\rm r}^2\boldsymbol{H}_{\rm rd}\boldsymbol{H}_\theta\boldsymbol{H}_\theta^H\boldsymbol{H}_{\rm rd}^H + \sigma_{\rm d}^2\boldsymbol{I}_N$. The CRBs are given by the diagonal elements of the inverse of the Fisher information matrix $\boldsymbol{\Gamma}^{\rm (f)}$. If desired, a single scalar quantity representing the overall CRB can be computed by find the trace of this matrix: $CRB_{\boldsymbol{\xi}_{\rm f}} = {\rm tr}\left((\boldsymbol{\Gamma}^{\rm (f)})^{-1}\right)$.

5.5 Multiple Relays

The multi-relay case is also an intuitive extension from the basic one-way relay system. With the analysis for the one-way relay, we can modify the estimation method

and CRB analysis. In the multi-relay case, the distance between the source and the destination is fixed. The relays are placed in an equally-spaced manner in series between the source and the destination. Assume there are M relays which satisfy $M(L-1) < N$ (There is a guard time of $L-1$ symbols for each relay). Each relay works in FD mode with AF relay protocol. The relays have their own RSI, and they do not perform estimation or equalization to keep relay complexity low. The estimation and equalization are performed only at the destination. The channel between the $(i-1)$th relay and the ith relay is flat fading with coefficients h_i for $i = 2, 3, \cdots, M$. The channels from the source to the first relay and from the last relay to the destination are h_1 and h_{M+1}. Channel coefficients h_i for $i = 1, \cdots, M+1$ are Gaussian random variables with zero-mean and variance σ_h^2. Each relay has its own RSI channel $h_{\mathrm{rr}i}$ and power scaling factor α_i which is given by

$$\alpha_i^2 = \frac{P_{\mathrm{r}}}{P_{\mathrm{s}_i}\sigma_h^2 + P_{\mathrm{r}}\sigma_{\mathrm{rr}}^2 + \sigma_{\mathrm{r}}^2}, \tag{5.56}$$

where P_{s_i} is the received power of the desired signal at the ith relay. We also assume all the relays have the same average transmit power P_{r} and average RSI power for simplicity.

The distance between the source and the destination is fixed in our model and M relays are placed in the line between the source and the destination in an equally spaced manner. Assume the distance between the source and the destination is normalized and the corresponding path loss is K dB. Then by using a simplified path loss model [95], the path loss between two relays is

$$K_m dB = KdB + 10\gamma \log_{10}(M+1), \tag{5.57}$$

where γ is the path loss exponent. We incorporate the path loss into h_i which leads to $\sigma_h^2 = 1/K_m$ and $P_{\mathrm{s}_i} = P_{\mathrm{r}}K(M+1)^{\gamma}$.

The transmit signal at the mth relay is

$$\boldsymbol{y}_m = \prod_{i=1}^{m} (\alpha_i h_i \boldsymbol{H}_{\theta i})\, \boldsymbol{x} + \sum_{i=1}^{m} \left[\left(\prod_{n=i+1}^{m} \alpha_n h_n \prod_{n=i}^{m} \boldsymbol{H}_{\theta n} \right) \boldsymbol{n}_{\mathrm{r}i} \right], \tag{5.58}$$

where $\boldsymbol{H}_{\theta i}$ is the RSI channel at the ith relay defined similarly as $\boldsymbol{H}_\theta$ with $\theta_i = \alpha_i h_{\mathrm{rr}i}$, and $\boldsymbol{n}_{\mathrm{r}i}$ is the additive Gaussian white noise at the ith relay. The received signal at the destination from the mth relay is given by

$$\boldsymbol{y}_{\mathrm{d}} = h_{M+1}\boldsymbol{y}_M + \boldsymbol{n}_{\mathrm{d}} = h_{M+1} \prod_{i=1}^{M} (\alpha_i h_i \boldsymbol{H}_{\theta i})\, \boldsymbol{x} + \sum_{i=1}^{M} \left[\left(\prod_{n=i+1}^{m} \alpha_n h_n \prod_{n=i}^{m} \boldsymbol{H}_{\theta n} \right) \boldsymbol{n}_{\mathrm{r}i} \right] + \boldsymbol{n}_{\mathrm{d}}. \tag{5.59}$$

Define $\boldsymbol{H}^{(n)} = \prod_{i=n}^{M} \boldsymbol{H}_{\theta i}$ and its corresponding function $t^{(n)}(\lambda)$. By using the property of product of Toeplitz matrix for large N, we have

$$\boldsymbol{H}^{(n)} = \prod_{i=n}^{M} \boldsymbol{T}(t_{\theta_i}(\lambda)) = \boldsymbol{T}\left(\prod_{i=n}^{M} t_{\theta_i}(\lambda) \right), \tag{5.60}$$

where $t_{\theta_i}(\lambda)$ is defined the same as (5.28) with θ_i. $\boldsymbol{H}^{(n)}$ is also a Toeplitz matrix and the elements in its first row defined through an inverse Fourier transform

$$h_k^{(n)} = \frac{1}{2\pi} \int_0^{2\pi} t^{(n)}(\lambda) e^{-jk\lambda} d\lambda, \tag{5.61}$$

where $t^{(n)}(\lambda) = \prod_{i=n}^{M} t_{\theta_i}(\lambda)$. Thus, we can approximate $\boldsymbol{y}_{\mathrm{d}}$ for large N as

$$\boldsymbol{y}_{\mathrm{d}} = z_M \boldsymbol{H}^{(1)} \boldsymbol{x} + \sum_{i=1}^{M} \left[\left(\prod_{n=i}^{M} \alpha_n h_n \right) / (\alpha_i h_i) \boldsymbol{H}^{(i)} \boldsymbol{n}_{\mathrm{r}i} \right] + \boldsymbol{n}_{\mathrm{d}}, \tag{5.62}$$

where $z_M = h_{M+1} \prod_{i=1}^{M} \alpha_i h_i$. The first row of $\boldsymbol{H}^{(1)}$ is $[1, h_2^{(1)}, \cdots, h_{M(L-1)}^{(1)}, 0, \cdots, 0]^T$ which is an $N \times 1$ vector (Assume $M(L-1) < N$). The channel parameters to be estimated is $\boldsymbol{\xi}_M = [z_M, h_2^{(1)}, h_3^{(1)}, \cdots, h_{M(L-1)}^{(1)}]^T$. The superscript of $h_m^{(n)}$ means the overall channel is the channel from the nth relay to the last relay while the subscript means the index of the taps of the overall ISI channel, i.e. the index of elements of $\boldsymbol{\xi}_M$. The signal model of (5.62) is the same to that of (5.51) except additional noise terms.

We can also extend our ML estimator to estimate the channel parameters using the same way in the frequency-selective case where z_M and $h_k^{(1)}$ are analogous to h and θ^k in (5.51) respectively. The advantage of estimating the multi-relay channel at the destination rather than at each relay is to keep the relays low complexity with just analog signal processing capability. However, the performance is better if estimation and equalization are performed at each relay, at the cost of complexity.

The CRB for multiple relays can be derived and analyzed similarly to the single relay case. We derive the CRBs for the first two strongest channel taps z_M and $h_2^{(1)}$ which dominate the data detection. The CRBs for other parameters can also be found similarly to (5.55). The CRB of $h_2^{(1)}$ is given by

$$CRB_{h_2^{(1)}} = \frac{|t^{(M)}(\lambda)|^2|(\sum_{i=1}^{M}|c_i|^2|t_{\theta_i}(\lambda)|^2+1)}{J_1\left(\sum_{i=1}^{M}|c_i|^2|t_{\theta_i}(\lambda)|^2+1\right)+||\boldsymbol{x}||^2||z_M||^2J_2}, \tag{5.63}$$

where $c_i = \prod_{n=i}^{M}\alpha_n h_n/(\alpha_i h_i)$ and

$$J_1 = |c_1|^4\frac{1}{2\pi}\int_0^{2\pi}\frac{|t^{(M)}(\lambda)|^2|g^{(M)}(\lambda)|^2}{(\sum_{i=1}^{M}|c_i|^2|t_{\theta_i}(\lambda)|^2+1)^2}, \tag{5.64}$$

$$J_2 = |t^{(M)}(\lambda)|^2|g^{(M)}(\lambda)|^2 - |p^{(M)}(\lambda)|^2. \tag{5.65}$$

Define the following functions

$$g^{(M)}(\lambda) = \frac{\partial t^{(M)}(\lambda)}{\partial\lambda}, \tag{5.66}$$

$$p^{(M)}(\lambda) = \frac{1}{2}\left[(t^{(M)}(\lambda))^* g^{(M)}(\lambda) + t^{(M)}(\lambda)(g^{(M)}(\lambda))^*\right]. \tag{5.67}$$

For z_M we have

$$CRB_{z_M} = \frac{[|z_M|^2|g^{(M)}(\lambda)|^2| + J_1(\sum_{i=1}^{M}|c_i|^2|t_{\theta_i}(\lambda)|^2+1)](\sum_{i=1}^{M}|c_i|^2|t_{\theta_i}(\lambda)|^2+1)}{J_1\left(\sum_{i=1}^{M}|c_i|^2|t_{\theta_i}(\lambda)|^2+1\right)+||\boldsymbol{x}||^2||z_M||^2J_2}. \tag{5.68}$$

We further approximate the CRBs and have simple expressions to find how the number of relays affects the CRBs. From (5.28) we have $|t_{\theta_i}(\lambda)| \approx 1$ for small θ_i.

We also assume the training power is large so that $J \ll ||\boldsymbol{x}||^2$. Therefore, the CRB becomes

$$CRB_{h_2^{(1)}} \approx \frac{\sum_{i=1}^{M} |c_i|^2 + 1}{|z_M|^2 ||\boldsymbol{x}||^2}, \quad CRB_{z_M} \approx \frac{\sum_{i=1}^{M} |c_i|^2 + 1}{||\boldsymbol{x}||^2}. \tag{5.69}$$

By plugging in $|c_i|^2 = (\alpha_i^2)^{M-i} \prod_{n=i+1}^{M} |h_i|^2$, and $\alpha_i^2 = \frac{P_{\mathrm{r}}}{P_{\mathrm{r}} K (M+1)^{\gamma} + P_{\mathrm{r}} \sigma_{\mathrm{rr}}^2 + 1}$, we have the CRB expressions as a function of M.

$$CRB_{h_2^{(1)}} = \frac{\sum_{i=1}^{M} (K(M+1)^{\gamma} + k_1)^{i-M} (\prod_{n=i+1}^{M} |h_i|^2)^{i-M} + 1}{||\boldsymbol{x}||^2 (L(M+1)^{\gamma} + k_1)^{-M} \prod_{n=i+1}^{M} |h_i|^2}, \tag{5.70}$$

$$CRB_{z_M} = \frac{\sum_{i=1}^{M} (K(M+1)^{\gamma} + k_1)^{i-M} (\prod_{n=i+1}^{M} |h_i|^2)^{i-M} + 1}{||\boldsymbol{x}||^2}. \tag{5.71}$$

where $k_1 = \sigma_{\mathrm{rr}}^2 + 1/P_{\mathrm{r}}$. Equation (5.70) and (5.71) are simple functions of M. Intuitively, the estimates of z_M will become more inaccurate as the noise goes strong for increasing M. However, as the number of relays increases, the RSI for each relay accumulates at the destination, which makes the RSI channel $h_2^{(1)}$ stronger and easier to estimate. Thus there is an optimal M which minimizes the sum MSE of z_M and $h_2^{(1)}$. Since M is an integer and is not quite large, the optimal number of relays with respect to the minimum sum CRBs of (5.70) and (5.71) can be found by searching over M.

5.6 Numerical Results

We first simulate the performance of the proposed ML estimator and compare it with the corresponding CRBs. We set $P_r = 30$ dB and $\sigma_{\mathrm{rr}}^2 = -10$ dB. For the channels we set $\sigma_{\mathrm{sr}}^2 = \sigma_{\mathrm{rd}}^2 = 1$ and the realization of h_{sr} and h_{rd} are drawn from their distributions. The variances of noise at the relay and the destination are set to 1. For each block we estimate the channels and calculate the mean squared error (MSE) which is averaged over multiple independent realizations of the channels. The training length is $N = 140$ according to the LTE FDD downlink standard.

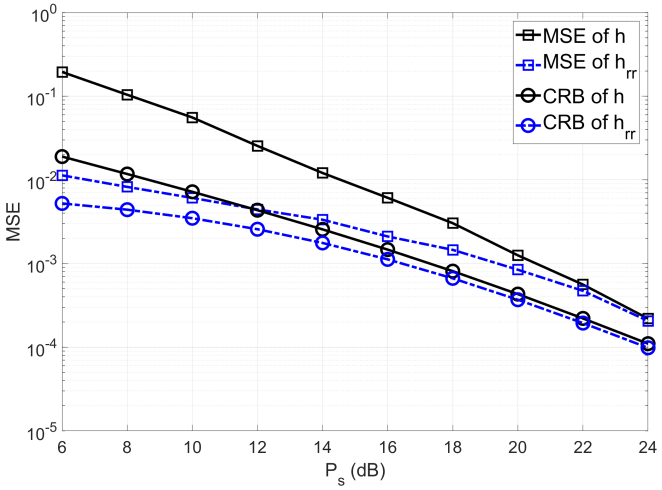

Figure 5.2: Performance of the ML estimator compared with the CRB - when P_{s} is small, the RSI dominates the signal, which makes the parameter hard to estimate and results in a large gap between MSE and CRB.

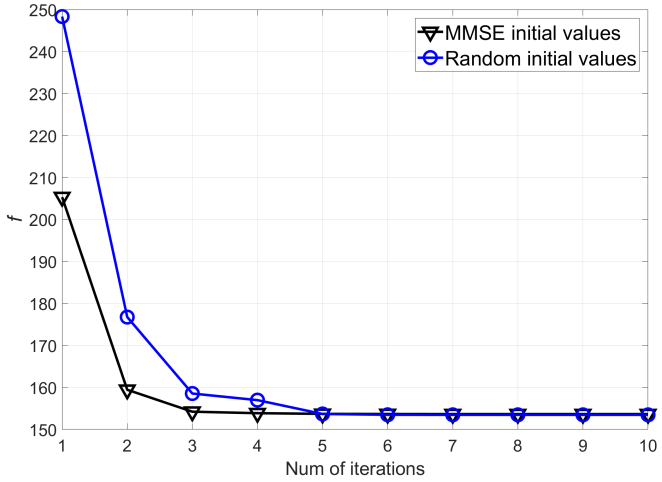

Figure 5.3: Number of iterations to convergence for different initialization - the objective function converges in 3 iterations with MMSE-based initialization while it needs 2 more iterations to converge with random initialization.

In Figure 5.2, we compare the MSEs of h and θ to their CRBs. For h, we obtain the simulated MSEs of h_x and h_y because our optimization only deals with real numbers. To make a fair comparison with its CRB which is derived for complex numbers, we use the fact that the MSE of h is the sum of the MSEs of its real and imaginary parts. The comparisons for θ are similar. When P_{s} is small, the RSI dominates the signal, which makes the parameter hard to estimate and results in a large gap between MSE and CRB. Moreover, the colored noise $d\boldsymbol{H}_\theta \boldsymbol{n}_{\mathrm{r}}$ also degrades the estimation performance because we use the expectation value of d in the estimation. The effect of colored noise reduces when P_{s} is large. For θ, the MSE does not decrease when P_{s} is less than 10 dB. The MSE for θ is also affected by the relay power P_{r}. It can be seen analytically from (5.48) that when the amplitude of P_{s} is close to that of $P_{\mathrm{r}}\sigma_{\mathrm{rr}}^2$, the decrease in α is apparent, which leads to a decrease in the CRB.

Figure 5.3 illustrates the convergence speed of the objective function f for different initialization methods, namely, random initialization and MMSE-based initialization. We calculate the average of f in each step for the same h and θ. We observe that with MMSE-based initialization, the objective function converges in 3 iterations while it needs 2 more iterations to converge with random initialization. Thus MMSE-based initialization increases the convergence speed of the algorithm.

We compare the CRBs of θ with different training sequences in Figure 5.4. We generate a training sequence which consists of i.i.d Bernoulli symbols which are random $+1$ and -1 with equal probability to compare with the optimal training sequence. The optimal and approximately optimal curves are almost overlapped. We observe that for different θ values, the roots calculated from the 8th order equation do not fall in the interval $[(1-|\theta|)^2, (1+|\theta|)^2]$ discussed in Section 5.3.2. Thus the optimal solution is on the boundary values which is consistent with the approximately optimal solution. Therefore the simulation results of the optimal and the approximately op-

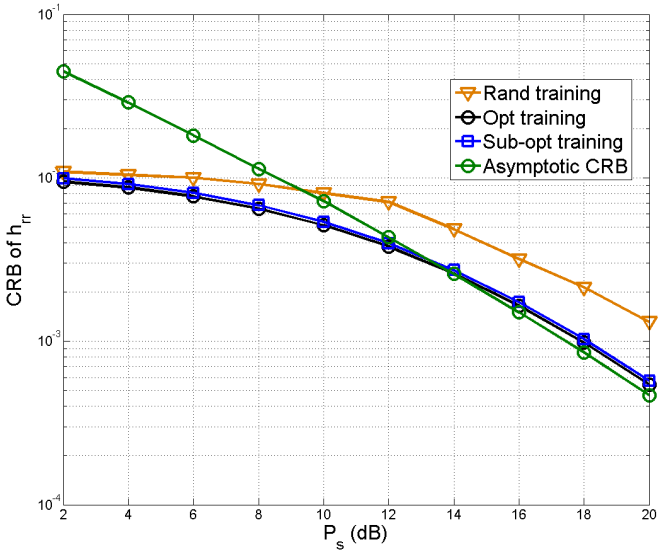

Figure 5.4: Comparison of optimal, approximately optimal, and random training sequences - the optimal training sequences save approximately 3 dB in power compared to the random training sequences and is almost overlapped with the approximately optimal one.

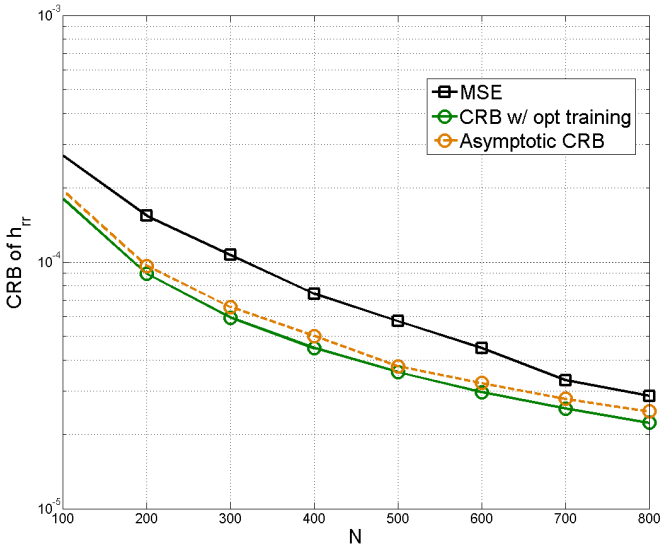

Figure 5.5: Effect of training length N on the CRB - the asymptotic CRB is an approximation of the exact CRB when the training length goes to infinity, and has a closed-form expression which can be efficiently calculated and analyzed.

timal cases are very close. Figure 5.4 also shows that the optimal training sequences save approximately 3 dB in power compared to the case of random training sequences.

Figure 5.5 shows the influences of training length N on the simulated CRB and the CRB calculated asymptotically, with the optimal training sequence. As N increases, the MSE gradually gets close to the CRB as we expect, since the ML estimator is asymptotically efficient (when N goes to infinity) [93] which shows the estimate of the RSI channel gets more accurate. The asymptotic CRB from (5.43) is an approximation of the CRB from (5.23) when the training length goes to infinity, and has a closed-form expression which can be efficiently calculated and analyzed. The small gap in the simulation shows the accuracy of the approximation.

In Figure 5.6, we compare the performance of different detectors including the Viterbi equalizer and matched filter (MF) detector with channel tap length $L = 3$. The Viterbi equalizer we use is the standard one for ISI channel [95]. However, in our system the ISI is caused by the RSI and forms a channel with taps $[h, h\theta, h\theta^2]^T$ which can be obtained from the estimates of h and θ. Thus, the standard Viterbi equalizer can be applied for RSI mitigation. On the other hand, the MF detects the signal by multiplying the received signal by the strongest tap of the ISI channel which is h. There are also two cases for MF detector. In one case, MF detector is directly used to the received signal which has colored noise. The other case is obtained by first applying a noise whitening filter to the received signal and then doing MF detection. So the noise is whitened in this case. From the perspective of how much CSI is needed, the former case only needs h while the latter needs both h and θ. Figure 5.6 shows the Viterbi equalizer outperforms any MF detector since the equalizer cancels the RSI while MF treats the RSI as noise. For the two MF detectors, the one that whitens the noise has better performance which comes from the noise whitening filter

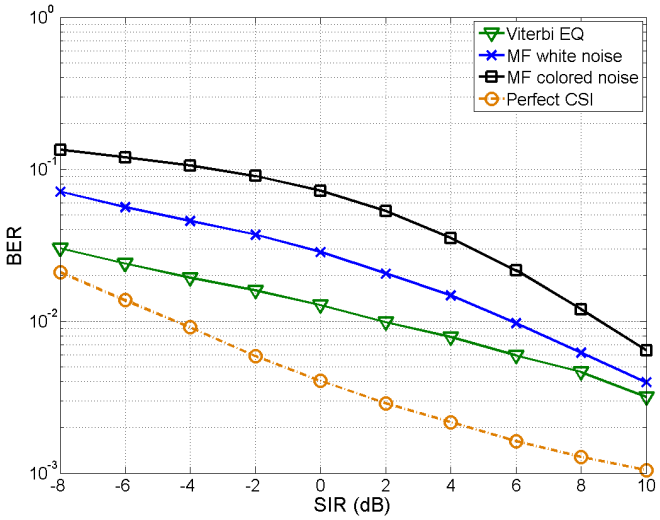

Figure 5.6: BER comparison of different detectors - the Viterbi equalizer can eliminate the ISI caused by the RSI channel. The MF detects the signal by multiplying the received signal by the strongest tap of the ISI channel. The Viterbi equalizer outperforms the MF detector since the equalizer cancels the RSI while MF treats the RSI as noise.

by using the CSI of θ. The fact that canceling the RSI and whitening the noise lead to better performance illustrates the benefits of estimating the RSI channel θ.

Figures 5.7 and 5.8 show the MSE of the two extensions. Note that the estimator are derived by using $\boldsymbol{H}_{\mathrm{f}}$ in (5.53) and $\boldsymbol{H}^{(1)}$ in (5.62) which are the approximation of the exact channels for frequency-selective case and multi-relay case respectively. The MSE is calculated by comparing the estimates of the approximation to the exact channels. Figure 5.7 shows that in the frequency-selective case, the MSE reduces with the training length N increasing, implying that the asymptotic approximation $\boldsymbol{H}_{\mathrm{f}}$ gets closer to the exact channels. The reducing MSE shows the accuracy of the approximation.

Figure 5.8 shows the MSEs of z_M and $h_2^{(1)}$ compared with their CRBs in the multi-relay case. Specifically, the total path-loss between the source and the relay is $K = -60$ dB and path-loss exponent is $\gamma = 3.71$ for the outdoor environment.

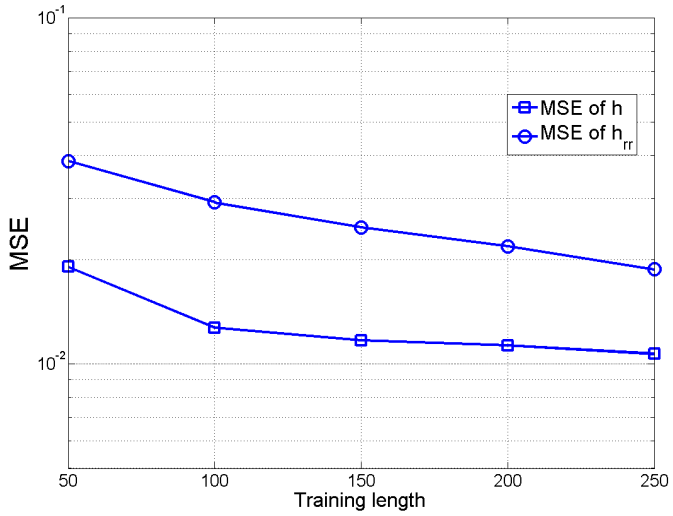

Figure 5.7: MSE with increasing N in frequency-selective case - the MSE reduces with the training length N increasing, implying that the asymptotic approximation $\boldsymbol{H}_{\mathrm{f}}$ gets closer to the exact channels.

As M increases, the MSE of z_M increases because more noise and interference are added. On the other hand, the MSE of $h_2^{(1)}$ decreases, since the RSI channel is easier to estimate as the RSI gets stronger. The asymptotic CRBs derived by (5.70) and (5.71) are close to the simulated CRBs. Since M is an integer and not large, one can search over the best M by using (5.70) and (5.71).

5.7 Conclusion

In this chapter, we propose an ML channel estimator in FD relays to estimate the end-to-end channel as well as the RSI channel at the destination. The log-likelihood function is maximized through the BFGS algorithm. The algorithm is initialized by a linear MMSE estimator to prevent local minima and increase the convergence speed. The corresponding CRBs are derived to evaluate the accuracy of the estimates. By using asymptotic properties of Toeplitz matrices, we show that the optimal training sequence is a sinusoid. To find the frequency, we minimize the CRBs and propose the corresponding optimal training sequence and a practical approximately optimal

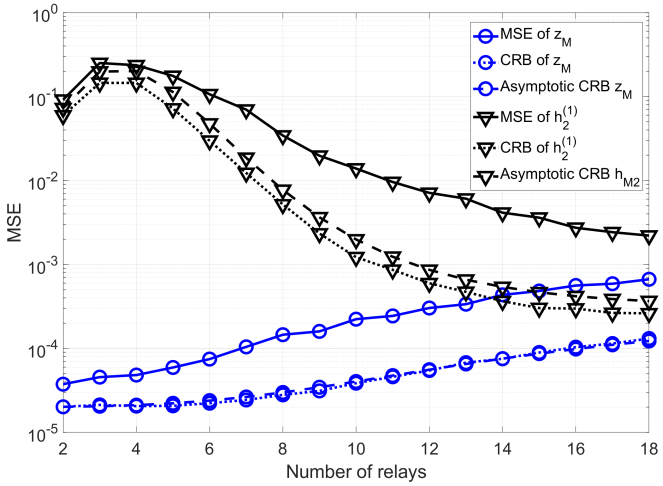

Figure 5.8: CRB for multiple relays - as M increases, the MSE of z_M increases because more noise and interference are added. The MSE of $h_2^{(1)}$ decreases since the RSI channel is easier to estimate as the RSI gets stronger.

training sequence. Extensions of our estimation method to frequency-selective and multi-relay case are also considered.

Chapter 6

SIGNAL DETECTION IN FULL-DUPLEX COGNITIVE RADIOS

In this chapter, we propose the signal detection problem in the presence of RSI. Different from FD relays, FD radios can also be used in spectrum sensing devices which detect signals from others while transmit their own data. The cognitive radio system is such a scenario that two types of users, unlicensed secondary users (SUs) and licensed primary users (PUs), share the spectrum through spectrum sensing [96, 97]. Underlay and overlay are two spectrum sharing schemes that SUs are allowed to access the spectrum bands of PUs. In the underlay scheme [98], the SUs are allowed to transmit if the interference caused by the SUs' transmission to PUs is below some threshold. In contrast, overlay spectrum sharing [99], which is adopted in this thesis, allows the SUs to access only the empty spectrum of PUs. The reliability and efficiency of identifying the spectrum holes by spectrum sensing are the key components to protect PUs' transmission and maximize SUs' throughput.

In conventional cognitive radio systems, PUs and SUs are half-duplex devices. Thus, the operation of SUs is time-slotted, and each slot is divided into spectrum sensing sub-slot and transmission sub-slot. The SUs will sense the PUs' spectrum bands in the sensing sub-slot and decide whether to transmit by accessing the spectrum bands in the following transmission sub-slot. Though optimization and cooperation of spectrum sensing are investigated, the half-duplex based system still suffers from two major problems. First, the SUs have to sacrifice their transmission time for spectrum sensing. The sensing is periodic so it wastes more transmission time for long and continuous spectrum holes. Second, the SUs cannot sense the spectrum when they transmit. Therefore, if the PUs arrive or leave during the SUs' transmis-

sion sub-slots, the SUs cannot notice the PUs' state change until the next sensing sub-slot, which leads to long collision for the PUs' arrival or transmission time waste for the PUs' departure.

The FD enhances the utilization of the spectrum holes and protection of the PUs' transmission by letting the SUs keep sensing the spectrum all the time. Hence, the spectrum efficiency in cognitive radio systems is improved. However, due to the existence of RSI, the spectrum sensing needs to incorporate the RSI. Several works have discussed FD cognitive radio systems where the SU is an FD device and it senses the activity of the PU while simultaneously transmitting its own data to its corresponding receiver [100–104]. In [102], the probabilities of miss detection and false alarm are compared in half-duplex and FD cognitive radio systems under energy detection. Different implementations of FD including two-antenna and signal antenna FD are also considered. The authors in [103] propose and analyze a simultaneous sensing and transmission scheme for a two-antenna FD SU. The trade-off between the SU's transmission rate and the detection accuracy is investigated where increasing SU's power improves the rate but leads to more RSI and reduces the detection accuracy. In [104], the authors consider cooperation between the primary and the secondary system. A cognitive FD relay forwards the primary signal and transmits its own cognitive signal. With MIMO at the relay, beamforming is used to differentiate the forwarding primary signal and the cognitive secondary signal.

We focus on the trade-off between transmission rate and the detection accuracy in an FD cognitive radio system with MIMO. Different from the single antenna case where the SU's power is the only parameter affecting the trade-off [103], the beamformer and combiner used for the transmitting and receiving antenna sets of the FD SU can have a significant impact on the trade-off. We use the sum-rate of PU and SU

as a metric and discuss how different choices of the beamformer and combiner affect the sum-rate.

6.1 System Model

We consider a cognitive radio system consisting of one PU and one SU pair as shown in Figure 6.1. Node B is the FD secondary transmitter equipped with two sets of antennas, where each set has N_{B} antennas and is used for either transmitting or spectrum sensing. Other nodes include primary transmitter (node A), primary receiver (node AR), and secondary receiver (node BR), and each has a single antenna. The PU either transmits its message to its receiver or be idle while the secondary user senses whether the PU accesses the spectrum. If PU is transmitting, SU is silent and senses the spectrum. If PU is idle, SU transmits its messages to its receiver but still keep detecting whether PU becomes active again, which is feasible by FD. The channels for the PU and the SU pair are h_{A} and $\boldsymbol{h}_{\mathrm{B}}$ respectively. Let $\boldsymbol{h}_{\mathrm{AB}}$ be the channel between PU and SU which is used in the spectrum sensing. The N_{B} by N_{B} channel matrix $\boldsymbol{H}_{\mathrm{rr}}$ is the RSI channel for SU. All the channels are assumed to be flat fading and time-invariant. We assume the SU knows the channels related to it, i.e., $\boldsymbol{h}_{\mathrm{B}}$, $\boldsymbol{h}_{\mathrm{AB}}$, and $\boldsymbol{H}_{\mathrm{rr}}$. The beamforming vector $\boldsymbol{b}$ and combiner $\boldsymbol{w}$ are used at the transmitter and receiver side at SU respectively. We assume PU has the prior probabilities p_0 for its state transition from "idle" to "active" and p_1 for that from "active" to "idle", which are fixed and known. However, the sensing is performed in the presence of RSI from SU. There is a trade-off in the system that increasing SU's rate, which leads to more RSI, decreases the accuracy of spectrum sensing.

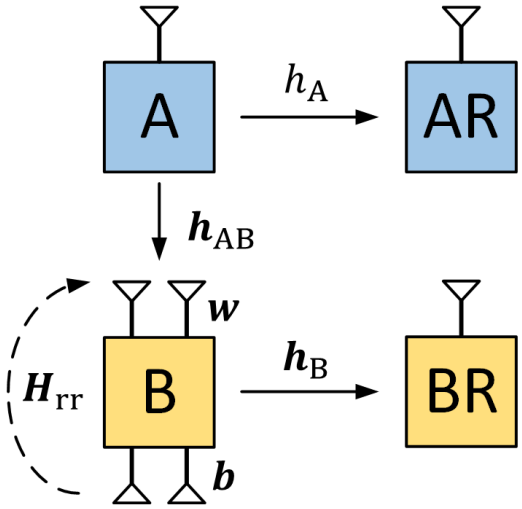

Figure 6.1: An FD cognitive radio system - An FD cognitive radio system consisting of one PU and one SU pair. The secondary transmitter is an FD device equipped with two sets of antennas, where each set has N_{B} antennas and is used for either transmitting or spectrum sensing. The PU either transmits or be idle while the SU keeps sensing the spectrum all the time to decide when to transmit.

6.2 Simultaneous Sensing and Transmission

6.2.1 Energy Detection

Working in FD mode, the SU can detect the PU's states when transmitting its own signal. However, the SU's detection is affected by its RSI and also depends on whether it transmits or not. When the SU is silent, there is no RSI and the spectrum sensing is the same as that in the conventional half-duplex cognitive radio system. On the other hand, when the SU transmits, its received signal for detection contains RSI. Therefore, we will consider two cases of spectrum sensing for either the SU is transmitting or silent.

When the SU is silent, the cases when the PU is active or idle are referred to as hypothesis $\mathcal{H}_{01}$ and $\mathcal{H}_{00}$ respectively. The received signal of the SU under each

hypothesis is

$$y[n] = \begin{cases} \boldsymbol{w}^H(\boldsymbol{h}_{\mathrm{AB}}\sqrt{P_{\mathrm{A}}}x_{\mathrm{A}}[n] + v[n]), & \mathcal{H}_{01} \\ \boldsymbol{w}^H v[n], & \mathcal{H}_{00}, \end{cases} \tag{6.1}$$

where x_{A} is the transmit signal of the PU with $|x_{\mathrm{A}}[n]|^2 = 1$, P_{A} is the PU's transmit power, the channel $\boldsymbol{h}_{\mathrm{AB}}$ is an $N_{\mathrm{B}} \times 1$ vector, and v is the complex Gaussian noise with zero mean and variance σ_{v}^2.

When the SU is transmitting, RSI exists in the received signal. The hypothesis $\mathcal{H}_{11}$ and $\mathcal{H}_{10}$ are under which the SU is transmitting while the PU is active or idle respectively. SU's received signal can be expressed as

$$y[n] = \begin{cases} \boldsymbol{w}^H(\boldsymbol{h}_{\mathrm{AB}}\sqrt{P_{\mathrm{A}}}x_{\mathrm{A}}[n] + \boldsymbol{H}_{\mathrm{rr}}\boldsymbol{b}\sqrt{P_{\mathrm{B}}}x_{\mathrm{B}}[n] + v[n]), & \mathcal{H}_{11} \\ \boldsymbol{w}^H(\boldsymbol{H}_{\mathrm{rr}}\boldsymbol{b}\sqrt{P_{\mathrm{B}}}x_{\mathrm{B}}[n] + v[n]), & \mathcal{H}_{10}, \end{cases} \tag{6.2}$$

where $\boldsymbol{b}$ and $\boldsymbol{w}$ are $N_{\mathrm{B}} \times 1$ vectors, and $x_{\mathrm{B}}[n]$ is the transmit signal of the SU with $|x_{\mathrm{B}}[n]|^2 = 1$.

Energy detection is adopted for the spectrum sensing. The average received power in a time interval is used as the test statistics as follows:

$$M = \frac{1}{N}\sum_{n=1}^{N} |y[n]|^2, \tag{6.3}$$

where $y[n]$ is the nth sample in the test interval given by (6.1) and (6.2) for different cases of SU's activities. The spectrum is considered to be occupied when M is greater than a certain threshold, otherwise the spectrum is idle and can be accessed by the SU. Since the received signals are different for SU's activities, i.e., the received signal is affected by RSI when SU is transmitting and has no RSI when SU is silent, we use two thresholds and calculate the probabilities of false alarm and detection for both cases. Let ϵ_0 and ϵ_1 be the thresholds when the SU is silent and transmitting. The

probability set for SU being silent is

$$p_{\mathrm{f}}(\epsilon_0) = \Pr(M > \epsilon_0 | \mathcal{H}_{00}), \tag{6.4}$$

$$p_{\mathrm{d}}(\epsilon_0) = \Pr(M > \epsilon_0 | \mathcal{H}_{01}). \tag{6.5}$$

Similarly, the other probability set when SU is transmitting is $\{p_{\mathrm{fI}}(\epsilon_1), p_{\mathrm{dI}}(\epsilon_1)\}$.

Either the PU is transmitting or idle, the received signal of the SU $y(n)$ is assumed to be i.i.d. in the test interval. If N is sufficiently large, by the central limit theorem, the PDF of M can be approximated by a Gaussian distribution with mean $\mathrm{E}\left[|y[n]|^2\right]$ and variance $\frac{1}{N}\mathrm{var}\left[|y[n]|^2\right]$. Therefore, we can derive the statistics of M under each hypothesis. Let m_{01} and σ_{01}^2 be the mean and variance of M when the PU is transmitting and the SU is silent under $\mathcal{H}_{01}$. We have

$$m_{01} = \mathrm{E}\left[|y[n]|^2\right] = P_{\mathrm{A}} \boldsymbol{w}^H \boldsymbol{h}_{\mathrm{AB}} \boldsymbol{h}_{\mathrm{AB}}^H \boldsymbol{w} + \sigma_{\mathrm{v}}^2 ||\boldsymbol{w}||^2, \tag{6.6}$$

$$\sigma_{01}^2 = \frac{1}{N}\mathrm{var}\left[|y[n]|^2\right] = \frac{1}{N}\left(\mathrm{E}\left[|y[n]|^4\right] - \left(\mathrm{E}\left[|y[n]|^2\right]\right)^2\right) \tag{6.7}$$

$$= \frac{1}{N}\left(P_{\mathrm{A}} \boldsymbol{w}^H \boldsymbol{h}_{\mathrm{AB}} \boldsymbol{h}_{\mathrm{AB}}^H \boldsymbol{w} + \sigma_{\mathrm{v}}^2 ||\boldsymbol{w}||^2\right)^2, \tag{6.8}$$

where the derivation of $\mathrm{E}\left[|y[n]|^4\right]$ uses the property of absolute moments of the Gaussian random variable.

Similarly, we derive the statistics for other hypothesis as follows. For $\mathcal{H}_{00}$ where the PU is idle and the SU is silent, we have

$$m_{00} = \sigma_{\mathrm{v}}^2 ||\boldsymbol{w}||^2, \tag{6.9}$$

$$\sigma_{00}^2 = \frac{1}{N}\sigma_{\mathrm{v}}^4 ||\boldsymbol{w}||^4. \tag{6.10}$$

For $\mathcal{H}_{11}$ where both the PU and the SU are transmitting,

$$m_{11} = P_{\mathrm{A}} \boldsymbol{w}^H \boldsymbol{h}_{\mathrm{AB}} \boldsymbol{h}_{\mathrm{AB}}^H \boldsymbol{w} + P_{\mathrm{B}} \boldsymbol{w}^H \boldsymbol{H}_{\mathrm{rr}} \boldsymbol{b}\boldsymbol{b}^H \boldsymbol{H}_{\mathrm{rr}}^H \boldsymbol{w} + \sigma_{\mathrm{v}}^2 ||\boldsymbol{w}||^2, \tag{6.11}$$

$$\sigma_{11}^2 = \frac{1}{N}\left(P_{\mathrm{A}} \boldsymbol{w}^H \boldsymbol{h}_{\mathrm{AB}} \boldsymbol{h}_{\mathrm{AB}}^H \boldsymbol{w} + P_{\mathrm{B}} \boldsymbol{w}^H \boldsymbol{H}_{\mathrm{rr}} \boldsymbol{b}\boldsymbol{b}^H \boldsymbol{H}_{\mathrm{rr}}^H \boldsymbol{w} + \sigma_{\mathrm{v}}^2 ||\boldsymbol{w}||^2\right)^2. \tag{6.12}$$

Last, for $\mathcal{H}_{10}$ where the PU is idle and the SU is transmitting,

$$m_{10} = P_{\mathrm{B}} \boldsymbol{w}^H \boldsymbol{H}_{\mathrm{rr}} \boldsymbol{b}\boldsymbol{b}^H \boldsymbol{H}_{\mathrm{rr}}^H \boldsymbol{w} + \sigma_{\mathrm{v}}^2 ||\boldsymbol{w}||^2, \tag{6.13}$$

$$\sigma_{10}^2 = \frac{1}{N} \left(P_{\mathrm{B}} \boldsymbol{w}^H \boldsymbol{H}_{\mathrm{rr}} \boldsymbol{b}\boldsymbol{b}^H \boldsymbol{H}_{\mathrm{rr}}^H \boldsymbol{w} + \sigma_{\mathrm{v}}^2 ||\boldsymbol{w}||^2 \right)^2. \tag{6.14}$$

With the statistics, we are able to calculate the sensing probabilities. When the SU is silent, the threshold ϵ_0 is used. Thus,

$$p_{\mathrm{f}}(\epsilon_0) = Q\left(\frac{\epsilon_0 - m_{00}}{\sigma_{00}} \right), \tag{6.15}$$

$$p_{\mathrm{d}}(\epsilon_0) = Q\left(\frac{\epsilon_0 - m_{01}}{\sigma_{01}} \right), \tag{6.16}$$

where $Q(\cdot)$ denotes the Q-function. When the SU is transmitting with threshold ϵ_1, we have

$$p_{\mathrm{fI}}(\epsilon_1) = Q\left(\frac{\epsilon_1 - m_{10}}{\sigma_{10}} \right), \tag{6.17}$$

$$p_{\mathrm{dI}}(\epsilon_1) = Q\left(\frac{\epsilon_1 - m_{11}}{\sigma_{11}} \right). \tag{6.18}$$

6.2.2 Sum-Rate Metric

To represent the trade-off between the transmitting rate and the accuracy of detection, we define sum-rate of the PU and the SU as a metric. We first define the probabilities that a spectrum waste happens. Let $p_{\mathrm{collision}}$ be the probability of both the PU and SU are transmitting, i.e., a collision happens which is the situation that the PU becomes active from its previous state (either active or idle) and the SU misdetects the PU's signal. Therefore, we can write $p_{\mathrm{collision}}$ as the following,

$$p_{\mathrm{collision}} = p_0(1 - p_{\mathrm{dI}}(\epsilon_1)) + (1 - p_1)(1 - p_{\mathrm{d}}(\epsilon_0)), \tag{6.19}$$

where p_0 and p_1 are prior probabilities of the PU changing its states defined in Section 6.1. Another spectrum waste situation is that both the PU and the SU are idle, which

happens when the PU becomes idle but the SU has a false alarm. Let p_{idle} be the probability of that both the PU and the SU are idle which can be expressed as

$$p_{\text{idle}} = p_1 p_{\text{f}}(\epsilon_0) + (1 - p_0) p_{\text{fl}}(\epsilon_1). \tag{6.20}$$

After defining the probabilities of situations that can cause wastes of transmission time, we can define the sum-rate as

$$R_{\text{sum}} = R_{\text{A}}(1 - p_{\text{collision}}) + R_{\text{B}}(1 - p_{\text{idle}}), \tag{6.21}$$

where R_{A} and R_{B} are the transmission rate of the PU and the SU respectively, and are given by

$$R_{\text{A}} = \log\left(1 + \frac{P_{\text{A}}|h_{\text{A}}|^2}{\sigma_{\text{v}}^2}\right), \tag{6.22}$$

$$R_{\text{B}} = \log\left(1 + \frac{P_{\text{B}}|\boldsymbol{b}^H \boldsymbol{h}_{\text{B}}|^2}{N_{\text{B}}\sigma_{\text{v}}^2}\right). \tag{6.23}$$

We propose different schemes for choosing the beamformer $\boldsymbol{b}$ and the combiner $\boldsymbol{w}$ to see how they affect the trade-off through sum-rate.

6.2.3 Beamforming and Combining Schemes

We begin with the schemes for the combiner $\boldsymbol{w}$. When using multiple antennas at the receiver, maximum-ratio combining (MRC) can maximize the received SNR. MRC is also used in energy detection in half-duplex systems. In FD systems, MRC may enhance the RSI in the received signal but the enhancement of RSI is not as strong as that of the desired signal. Thus, the MRC scheme for $\boldsymbol{w}$ still improve the SNR for the desired signal in the presence of RSI. Such a combiner can be expressed as

$$\boldsymbol{w}_{\text{MRC}} = \frac{\boldsymbol{h}_{\text{AB}}}{||\boldsymbol{h}_{\text{AB}}||}, \tag{6.24}$$

where the combiner is normalized to keep the power constraint. Selection combining (SC) is commonly used for its simplicity. If the FD system has multiple antennas at both transmitter and receiver, one receiving antenna can receive multiple copies of RSI from the transmitting antennas. Thus, selecting the receiving antenna with the best SINR is an efficient way to reduce the effect of RSI. The SC scheme combiner is

$$w_{\mathrm{SC}i} = \begin{cases} 1, & i = \arg\max_i \frac{|h_{\mathrm{AB}i}|^2}{||\boldsymbol{h}_{\mathrm{rr}}^{(i)}||}, \\ 0, & \text{otherwise}, \end{cases} \tag{6.25}$$

where $w_{\mathrm{SC}i}$ and $h_{\mathrm{AB}i}$ are the ith elements of $\boldsymbol{w}_{\mathrm{SC}}$ and $\boldsymbol{h}_{\mathrm{AB}}$ respectively, and $\boldsymbol{h}_{\mathrm{rr}}^{(i)}$ is the ith row of $\boldsymbol{H}_{\mathrm{rr}}$.

For the schemes of beamformer, one natural choice is to maximize the SU's (node B's) rate. However, such beamformers may enhance the RSI and reduce the detection accuracy, which leads to a decrease of the sum-rate. The max-B-rate scheme beamformer is given by

$$\boldsymbol{b}_{\mathrm{max-B-rate}} = \frac{\boldsymbol{h}_B}{||\boldsymbol{h}_{\mathrm{B}}||}. \tag{6.26}$$

Note that if the channel of SU to its receiver is a matrix, $\boldsymbol{b}_{\mathrm{max-B-rate}}$ is the eigenvector corresponding to the maximum eigenvalue of $\boldsymbol{h}_B\boldsymbol{h}_B^H$. We can also use the beamformer to help reduce the RSI at the receiver to improve the detection probabilities. Though such a scheme does not increase the SU's rate directly, it can still improve the sum-rate by reducing the probabilities of spectrum waste. The min-B-RSI scheme beamformer $\boldsymbol{b}_{\mathrm{min-B-RSI}}$ can be obtained by finding the normalized eigenvector corresponding to the minimum eigenvalue of $\boldsymbol{H}_{\mathrm{rr}}^H\boldsymbol{w}\boldsymbol{w}^H\boldsymbol{H}_{\mathrm{rr}}$.

6.3 Numerical Results

In this section, we simulate the sum-rate R_{sum} by combining different schemes of $\boldsymbol{w}$ and $\boldsymbol{b}$. As shown in Figure 6.2, R_{sum} has local maximum points when using the

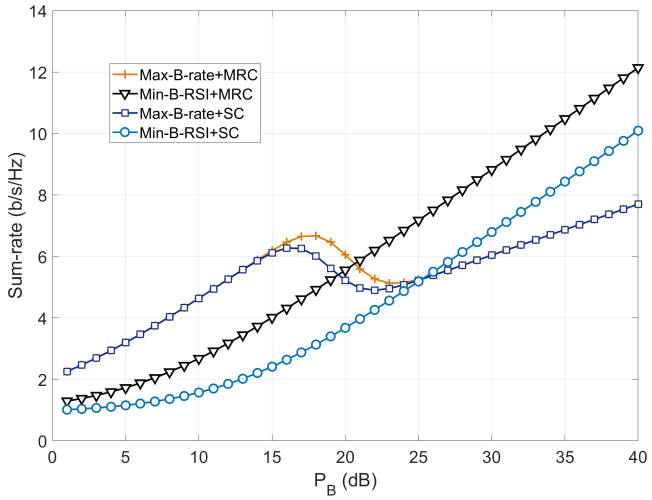

Figure 6.2: Sum-rate for different schemes of $\boldsymbol{b}$ and $\boldsymbol{w}$ - for the max-B-rate scheme, R_{sum} has a local maximum and decreases for large P_{B} which leads to strong RSI and large p_{fI}. R_{sum} increases again but is dominated by R_{B}. For the min-B-RSI scheme, R_{sum} is a monotonically increasing function of P_{B}. The min-B-RSI scheme efficiently utilizes the transmission time of the PU and the SU and performs better for large P_{B}.

max-B-rate scheme of $\boldsymbol{b}$. When P_{B} is less than 18 dB, R_{sum} increases due to the augment in R_{B}. However, continuing to increase P_{B} leads to strong RSI and rises p_{fI}. Consequently, p_{idle} is large for large P_{B}, which results in a decrease in R_{sum}. When P_{B} is greater than 25 dB, R_{sum} increases again because the augment in R_{B} due to large P_{B} can compensate the rate loss caused by large p_{idle}. Though R_{sum} increases again in this situation, the system still wastes lots of transmission time due to large p_{idle}. The sum-rate is dominated by R_{B} and the PU has little impact on R_{sum}. For the min-B-RSI $\boldsymbol{b}$ scheme, R_{sum} is a monotonically increasing function of P_{B}. In this scheme, p_{fI} and p_{dI} are kept in reasonable range for large P_{B}. Though min-B-RSI scheme is worse than max-B-rate scheme for P_{B} less than 23 dB, it efficiently utilizes the transmission time of the PU and the SU, and performs better for large P_{B}. For $\boldsymbol{w}$, MRC performs better than SC.

We also simulate how the RSI affects p_{idle}, as shown in Figure 6.3. The parameter σ_{rr}^2 is the variance of the RSI channel, i.e., variance of the elements of $\boldsymbol{H}_{\text{rr}}$. It char-

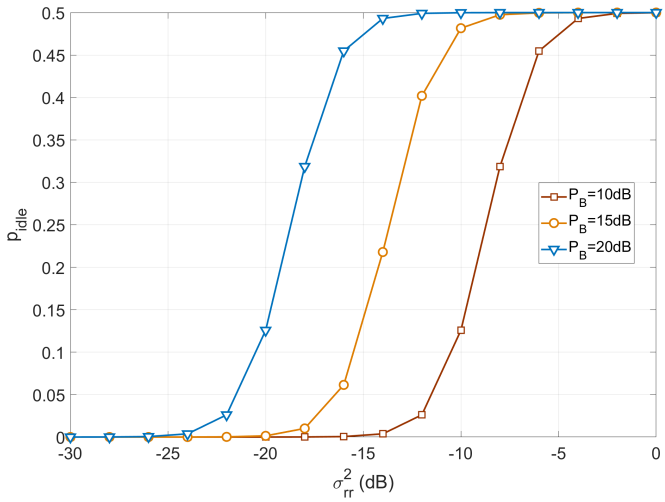

Figure 6.3: Probability of both the PU and the SU being idle - when the average RSI power is below -5 dB, p_{idle} increases slowly with increased RSI but goes up fast when RSI is greater than -5 dB. This can be used as a threshold for RSI when design the system.

acterizes the ability of SIC so that the average RSI power is equal to $P_{\text{B}}\sigma_{\text{rr}}^2$, e.g., for the rightmost plot in Figure 6.3, $P_{\text{B}} = 10$ dB and when $\sigma_{\text{rr}}^2 = -15$ dB, the average RSI power is $10 + (-15) = -5$ dB. We can see when the average RSI power is below -5 dB for all the three plots, p_{idle} increases slowly with increased RSI but goes up fast when RSI is greater than -5 dB. This can be used as a threshold for RSI when design the system.

6.4 Conclusion

We consider the simultaneously transmitting and sensing problem in an FD cognitive radio system with MIMO. The probabilities of detection in the presence of RSI are derived. The sum-rate of PU and SU is proposed as a metric to characterize the trade-off between transmission rate and the detection accuracy. Different beamforming and combining schemes are compared and how the schemes affect the sum-rate is discussed.

Chapter 7

CONCLUSIONS

In this dissertation, we study channel estimation in half and full duplex relays, aiming to provide spectrally efficient training schemes with high performance for FD relays. The training schemes take full advantages of the FD relaying protocol and take the RSI channels into account.

The impact of channel estimation on spectral efficiency in half-duplex MIMO TWR systems is investigated. The trade-off between training and data energy is optimized in the MIMO TWR scenario. We derive the ratio of training-versus-data for both the symmetric case and the asymmetric case of the two source powers. To maximize the spectral efficiency, data time is set to its maximum value since the achievable rate is a monotonically increasing function of the data time. In the asymmetric case, we show that the difference of two SNRs is either a concave or convex function of the training-versus-data ratio which enables the maximization of the minimum SNR of the two sources via the ratio.

To utilize the inherent spectrally efficient structures of both FD and TWRs, the efficient and high performance one-block training scheme is proposed to obtain the CSI in the presence of RSI. An ML estimator solved by the BFGS algorithm is derived to estimate the cascaded channel, the individual channel as well as the RSI channel simultaneously. The initialization, complexity and convergence of the algorithm are also discussed. The two baselines, including the multi-block training scheme with LS estimator and the cross-correlation method, are proposed for comparison. The CRBs for the three schemes are derived and analyzed to show how the channel parameters and transmit powers affect the training performance via Fisher information. We

show analytically that exploiting the channel structure arising from the RSI channel increases its Fisher information, which demonstrates the benefit of estimating the RSI channel.

The FD one-way relay system is considered for fundamental and analytic results of the effect of RSI on spectral efficiency. We propose an ML channel estimator in FD relays to estimate the end-to-end channel and the RSI channel at the destination. The corresponding CRBs are derived in closed form and analyzed by using asymptotic properties of Toeplitz matrices. We show that the optimal training sequence is a sinusoid. To find the frequency, we minimize the CRBs with respect to the corresponding training sequence. A practical approximately optimal training sequence is also proposed. Extensions of our estimation method to frequency selective and multi-relay case are also considered.

The simultaneously transmitting and sensing problem in an FD cognitive radio system with MIMO is considered. The probabilities of detection in the presence of RSI are derived. The sum-rate of PU and SU is proposed as a metric to characterize the trade-off between transmission rate and the detection accuracy. Different beamforming and combining schemes are compared and how the schemes affect the sum-rate is discussed.

References

[1] H. Ju, E. Oh, and D. Hong, "Catching resource-devouring worms in next-generation wireless relay systems: Two-way relay and full-duplex relay," *IEEE Communications Magazine*, vol. 47, no. 9, Sep. 2009.

[2] K. Ratajczak, K. Bakowski, and K. Wesolowski, "Two-way relaying for 5G systems: Comparison of network coding and MIMO techniques," in *Proc. IEEE Wireless Communications and Networking Conference (WCNC)*, Apr. 2014, pp. 376–381.

[3] S.-K. Hong, J. Brand, J. Choi, M. Jain, J. Mehlman, S. Katti, and P. Levis, "Applications of self-interference cancellation in 5G and beyond," *IEEE Communications Magazine*, vol. 52, no. 2, pp. 114–121, Feb. 2014.

[4] Z. Zhang, X. Chai, K. Long, A. V. Vasilakos, and L. Hanzo, "Full duplex techniques for 5G networks: self-interference cancellation, protocol design, and relay selection," *IEEE Communications Magazine*, vol. 53, no. 5, pp. 128–137, May 2015.

[5] C. E. Shannon, "Two-way communication channels," in *Proc. 4th Berkeley Symp. Math. Stat. Prob*, vol. 1, Sep. 1961, pp. 611–644.

[6] S. Katti, S. Gollakota, and D. Katabi, "Embracing wireless interference: analog network coding," *ACM SIGCOMM Computer Communication Review*, vol. 37, no. 4, pp. 397–408, Aug 2007.

[7] B. Rankov and A. Wittneben, "Achievable rate regions for the two-way relay channel," in *Proc. IEEE International Symposium on Information Theory (ISIT)*, Jul. 2006, pp. 1668–1672.

[8] C. Esli and A. Wittneben, "Multiuser MIMO two-way relaying for cellular communications," in *Proc. IEEE International Symposium on Personal, Indoor and Mobile Radio Communications (PIMRC)*, Sep. 2009, pp. 1–6.

[9] J. Joung and A. H. Sayed, "Multiuser two-way amplify-and-forward relay processing and power control methods for beamforming systems," *IEEE Transactions on Signal Processing*, vol. 58, no. 3, pp. 1833–1846, Mar. 2010.

[10] H. Cui, L. Song, and B. Jiao, "Multi-pair two-way amplify-and-forward relaying with very large number of relay antennas," *IEEE Transactions on Wireless Communications*, vol. 13, no. 5, pp. 2636–2645, May 2014.

[11] A. Al-Fuqaha, M. Guizani, M. Mohammadi, M. Aledhari, and M. Ayyash, "Internet of things: A survey on enabling technologies, protocols, and applications," *IEEE Communications Surveys & Tutorials*, vol. 17, no. 4, pp. 2347–2376, Jun. 2015.

[12] S. Zhang, C. Tepedelenlioğlu, A. Spanias, and M. Banavar, "Distributed network structure estimation using consensus methods," *Synthesis Lectures on Communications*, vol. 10, no. 1, pp. 1–88, Mar. 2018.

[13] S. Wu, H. Guo, J. Xu, S. Zhu, and H. Wang, "In-band full duplex wireless communications and networking for IoT devices: Progress, challenges and opportunities," *Future Generation Computer Systems*, Nov. 2017.

[14] E. C. Van Der Meulen, "Three-terminal communication channels," *Advances in Applied Probability*, pp. 120–154, Apr. 1971.

[15] T. Cover and A. E. Gamal, "Capacity theorems for the relay channel," *IEEE Transactions on Information Theory*, vol. 25, no. 5, pp. 572–584, Jun. 1979.

[16] J. N. Laneman, D. N. Tse, and G. W. Wornell, "Cooperative diversity in wireless networks: Efficient protocols and outage behavior," *IEEE Transactions on Information Theory*, vol. 50, no. 12, pp. 3062–3080, Dec. 2004.

[17] A. G. Stove, "Linear FMCW radar techniques," in *Proc. Inst. Elect. Eng. F (Radar and Signal Processing)*, vol. 139, Oct. 1992, pp. 343–350.

[18] M. Heino, D. Korpi, T. Huusari, E. Antonio-Rodriguez, S. Venkatasubramanian, T. Riihonen, L. Anttila, C. Icheln, K. Haneda, and R. Wichman, "Recent advances in antenna design and interference cancellation algorithms for in-band full duplex relays," *IEEE Communications Magazine*, vol. 53, no. 5, pp. 91–101, May 2015.

[19] A. Sabharwal, P. Schniter, D. Guo, D. W. Bliss, S. Rangarajan, and R. Wichman, "In-band full-duplex wireless: Challenges and opportunities," *IEEE Journal on Selected Areas in Communications*, vol. 32, no. 9, pp. 1637–1652, Sep. 2014.

[20] G.-P. Liu, R. Yu, H. Ji, V. Leung, and X. Li, "In-band full-duplex relaying: A survey, research issues and challenges," *IEEE Communications Surveys & Tutorials*, vol. 17, no. 2, pp. 500–524, Jan. 2015.

[21] T. Riihonen, K. Haneda, S. Werner, and R. Wichman, "SINR analysis of full-duplex OFDM repeaters," in *Proc. IEEE International Symposium on Personal, Indoor and Mobile Radio Communications*, Sep. 2009, pp. 3169–3173.

[22] L. Jimenez Rodríguez, N. H. Tran, and T. Le-Ngoc, "Performance of full-duplex af relaying in the presence of residual self-interference," *IEEE Journal on Selected Areas in Communications*, vol. 32, no. 9, pp. 1752–1764, Jun. 2014.

[23] R. Ahlswede, N. Cai, S.-Y. Li, and R. W. Yeung, "Network information flow," *IEEE Transactions on Information Theory*, vol. 46, no. 4, pp. 1204–1216, Jul. 2000.

[24] S. Zhang, S. C. Liew, and P. P. Lam, "Hot topic: physical-layer network coding," in *Proc. International Conference on Mobile Computing and Networking*, Sep. 2006, pp. 358–365.

[25] P. Popovski and H. Yomo, "Physical network coding in two-way wireless relay channels," in *Proc. IEEE International Conference on Communications ICC*, Jun. 2007, pp. 707–712.

[26] M. P. Wilson, K. Narayanan, H. D. Pfister, and A. Sprintson, "Joint physical layer coding and network coding for bidirectional relaying," *IEEE Transactions on Information Theory*, vol. 56, no. 11, pp. 5641–5654, Nov. 2010.

[27] R. H. Louie, Y. Li, and B. Vucetic, "Practical physical layer network coding for two-way relay channels: performance analysis and comparison," *IEEE Transactions on Wireless Communications*, vol. 9, no. 2, pp. 764–777, Feb. 2010.

[28] Y. Yang, H. Hu, J. Xu, and G. Mao, "Relay technologies for WiMAX and LTE-advanced mobile systems," *IEEE Communications Magazine*, vol. 47, no. 10, Oct. 2009.

[29] A. Ghosh, R. Ratasuk, B. Mondal, N. Mangalvedhe, and T. Thomas, "LTE-advanced: next-generation wireless broadband technology," *IEEE wireless communications*, vol. 17, no. 3, Jun. 2010.

[30] T. Riihonen, S. Werner, and R. Wichman, "Mitigation of loopback self-interference in full-duplex MIMO relays," *IEEE Transactions on Signal Processing*, vol. 59, no. 12, pp. 5983–5993, Dec. 2011.

[31] B. P. Day, A. R. Margetts, D. W. Bliss, and P. Schniter, "Full-duplex MIMO relaying: Achievable rates under limited dynamic range," *IEEE Journal on Selected Areas in Communications*, vol. 30, no. 8, pp. 1541–1553, Sep. 2012.

[32] D. Kim, H. Ju, S. Park, and D. Hong, "Effects of channel estimation error on full-duplex two-way networks," *IEEE Transactions on Vehicular Technology*, vol. 62, no. 9, pp. 4666–4672, Nov. 2013.

[33] B. P. Day, A. R. Margetts, D. W. Bliss, and P. Schniter, "Full-duplex bidirectional MIMO: Achievable rates under limited dynamic range," *IEEE Transactions on Signal Processing*, vol. 60, no. 7, pp. 3702–3713, Jul. 2012.

[34] A. Masmoudi and T. Le-Ngoc, "Channel estimation and self-interference cancelation in full-duplex communication systems," *IEEE Transactions on Vehicular Technology*, vol. 66, no. 1, pp. 321–334, Jan. 2017.

[35] M. Duarte, C. Dick, and A. Sabharwal, "Experiment-driven characterization of full-duplex wireless systems," *IEEE Transactions on Wireless Communications*, vol. 11, no. 12, pp. 4296–4307, Dec. 2012.

[36] D. Bliss, P. Parker, and A. Margetts, "Simultaneous transmission and reception for improved wireless network performance," in *Proc. IEEE Statistic Singal Processing Workshop*, Aug. 2007, pp. 478–482.

[37] H. Ju, E. Oh, and D. Hong, "Improving efficiency of resource usage in two-hop full duplex relay systems based on resource sharing and interference cancellation," *IEEE Transactions on Wireless Communications*, vol. 8, no. 8, Aug. 2009.

[38] B. Rankov and A. Wittneben, "Spectral efficient protocols for half-duplex fading relay channels," *IEEE Journal on selected Areas in Communications*, vol. 25, no. 2, Feb. 2007.

[39] Y. Han, S. H. Ting, C. K. Ho, and W. H. Chin, "Performance bounds for two-way amplify-and-forward relaying," *IEEE Transactions on Wireless Communications*, vol. 8, no. 1, pp. 432–439, Jan. 2009.

[40] K.-J. Lee, K. W. Lee, H. Sung, and I. Lee, "Sum-rate maximization for two-way MIMO amplify-and-forward relaying systems," in *Proc. IEEE 69th Vehicular Technology Conference, VTC Spring*, Apr. 2009, pp. 1–5.

[41] P. Lioliou, M. Viberg, M. Coldrey, and F. Athley, "Self-interference suppression in full-duplex mimo relays," in *Proc. IEEE 44th Asilomar Conference on Signals, Systems and Computers*, Nov. 2010, pp. 658–662.

[42] I. Krikidis, H. A. Suraweera, P. J. Smith, and C. Yuen, "Full-duplex relay selection for amplify-and-forward cooperative networks," *Wireless Communications, IEEE Transactions on*, vol. 11, no. 12, pp. 4381–4393, Dec. 2012.

[43] L. Jimenez Rodríguez, N. H. Tran, and T. Le-Ngoc, "Optimal power allocation and capacity of full-duplex af relaying under residual self-interference," *IEEE Wireless Communications Letters*, vol. 3, no. 2, pp. 233–236, Apr. 2014.

[44] C. Esli and A. Wittneben, "One-and two-way decode-and-forward relaying for wireless multiuser MIMO networks," in *Proc. IEEE Global Telecommunications Conference (GLOBECOM)*, Nov. 2008, pp. 1–6.

[45] Q. F. Zhou, Y. Li, F. C. Lau, and B. Vucetic, "Decode-and-forward two-way relaying with network coding and opportunistic relay selection," *IEEE Transactions on Communications*, vol. 58, no. 11, pp. 3070–3076, Nov. 2010.

[46] E. Antonio-Rodríguez, R. López-Valcarce, T. Riihonen, S. Werner, and R. Wichman, "Adaptive self-interference cancellation in wideband full-duplex decode-and-forward mimo relays," in *Proc. IEEE 14th Workshop on Signal Processing Advances in Wireless Communications (SPAWC)*, Jun. 2013, pp. 370–374.

[47] M. Mohammadi, B. K. Chalise, H. A. Suraweera, C. Zhong, G. Zheng, and I. Krikidis, "Throughput analysis and optimization of wireless-powered multiple antenna full-duplex relay systems," *IEEE Transactions on communications*, vol. 64, no. 4, pp. 1769–1785, Apr. 2016.

[48] M. Khafagy, A. Ismail, M.-S. Alouini, and S. Aissa, "On the outage performance of full-duplex selective decode-and-forward relaying," *IEEE Communications Letters*, vol. 17, no. 6, pp. 1180–1183, Apr. 2013.

[49] L. J. Rodríguez, N. Tran, and T. Le-Ngoc, *Amplify-and-Forward Relaying in Wireless Communications*. Basel, Switzerland: Springer, 2015.

[50] T. Riihonen, S. Werner, and R. Wichman, "Optimized gain control for single-frequency relaying with loop interference," *IEEE Transactions on Wireless Communications*, vol. 8, no. 6, pp. 2801–2806, Jun. 2009.

[51] ——, "Hybrid full-duplex/half-duplex relaying with transmit power adaptation," *IEEE Transactions on Wireless Communications*, vol. 10, no. 9, pp. 3074–3085, Sep. 2011.

[52] T. M. Kim and A. Paulraj, "Outage probability of amplify-and-forward cooperation with full duplex relay," in *Proc. IEEE Wireless Communications and Networking Conference (WCNC)*, Apr. 2012, pp. 75–79.

[53] X. Li and C. Tepedelenlioğlu, "Maximum likelihood channel estimation for residual self-interference cancellation in full duplex relay," in *Proc. IEEE 49th Asilomar Conference on Signals, Systems and Computers*, Nov. 2015, pp. 807–811.

[54] X. Li, C. Tepedelenlioğlu, and H. Şenol, "Channel estimation for residual self-interference in full duplex amplify-and-forward two-way relays," *IEEE Transactions on Wireless Communications*, vol. 16, no. 8, pp. 4970–4983, Aug. 2017.

[55] ——, "Optimal training for residual self-interference for full duplex one-way relays," *submitted to IEEE Transactions on Communications, http://arxiv.org/abs/1709.06140*.

[56] D. Gunduz, A. Goldsmith, and H. V. Poor, "MIMO two-way relay channel: Diversity-multiplexing tradeoff analysis," in *Proc. IEEE 42th Asilomar Conference on Signals, Systems and Computers*, Nov. 2008, pp. 1474–1478.

[57] M. Benjillali and L. Szczecinski, "A simple detect-and-forward scheme in fading channels," *IEEE Communications Letters*, vol. 13, no. 5, May 2009.

[58] C. K. Lo, S. Vishwanath, and R. W. Heath, "Relay subset selection in wireless networks using partial decode-and-forward transmission," *IEEE Transactions on Vehicular Technology*, vol. 58, no. 2, pp. 692–704, Feb. 2009.

[59] H.-M. Wang, X.-G. Xia, and Q. Yin, "A linear analog network coding for asynchronous two-way relay networks," *IEEE Transactions on Wireless Communications*, vol. 9, no. 12, pp. 3630–3637, Dec. 2010.

[60] S. Chang and B. Kelley, "An efficient time synchronization scheme for broadband two-way relaying networks based on physical-layer network coding," *IEEE Communications Letters*, vol. 16, no. 9, pp. 1416–1419, Sep. 2012.

[61] F. Gao, R. Zhang, and Y.-C. Liang, "Channel estimation for OFDM modulated two-way relay networks," *IEEE Transactions on Signal Processing*, vol. 57, no. 11, pp. 4443–4455, Oct. 2009.

[62] S. Abdallah and I. Psaromiligkos, "Semi-blind channel estimation with superimposed training for OFDM-based af two-way relaying," *IEEE Transactions on Wireless Communications*, vol. 13, no. 5, pp. 2468–2477, May 2014.

[63] R. Wang, M. Tao, H. Mehrpouyan, and Y. Hua, "Channel estimation and optimal training design for correlated mimo two-way relay systems in colored environment," *IEEE Transactions on Wireless Communications*, vol. 14, no. 5, pp. 2684–2699, May 2015.

[64] C. W. Chiong, Y. Rong, and Y. Xiang, "Channel training algorithms for two-way MIMO relay systems," *IEEE Transactions on Signal Processing*, vol. 61, no. 16, pp. 3988–3998, Aug. 2013.

[65] Y. Rong, M. R. Khandaker, and Y. Xiang, "Channel estimation of dual-hop mimo relay system via parallel factor analysis," *IEEE Transactions on Wireless Communications*, vol. 11, no. 6, pp. 2224–2233, Jun. 2012.

[66] X. Li, B. Shen, B. D. Liu, and Y. J. Zhang, "A locality sensitive low-rank model for image tag completion," *IEEE Transactions on Multimedia*, vol. 18, no. 3, pp. 474–483, Mar. 2016.

[67] ——, "Ranking-preserving low-rank factorization for image annotation with missing labels," *IEEE Transactions on Multimedia*, vol. 20, no. 5, pp. 1169–1178, May 2018.

[68] F. Gao, R. Zhang, and Y.-C. Liang, "Optimal channel estimation and training design for two-way relay networks," *IEEE Transactions on Communications*, vol. 57, no. 10, pp. 3024–3033, Sep. 2009.

[69] G. Wang, F. Gao, W. Chen, and C. Tellambura, "Channel estimation and training design for two-way relay networks in time-selective fading environments," *IEEE Transactions on Wireless Communications*, vol. 10, no. 8, pp. 2681–2691, Aug. 2011.

[70] G. Wang, F. Gao, Y.-C. Wu, and C. Tellambura, "Joint cfo and channel estimation for OFDM-based two-way relay networks," *IEEE Transactions on Wireless Communications*, vol. 10, no. 2, pp. 456–465, Sep. 2011.

[71] T. Sjodin, H. Gacanin, and F. Adachi, "Two-slot channel estimation for analog network coding based on OFDM in a frequency-selective fading channel," in *Proc. IEEE Vehicular Technology Conference (VTC) Spring*, May. 2010, pp. 1–5.

[72] S. Zhang, F. Gao, and C.-X. Pei, "Optimal training design for individual channel estimation in two-way relay networks," *IEEE Transactions on Signal Processing*, vol. 60, no. 9, pp. 4987–4991, Sep. 2012.

[73] D.-H. Kim, M. Ju, and H.-M. Kim, "Optimal training signal design for estimation of correlated MIMO channels in two-way amplify-and-forward relay systems," *IEEE Communications Letters*, vol. 17, no. 3, pp. 491–494, Mar. 2013.

[74] R. Wang, M. Tao, H. Mehrpouyan, and Y. Hua, "Channel estimation and optimal training design for correlated MIMO two-way relay systems in colored environment," *IEEE Transactions on Wireless Communications*, May 2014.

[75] X. Li, C. Tepedelenlioğlu, and H. Şenol, "Optimal power allocation between training and data for MIMO two-way relay channels," *IEEE Communications Letters*, vol. 19, pp. 1941–1944, Nov. 2015.

[76] T. Riihonen, S. Werner, and R. Wichman, "Residual self-interference in full-duplex MIMO relays after null-space projection and cancellation," in *Proc. IEEE 44th Asilomar Conference on Signals, Systems and Computers*, Nov. 2010, pp. 653–657.

[77] F. S. Tabataba, P. Sadeghi, C. Hucher, and M. R. Pakravan, "Impact of channel estimation errors and power allocation on analog network coding and routing in two-way relaying," *IEEE Transactions on Vehicular Technology*, vol. 61, no. 7, pp. 3223–3239, Oct. 2012.

[78] G. Zheng, "Joint beamforming optimization and power control for full-duplex MIMO two-way relay channel," *IEEE Transactions on Signal Processing*, vol. 63, no. 3, pp. 555–566, Feb. 2015.

[79] X. Xiong, X. Wang, T. Riihonen, and X. You, "Channel estimation for full-duplex relay systems with large-scale antenna arrays," *IEEE Transactions on Wireless Communications*, vol. 15, no. 10, pp. 6925–6938, Oct. 2016.

[80] H. Şenol, X. Li, and C. Tepedelenlioğlu, "Rapidly time-varying channel estimation for full-duplex amplify-and-forward one-way relay networks," *IEEE Transactions on Signal Processing*, vol. 66, no. 11, pp. 3056–3069, Jun. 2018.

[81] A. Masmoudi and T. Le-Ngoc, "A maximum-likelihood channel estimator for self-interference cancellation in full-duplex systems," *IEEE Transactions on Vehicular Technology*, vol. 65, no. 7, pp. 5122–5132, Oct. 2016.

[82] Y.-H. Kim and J.-H. Lee, "Channel estimation for self-interference cancellation in full-duplex wireless systems," *Wireless Personal Communications*, pp. 1–14, Oct. 2015.

[83] S. Huberman and T. Le-Ngoc, "MIMO full-duplex precoding: A joint beamforming and self-interference cancellation structure," *IEEE Transactions on Wireless Communications*, vol. 14, no. 4, pp. 2205–2217, Apr. 2015.

[84] H. Q. Ngo, H. A. Suraweera, M. Matthaiou, and E. G. Larsson, "Multipair full-duplex relaying with massive arrays and linear processing," *IEEE Journal on Selected Areas in Communications*, vol. 32, no. 9, pp. 1721–1737, Sep. 2014.

[85] A. C. Cirik, M. C. Filippou, and T. Ratnarajaht, "Transceiver design in full-duplex MIMO cognitive radios under channel uncertainties," *IEEE Transactions on Cognitive Communications and Networking*, vol. 2, no. 1, pp. 1–14, Mar. 2016.

[86] O. Taghizadeh, M. Rothe, A. C. Cirik, and R. Mathar, "Distortion-loop analysis for full-duplex amplify-and-forward relaying in cooperative multicast scenarios," in *Proc. IEEE International Conference on Signal Processing and Communmunication Systems*, Dec. 2015, pp. 1–9.

[87] O. Taghizadeh, T. Yang, A. C. Cirik, and R. Mathar, "Distortion-loop-aware amplify-and-forward full-duplex relaying with multiple antennas," in *Proc. IEEE International Symposium on Wireless Communication Systems*, Sep. 2016, pp. 54–58.

[88] J. G. Proakis, *Digital communications*, 4th ed. New York, NY, USA: McGraw Hill, 2001.

[89] A. Vosoughi and Y. Jia, "How does channel estimation error affect average sum-rate in two-way amplify-and-forward relay networks?" *IEEE Transactions on Wireless Communications*, vol. 11, no. 5, pp. 1676–1687, Oct. 2012.

[90] J. Nocedal and S. Wright, *Numerical Optimization*. New York, NY, USA: Springer, 2006.

[91] S. Chang and B. Kelley, "An efficient time synchronization scheme for broadband two-way relaying networks based on physical-layer network coding," *IEEE Communications Letters*, vol. 16, no. 9, pp. 1416–1419, Sep. 2012.

[92] K. P. Murphy, *Machine Learning: A Probabilistic Perspective*. Cambridge, MA, USA: MIT Press, 2012.

[93] S. M. Kay, *Fundamentals of Statistical Signal Processing: Estimation Theory*. Englewood Cliffs, NJ, USA: Prentice-Hall, 1993.

[94] R. M. Gray, *Toeplitz and Circulant Matrices: A Review*. LP Breda, The Netherlands: Now Publishers, 2006.

[95] A. Goldsmith, *Wireless Communications*. New York, NY, USA: Cambridge University Press, 2005.

[96] R. Zeng and C. Tepedelenlioğlu, "Fundamental performance trade-offs in cooperative cognitive radio systems," *IEEE Transactions on Cognitive Communications and Networking*, vol. 3, no. 2, pp. 169–179, Jun. 2017.

[97] ——, "Optimal achievable rate trade-off in cooperative cognitive radio systems," *Proc. IEEE International Conference on Acoustics Speech and Signal Processing (ICASSP)*, Mar. 2017.

[98] ——, "Underlay cognitive multi-user diversity with random number of secondary users," *IEEE Transactions on Wireless Communications*, vol. 13, no. 10, pp. 5571–5581, Oct. 2014.

[99] ——, "Multiple device-to-device users overlaying cellular networks," in *Proc. IEEE Wireless Communications and Networking Conference (WCNC)*, Mar. 2017, pp. 1–6.

[100] J. I. Choi, S. Hong, M. Jain, S. Katti, P. Levis, and J. Mehlman, "Beyond full duplex wireless," in *Proc. IEEE 46th Asilomar Conference on Signals, Systems and Computers*. IEEE, Nov. 2012, pp. 40–44.

[101] E. Ahmed, A. Eltawil, and A. Sabharwal, "Simultaneous transmit and sense for cognitive radios using full-duplex: A first study," in *Proc. IEEE Antennas and Propagation Society International Symposium (APSURSI)*. IEEE, 2012, pp. 1–2.

[102] T. Riihonen and R. Wichman, "Energy detection in full-duplex cognitive radios under residual self-interference," in *Proc. IEEE International Conference on Cognitive Radio Oriented Wireless Networks and Communications (CROWNCOM)*, Jun. 2014, pp. 57–60.

[103] Y. Liao, T. Wang, L. Song, and Z. Han, "Listen-and-talk: Protocol design and analysis for full-duplex cognitive radio networks," *IEEE Transactions on Vehicular Technology*, vol. 66, no. 1, pp. 656–667, Jan. 2017.

[104] G. Zheng, I. Krikidis, and B. orn Ottersten, "Full-duplex cooperative cognitive radio with transmit imperfections," *IEEE Transactions on Wireless Communications*, vol. 12, no. 5, pp. 2498–2511, May 2013.

APPENDIX A

GRADIENTS USED IN THE BFGS ALGORITHM FOR FD TWR

We derive the gradients used in the BFGS method in Section 4.2.4. Before that the following derivatives are needed.

$$\frac{\partial \boldsymbol{\mu}}{\partial \theta_x} = \boldsymbol{B}_\theta(\boldsymbol{X}_{\mathrm{t}}\boldsymbol{h} + d\boldsymbol{x}_{\mathrm{r}}) \qquad \frac{\partial \boldsymbol{\mu}}{\partial \theta_y} = j\boldsymbol{B}_\theta(\boldsymbol{X}_{\mathrm{t}}\boldsymbol{h} + d\boldsymbol{x}_{\mathrm{r}}) \tag{A.1}$$

$$\frac{\partial \boldsymbol{C}}{\partial \theta_x} = |d|^2\sigma_{\mathrm{n}}^2\left(\boldsymbol{B}_\theta\boldsymbol{H}_\theta^H + \boldsymbol{H}_\theta\boldsymbol{B}_\theta^H\right) \qquad \frac{\partial \boldsymbol{C}}{\partial \theta_y} = |d|^2\sigma_{\mathrm{n}}^2\left(j\boldsymbol{B}_\theta\boldsymbol{H}_\theta^H - j\boldsymbol{H}_\theta\boldsymbol{B}_\theta^H\right). \tag{A.2}$$

where $\boldsymbol{B}_\theta = \frac{\partial \boldsymbol{H}_\theta}{\partial \theta}$ is also an $N \times N$ Toeplitz matrix given by the first column $[0, 1, 2\theta, \cdots, (L-1)\theta^{L-2}, 0, \cdots, 0]^T$ and the first row $[0, 0, \cdots, 0]$.

The gradients for both real and imaginary part are needed as inputs of the algorithm. The gradients of p_x and p_y are

$$\nabla f_{p_x} = \frac{\partial f}{\partial p_x} = -2\mathrm{Re}\left[(\boldsymbol{y}_1 - \boldsymbol{\mu})^H\boldsymbol{C}^{-1}\boldsymbol{H}_\theta\boldsymbol{x}_1\right] \tag{A.3}$$

$$\nabla f_{p_y} = \frac{\partial f}{\partial p_y} = -2\mathrm{Re}\left[(\boldsymbol{y}_1 - \boldsymbol{\mu})^H\boldsymbol{C}^{-1}j\boldsymbol{H}_\theta\boldsymbol{x}_1\right] \tag{A.4}$$

The derivatives of q are similar to those of p only by replacing $\boldsymbol{x}_1$ with $\boldsymbol{x}_2$ in (A.3). The derivatives with respect to h_{11} are

$$\nabla f_{h_{11x}} = \frac{\partial f}{\partial h_{11x}} = -2\mathrm{Re}\left[(\boldsymbol{y}_1 - \boldsymbol{\mu})^H\boldsymbol{C}^{-1}\boldsymbol{J}^{\mathrm{u}}\boldsymbol{x}_1\right] \tag{A.5}$$

$$\nabla f_{h_{11y}} = \frac{\partial f}{\partial h_{11y}} = -2\mathrm{Re}\left[(\boldsymbol{y}_1 - \boldsymbol{\mu})^H\boldsymbol{C}^{-1}j\boldsymbol{J}^{\mathrm{u}}\boldsymbol{x}_1\right] \tag{A.6}$$

For d, it's involved in both $\boldsymbol{\mu}$ and $\boldsymbol{C}$, thus

$$\begin{aligned}\nabla f_{d_x} = {} & \mathrm{tr}\left(2d_x\boldsymbol{C}^{-1}\boldsymbol{H}_\theta\boldsymbol{H}_\theta^H\right) - (\boldsymbol{y}_1 - \boldsymbol{\mu})^H\boldsymbol{C}^{-1}(2d_x\boldsymbol{H}_\theta\boldsymbol{H}_\theta^H)\boldsymbol{C}^{-1}(\boldsymbol{y}_1 - \boldsymbol{\mu}) \\ & - 2\mathrm{Re}\left[(\boldsymbol{y}_1 - \boldsymbol{\mu})^H\boldsymbol{C}^{-1}\boldsymbol{H}_\theta\boldsymbol{x}_{\mathrm{r}}\right]\end{aligned} \tag{A.7}$$

$$\begin{aligned}\nabla f_{d_y} = {} & \mathrm{tr}\left(2d_y\boldsymbol{C}^{-1}\boldsymbol{H}_\theta\boldsymbol{H}_\theta^H\right) - (\boldsymbol{y}_1 - \boldsymbol{\mu})^H\boldsymbol{C}^{-1}(2d_y\boldsymbol{H}_\theta\boldsymbol{H}_\theta^H)\boldsymbol{C}^{-1}(\boldsymbol{y}_1 - \boldsymbol{\mu}) \\ & - 2\mathrm{Re}\left[(\boldsymbol{y}_1 - \boldsymbol{\mu})^H\boldsymbol{C}^{-1}j\boldsymbol{H}_\theta\boldsymbol{x}_{\mathrm{r}}\right]\end{aligned} \tag{A.8}$$

and θ is similar to d for which we need the derivatives of $\boldsymbol{\mu}$ and $\boldsymbol{C}$ with respect with it. Using (A.1) and (A.2), we have

$$\begin{aligned}\nabla f_{\theta_x} = {} & \mathrm{tr}\left(|d|^2\sigma_{\mathrm{n}}^2\boldsymbol{C}^{-1}\left(\boldsymbol{B}_\theta\boldsymbol{H}_\theta^H + \boldsymbol{H}_\theta\boldsymbol{B}_\theta^H\right)\right) \\ & - 2\mathrm{Re}\left[(\boldsymbol{y}_1 - \boldsymbol{\mu})^H\boldsymbol{C}^{-1}\boldsymbol{B}_\theta(p\boldsymbol{x}_1 + q\boldsymbol{x}_2 + d\boldsymbol{x}_{\mathrm{r}})\right] \\ & - |d|^2\sigma_{\mathrm{n}}^2(\boldsymbol{y}_1 - \boldsymbol{\mu})^H\boldsymbol{C}^{-1}\left(\boldsymbol{B}_\theta\boldsymbol{H}_\theta^H + \boldsymbol{H}_\theta\boldsymbol{B}_\theta^H\right)\boldsymbol{C}^{-1}(\boldsymbol{y}_1 - \boldsymbol{\mu})\end{aligned} \tag{A.9}$$

$$\begin{aligned}\nabla f_{\theta_y} = {} & \mathrm{tr}\left(|d|^2\sigma_{\mathrm{n}}^2\boldsymbol{C}^{-1}\left(j\boldsymbol{B}_\theta\boldsymbol{H}_\theta^H - j\boldsymbol{H}_\theta\boldsymbol{B}_\theta^H\right)\right) \\ & - 2\mathrm{Re}\left[(\boldsymbol{y}_1 - \boldsymbol{\mu})^H\boldsymbol{C}^{-1}\boldsymbol{B}_\theta j(p\boldsymbol{x}_1 + q\boldsymbol{x}_2 + d\boldsymbol{x}_{\mathrm{r}})\right] \\ & - |d|^2\sigma_{\mathrm{n}}^2(\boldsymbol{y}_1 - \boldsymbol{\mu})^H\boldsymbol{C}^{-1}\left(j\boldsymbol{B}_\theta\boldsymbol{H}_\theta^H - j\boldsymbol{H}_\theta\boldsymbol{B}_\theta^H\right)\boldsymbol{C}^{-1}(\boldsymbol{y}_1 - \boldsymbol{\mu})\end{aligned} \tag{A.10}$$

APPENDIX B

ELEMENTS OF THE FISHER INFORMATION MATRIX FOR FD TWR

For the one-block training scheme, elements for the FIM can be obtained by (4.31). We derive all the Γ_{mn}, $m \neq n$ here. For different (m, n), they are given by the following.

$$\begin{aligned}
\Gamma_{12} =& \boldsymbol{x}_1^H \boldsymbol{H}_\theta^H \boldsymbol{C}^{-1} \boldsymbol{H}_\theta \boldsymbol{x}_2, & \Gamma_{13} =& \boldsymbol{x}_1^H \boldsymbol{H}_\theta^H \boldsymbol{C}^{-1} \boldsymbol{B}_\theta (p\boldsymbol{x}_1 + q\boldsymbol{x}_2 + d\boldsymbol{x}_\mathrm{r}), \\
\Gamma_{14} =& \boldsymbol{x}_1^H \boldsymbol{H}_\theta^H \boldsymbol{C}^{-1} \boldsymbol{H}_\theta \boldsymbol{x}_\mathrm{r}, & \Gamma_{15} =& \boldsymbol{x}_1^H \boldsymbol{H}_\theta^H \boldsymbol{C}^{-1} \boldsymbol{J}^\mathrm{u} \boldsymbol{x}_1, \\
\Gamma_{23} =& \boldsymbol{x}_2^H \boldsymbol{H}_\theta^H \boldsymbol{C}^{-1} \boldsymbol{B}_\theta (p\boldsymbol{x}_1 + q\boldsymbol{x}_2 + d\boldsymbol{x}_\mathrm{r}), & \Gamma_{24} =& \boldsymbol{x}_2^H \boldsymbol{H}_\theta^H \boldsymbol{C}^{-1} \boldsymbol{H}_\theta \boldsymbol{x}_\mathrm{r}, \\
\Gamma_{25} =& \boldsymbol{x}_2^H \boldsymbol{H}_\theta^H \boldsymbol{C}^{-1} \boldsymbol{J}^\mathrm{u} \boldsymbol{x}_1, & \Gamma_{35} =& (p\boldsymbol{x}_1 + q\boldsymbol{x}_2 + d\boldsymbol{x}_\mathrm{r})^H \boldsymbol{B}_\theta^H \boldsymbol{C}^{-1} \boldsymbol{J}^\mathrm{u} \boldsymbol{x}_1 \\
\Gamma_{45} =& \boldsymbol{x}_\mathrm{r}^H \boldsymbol{H}_\theta^H \boldsymbol{C}^{-1} \boldsymbol{J}^\mathrm{u} \boldsymbol{x}_1, & & \\
\Gamma_{34} =& (p\boldsymbol{x}_1 + q\boldsymbol{x}_2 + d\boldsymbol{x}_\mathrm{r})^H \boldsymbol{B}_\theta^H \boldsymbol{C}^{-1} \boldsymbol{H}_\theta \boldsymbol{x}_\mathrm{r} & & \\
& + d^* |d|^2 \sigma_\mathrm{n}^4 \mathrm{tr} \left(\boldsymbol{C}^{-1} \boldsymbol{H}_\theta \boldsymbol{B}_\theta^H \boldsymbol{C}^{-1} \boldsymbol{H}_\theta \boldsymbol{H}_\theta^H \right) & & \qquad \text{(B.1)}
\end{aligned}$$

and $\Gamma_{mn} = \Gamma_{nm}^*$.

We also derive the CRBs for the multi-block training scheme. Put (4.23) to (4.27) together to form a new received signal vector as

$$\boldsymbol{y}_\mathrm{M} = \left[\boldsymbol{y}_{\mathrm{P}2}^T \ \boldsymbol{y}_{\mathrm{P}4}^T \ \boldsymbol{y}_{\mathrm{P}3}^T \ \boldsymbol{y}_{\mathrm{P}1}^T \ \right]^T \qquad \text{(B.2)}$$

The mean of $\boldsymbol{y}_\mathrm{M}$ is given by

$$\boldsymbol{\mu}_\mathrm{M} = \left[\boldsymbol{\mu}_{\boldsymbol{h}}^T \ \boldsymbol{\mu}_\theta^T \ \boldsymbol{\mu}_{h_{\mathrm{r}1}}^T \ \boldsymbol{\mu}_{h_{11}}^T \ \right]^T \qquad \text{(B.3)}$$

where $\boldsymbol{\mu}_{\boldsymbol{h}} = p\boldsymbol{x}_{1\mathrm{t}} + q\boldsymbol{x}_{2\mathrm{t}}$, $\boldsymbol{\mu}_\theta = h_{\mathrm{r}1}\theta \boldsymbol{x}_{\mathrm{rt}}$, $\boldsymbol{\mu}_{h_{\mathrm{r}1}} = h_{\mathrm{r}1}\boldsymbol{x}_{\mathrm{rt}}$, and $\boldsymbol{\mu}_{h_{11}} = h_{11}\boldsymbol{x}_{1\mathrm{t}}$.

The covariance matrix of $\boldsymbol{y}_\mathrm{M}$ is

$$\boldsymbol{C}_\mathrm{M} = \begin{bmatrix} \boldsymbol{C}_{\boldsymbol{h}} & 0 & 0 & 0 \\ 0 & \boldsymbol{C}_\theta & 0 & 0 \\ 0 & 0 & \boldsymbol{C}_{h_{\mathrm{r}1}} & 0 \\ 0 & 0 & 0 & \boldsymbol{C}_{h_{11}} \end{bmatrix} = \sigma_\mathrm{v}^2 \begin{bmatrix} \alpha_1^2 |h_{\mathrm{r}1}|^2 + 1 & 0 & 0 & 0 \\ 0 & \alpha_2^2 |h_{\mathrm{r}1}|^2 + 1 & 0 & 0 \\ 0 & 0 & 1 & 0 \\ 0 & 0 & 0 & 1 \end{bmatrix} \otimes \boldsymbol{I}_N \qquad \text{(B.4)}$$

where $\otimes$ denotes the Kronecker product. $\boldsymbol{\mu}_\mathrm{M}$ is a $4N \times 1$ vector and $\boldsymbol{C}_\mathrm{M}$ is a $4N \times 4N$ diagonal matrix due to the uncorrelated noise in $\boldsymbol{y}_\mathrm{M}$.

Define $\boldsymbol{\xi}^{(\mathrm{M})} = [p \ q \ \theta \ h_{\mathrm{r}1} \ h_{11}]^T$. The (m, n)th element of the FIM is given by

$$\Gamma_{mn}^{(\mathrm{M})} = \frac{\partial \boldsymbol{\mu}_\mathrm{M}^H}{\partial \left(\xi_m^{(\mathrm{M})}\right)^*} \boldsymbol{C}_\mathrm{M}^{-1} \frac{\partial \boldsymbol{\mu}_\mathrm{M}}{\partial \xi_n^{(\mathrm{M})}} + \mathrm{tr} \left(\boldsymbol{C}_\mathrm{M}^{-1} \frac{\partial \boldsymbol{C}_\mathrm{M}}{\partial \left(\xi_m^{(\mathrm{M})}\right)^*} \boldsymbol{C}_\mathrm{M}^{-1} \frac{\partial \boldsymbol{C}_\mathrm{M}}{\partial \xi_n^{(\mathrm{M})}} \right). \qquad \text{(B.5)}$$

Only the diagonal elements, $\Gamma_{12}^{(\mathrm{M})}$, and $\Gamma_{21}^{(\mathrm{M})}$ are not zero. Thus the inverse of the FIM can be obtained by finding the inverse of a partitioned matrix. Define $D =$

$\Gamma_{11}^{(\mathrm{M})}\Gamma_{22}^{(\mathrm{M})} - \Gamma_{12}^{(\mathrm{M})}\Gamma_{21}^{(\mathrm{M})}$. The CRBs are given by the diagonal elements of inverse of the FIM, thus

$$
\begin{aligned}
CRB_{p}^{(\mathrm{M})} &= \left[\left(\mathbf{\Gamma}^{(\mathrm{M})}\right)^{-1}\right]_{11} = \Gamma_{22}^{(\mathrm{M})}/D \qquad & CRB_{q}^{(\mathrm{M})} &= \left[\left(\mathbf{\Gamma}^{(\mathrm{M})}\right)^{-1}\right]_{22} = \Gamma_{11}^{(\mathrm{M})}/D \\
CRB_{\theta}^{(\mathrm{M})} &= \left[\left(\mathbf{\Gamma}^{(\mathrm{M})}\right)^{-1}\right]_{33} = 1/\Gamma_{33} & CRB_{h_{\mathrm{r}1}}^{(\mathrm{M})} &= \left[\left(\mathbf{\Gamma}^{(\mathrm{M})}\right)^{-1}\right]_{44} = 1/\Gamma_{44} \\
CRB_{h_{11}}^{(\mathrm{M})} &= \left[\left(\mathbf{\Gamma}^{(\mathrm{M})}\right)^{-1}\right]_{55} = 1/\Gamma_{55}
\end{aligned}
\tag{B.6}
$$

APPENDIX C

MEAN AND COVARIANCE MATRIX OF $P(\boldsymbol{Y}|H,\theta)$

In (5.5), h and θ are parameters of interest and d is the nuisance parameter. The likelihood function $p(\boldsymbol{y}|h,\theta)$ is obtained through integrating $p(\boldsymbol{y}|h,\theta,d)$ with respect to d [93],

$$p(\boldsymbol{y}|h,\theta) = \int p(\boldsymbol{y}|h,\theta,d)p(d)\mathrm{d}d. \tag{C.1}$$

Since $p(\boldsymbol{y}|h,\theta,d)$ and $p(d)$ are Gaussian distributed, it can be shown that the distribution of $p(\boldsymbol{y}|h,\theta)$ is also Gaussian. Denoting the mean of $\boldsymbol{y}$ given h and θ to be $E[\boldsymbol{y}|h,\theta]$ and the covariance matrix as $V[\boldsymbol{y}|h,\theta]$. It can be shown that

$$E[\boldsymbol{y}|h,\theta] = E_d[E_{\boldsymbol{y}}[\boldsymbol{y}|h,\theta,d]] \tag{C.2}$$
$$V[\boldsymbol{y}|h,\theta] = V_d[E_{\boldsymbol{y}}[\boldsymbol{y}|h,\theta,d]] + E_d[V_{\boldsymbol{y}}[\boldsymbol{y}|h,\theta,d]]. \tag{C.3}$$

Since we know $p(\boldsymbol{y}|h,\theta,d)$ is a Gaussian distribution with mean $\boldsymbol{\mu}$ and co-variance matrix $\boldsymbol{C}$, then it is straight forward to get

$$E_{\boldsymbol{y}}[\boldsymbol{y}|h,\theta,d] = h\boldsymbol{H}_\theta, \quad V_{\boldsymbol{y}}[\boldsymbol{y}|h,\theta,d] = |d|^2\sigma_{\mathrm{r}}^2\boldsymbol{H}_\theta\boldsymbol{H}_\theta^H + \sigma_{\mathrm{d}}^2\boldsymbol{I}_N. \tag{C.4}$$

The distribution of $p(d)$ is also Gaussian with zero mean and variance α^2, thus

$$E_d[E_{\boldsymbol{y}}[\boldsymbol{y}|h,\theta,d]] = E_d[h\boldsymbol{H}_\theta] = h\boldsymbol{H}_\theta \tag{C.5}$$
$$V_d[E_{\boldsymbol{y}}[\boldsymbol{y}|h,\theta,d]] = V_d[h\boldsymbol{H}_\theta] = \boldsymbol{0}_{N\times N} \tag{C.6}$$
$$E_d[V_{\boldsymbol{y}}[\boldsymbol{y}|h,\theta,d]] = E_d[|d|^2\sigma_{\mathrm{r}}^2\boldsymbol{H}_\theta\boldsymbol{H}_\theta^H + \sigma_{\mathrm{d}}^2\boldsymbol{I}_N] = \alpha^2\sigma_{\mathrm{r}}^2\boldsymbol{H}_\theta\boldsymbol{H}_\theta^H + \sigma_{\mathrm{d}}^2\boldsymbol{I}_N. \tag{C.7}$$

Therefore, we can obtain the mean and covariance matrix of the Gaussian distribution $p(\boldsymbol{y}|h,\theta)$,

$$\boldsymbol{\mu} = E[\boldsymbol{y}|h,\theta] = h\boldsymbol{H}_\theta \tag{C.8}$$
$$\boldsymbol{C} = V[\boldsymbol{y}|h,\theta] = \alpha^2\sigma_{\mathrm{r}}^2\boldsymbol{H}_\theta\boldsymbol{H}_\theta^H + \sigma_{\mathrm{d}}^2\boldsymbol{I}_N. \tag{C.9}$$

APPENDIX D

GRADIENTS USED IN THE BFGS ALGORITHM FOR FD ONE-WAY RELAY

Now we derive the gradients of f with respect to θ_x and θ_y which are used in the BFGS algorithm. The gradients for both real and imaginary parts are needed as inputs of the algorithm. For θ, we first obtain the derivative of $\boldsymbol{H}_\theta$ with respect to θ, denoted as $\boldsymbol{B}_\theta$, which is also an $N \times N$ Toeplitz matrix with first column $[0, 1, 2\theta, \cdots, (L-1)\theta^{L-2}, 0, \cdots, 0]^T$ and first row $\mathbf{0}_{N\times 1}^T$.

Both $\boldsymbol{C}$ and $\boldsymbol{\mu}$ contain θ, therefore there are three terms in its gradient. We have

$$\begin{aligned}
&\nabla f_{\theta_x} = \mathrm{tr}\left(\alpha^2|d|^2\sigma_{\mathrm{n}}^2\boldsymbol{C}^{-1}(\boldsymbol{B}_\theta\boldsymbol{H}_\theta^H + \boldsymbol{H}_\theta\boldsymbol{B}_\theta^H)\right) - 2\mathrm{Re}\left[(\boldsymbol{y}-\boldsymbol{\mu})^H\boldsymbol{C}^{-1}h\boldsymbol{B}_\theta\boldsymbol{x}\right] \\
&- \alpha^2|d|^2\sigma_{\mathrm{n}}^2(\boldsymbol{y}-\boldsymbol{\mu})^H\boldsymbol{C}^{-1}(\boldsymbol{B}_\theta\boldsymbol{H}_\theta^H + \boldsymbol{H}_\theta\boldsymbol{B}_\theta^H)\boldsymbol{C}^{-1}(\boldsymbol{y}-\boldsymbol{\mu}), \qquad \text{(D.1)} \\
&\nabla f_{\theta_y} = \mathrm{tr}\left(j\alpha^2|d|^2\sigma_{\mathrm{n}}^2\boldsymbol{C}^{-1}(\boldsymbol{B}_\theta\boldsymbol{H}_\theta^H - \boldsymbol{H}_\theta\boldsymbol{B}_\theta^H)\right) - 2\mathrm{Re}\left[(\boldsymbol{y}-\boldsymbol{\mu})^H\boldsymbol{C}^{-1}jh\boldsymbol{B}_\theta\boldsymbol{x}\right] \\
&- j\alpha^2|d|^2\sigma_{\mathrm{n}}^2(\boldsymbol{y}-\boldsymbol{\mu})^H\boldsymbol{C}^{-1}(\boldsymbol{B}_\theta\boldsymbol{H}_\theta^H - \boldsymbol{H}_\theta\boldsymbol{B}_\theta^H)\boldsymbol{C}^{-1}(\boldsymbol{y}-\boldsymbol{\mu}). \qquad \text{(D.2)}
\end{aligned}$$

APPENDIX E

COEFFICIENTS OF $G'(X)$

To solve $G'(x) = 0$ we only need to solve the numerator of $G'(x)$ equals to zero which is given by

$$|h|^2\frac{2x^2+\alpha x}{\theta_{\mathrm{R}}^2} + |h|^2\frac{x^2+\alpha x}{8|\theta|^4}\cdot\frac{-\sqrt{\Delta}+m+m|\theta|^2-mx}{\sqrt{\Delta}}(1-|\theta|^2+m\sqrt{\Delta}-x)$$
$$-|h|^2\frac{2\alpha^2+3x}{16|\theta|^4}(1-|\theta|^2+m\sqrt{\Delta}-x)^2 = 0. \tag{E.1}$$

where $m = \theta_{\mathrm{I}}/\theta_{\mathrm{R}}$ and $\Delta = 4|\theta|^2-(1+|\theta|^2-x)^2$. $|h|^2$ can be canceled from (E.1) and thus the solution is not related to h. Move all the terms containing $\sqrt{\Delta}$ to the left hand side and the others to the right hand side, and take a square of both sides, we have

$$\begin{aligned}\mathrm{LHS} &= \Delta\Big[\frac{x(\alpha+x)(-1+|\theta|^2+m^2+m^2|\theta|^2+x-m^2x)}{|\theta|^4}\\ &\quad+\frac{m(2\alpha^2+3x)(-1+|\theta|^2+x)}{|\theta|^4}+\frac{\alpha x+2x^2}{R^2}\Big]^2,\\ \mathrm{RHS} &= \Big[\frac{m(\alpha x+2x^2)[(1-x)^2-|\theta|^4-\Delta]-(\alpha^2+\frac{3}{2}x)[(1-|\theta|^2-x)^2+m\Delta]}{|\theta|^4}\Big]^2.\end{aligned} \tag{E.2}$$

Simplify both sides, we have

$$\begin{aligned}\mathrm{LHS} &= (-x^2+d_1x+d_2)(e_2x^3+e_3x^2+e_4x+e_5)^2,\\ \mathrm{RHS} &= \left(f_1x^4+f_2x^3+f_3x^2+f_4x+f_5\right)^2,\end{aligned} \tag{E.3}$$

where

$$\begin{aligned} d_1 &= 2(1+|\theta|^2), & d_2 &= -(1-|\theta|^2)^2,\\ e_1 &= -1+|\theta|^2+m^2+m^2|\theta|^2, & e_2 &= 1+3m-m^2,\\ e_3 &= \alpha-\alpha m^2+e_1-2\alpha^2m+\frac{2|\theta|^4}{R^2}, & e_4 &= \alpha e_1+3m|\theta|^3-3m+\frac{\alpha|\theta|^4}{R^2},\\ e_5 &= 2\alpha^2m(|\theta|^2-1), \end{aligned} \tag{E.4}$$

and

$$\begin{aligned} f_1 &= 2m, \qquad f_2 = \frac{3}{2}-\frac{3}{2}m^2-4m-2|\theta|^2m+2\alpha m,\\ f_3 &= 2m-2|\theta|^2m-4\alpha m-2\alpha|\theta|^2m+\alpha^2-\alpha^2m^2+3m^2+3m^2|\theta|^2+3+3|\theta|^2,\\ f_4 &= 2\alpha m-2\alpha|\theta|^2m+\frac{3}{2}(1-m^2)(1-|\theta|^2)^2+2\alpha(m^2+m^2|\theta|^2-1+|\theta|^2),\\ f_5 &= \alpha^2(1-m^2)(1-|\theta|^2)^2. \end{aligned} \tag{E.5}$$

Finally, the coefficients are

$$
\begin{aligned}
&x^8 : f_1^2 + e_2^2, \\
&x^7 : 2f_1f_2 - d_1e_2^2 + 2e_2e_3, \\
&x^6 : (f_2^2 + 2f_1f_3) - (d_1e_2^2 + 2d_1e_2e_3 - e_3^2 - 2e_2e_4), \\
&x^5 : (2f_2f_3 + 2f_1f_4) - (2d_2e_2e_3 + d_1e_3^2 + 2d_1e_2e_4 - 2e_3e_4 - 2e_2e_5), \\
&x^4 : (f_3^2 + 2f_2f_4 + 2f_1f_5) - (d_2e_3^2 + 2d_2e_2e_4 + 2d_1e_3e_4 - e_4^2 + 2e_2e_5 - 2e_3e_5), \\
&x^3 : (2f_3f_4 + 2f_2f_5) - (2d_2e_3e_4 + d_1e_4^2 + 2d_2e_2e_5 + 2d_1e_3e_5 - 2e_4e_5), \\
&x^2 : (f_4^2 + 2f_3f_5) - (d_2e_4^2 + 2d_2e_3e_5 + 2d_2e_4e_5 - e_5^2), \\
&x : 2f_4f_5 - (2d_2e_4e_5 + d_1e_5^2), \\
&x^0 : f_5^2 - d_2e_5^2.
\end{aligned}
\tag{E.6}
$$